STATE UNIVERSITY OF NEW YORK AT BUFFALO

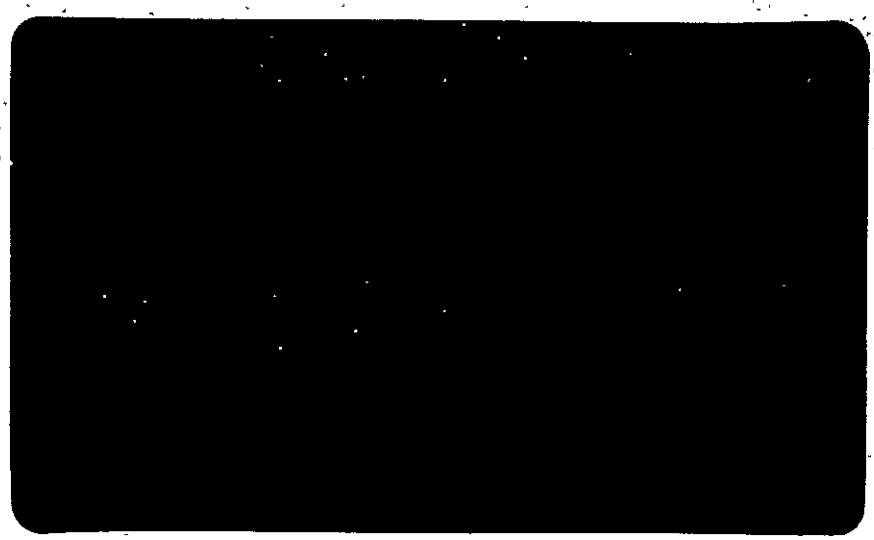

Laboratory for Power and Environmental Studies

Faculty of
Engineering and
Applied Sciences

NSG-7071

LAPES 77-003

EXPERIMENTAL AND THEORETICAL INVESTIGATION FOR THE SUPPRESSION OF THE PLASMA ARC DROP IN THE THERMIONIC CONVERTER

REPORT

DECEMBER 31, 1977

D.T. SHAW, C. N. MANIKOPOULOS, T. CHANG, C.H. LEE AND N. CHIU

WORK CARRIED OUT UNDER THE SUPPORT OF NASA, NSF AND ERDA.

Abstract

This work investigates ion generation and recombination mechanisms in the cesium plasma as they pertain to the advanced mode thermionic energy converter. We have thus studied the decay of highly ionized cesium plasma in the near afterglow in order to examine the recombination processes. We have found very low recombination in such a plasma which may prove to be of considerable importance in practical converters. Moreover we have investigated novel approaches of external cesium generation, i.e., vibrationally excited nitrogen as an energy source of ionization of cesium ion and microwave power as a means of resonant sustenance of the cesium plasma. Experimental data obtained so far show that all three techniques - i.e., the non-LTE high-voltage pulsing, the energy transfer from vibrationally excited diatomic gases, and the external pumping with a microwave resonant cavity - can produce plasmas with their densities significantly higher than the Richardson density. The implication of these findings as related to Lam's theory is discussed in the report.

Table of Contents

	Abstract	i
	Table of contents	ii
I.	Introduction	1
II.	Investigation of the transient cesium plasma	7
	1. Background	7
	2. The experimental setup	9
	3. Spectroscopic plasma diagnostics	11
	a. The spectroscopic apparatus	11
	b. Determination of electron temperature	13
	c. Measurement of electron density	15
	d. Measurement of the relative populations	16
	4. Experimental procedure	19
	5. The experimental results	20
	6. Theoretical calculation of the plasma relaxation	23
	7. Discussion	29
III.	Vibrationally excited molecular nitrogen as an ionization source in the thermionic plasma	35
	1. Background	35
	2. Experimental measurements	36
	3. Discussion of results	38
IV.	Plasma sustenance by the resonant application of microwave power	41
	1. Background	41
	2. Experimental setup	44
	a. The microwave cavity	44
	b. The vacuum system	47
	c. The microwave setup	48
	d. The electrical circuit	49
	3. The experimental results	49
	4. Discussion	53
V.	References	55
VI.	Figures	58

I. INTRODUCTION

The thermionic energy converter has been applied successfully to power systems in a variety of space vehicles. The primary needs in such applications are high power to weight ratio and reliable performance. In the advanced thermionic converter mode we now need to improve the converter efficiency and cost. To achieve a reasonable reduction in cost we envision operating parameters for the second generation converters which are in the range of:

Emitter temperature $\gtrsim 1400^{\circ}K$

Collector temperature $\simeq 700^{\circ}K$

Cesium reservoir temperature $\simeq 400 - 450^{\circ}K$

Interelectrode spacing $\lesssim 1$ cm

It is immediately noticeable that we are demanding a strikingly large reduction of the emitter temperature in comparison to the first generation converters where the emitter temperature was about $2500^{\circ}K$. The direct result of this emitter temperature reduction is the almost complete elimination of the source of the cesium ions previously generated by contact with the hot emitter. The cesium ionization required for space charge reduction cannot be produced by the "arc drop" as was the case of the first generation converter. In such converters, the arc drop (0.5 ev) is a measure of the energy used to heat electrons in order to ionize the cesium atoms. Actually only 5% of this energy is directly used for ionization of cesium. Most of it is lost by collisions of hot electrons with the confining walls, while some of it is lost by radiation. The ionization process of the first generation converter is very inefficient. Our task is to devise an ion generation scheme for the

second generation converter such that efficient ion generation occurs. This must be accomplished without disturbing the quality of the performance of the emitter and the collector electrodes.

It is evident that some external source of energy must be directed into the interelectrode spacing to produce cesium ions. The energy consumption of this source can then be interpreted as an equivalent "arc drop." The performance of the overall system of electrodes and plasma should result in considerable reduction of losses in order to achieve a viable converter.

The present work aims at studying ion generation and recombination in the thermionic cesium plasma and to investigate novel methods in ion generation and plasma sustenance. Plasma recombination studies are typically done in the afterglow of a thermionic converter in the pulsed mode. Furthermore, we investigate two externally supplied sources of cesium ion generation, i.e., vibrationally excited molecular nitrogen and resonantly applied microwave power. Both methods show promise in eventually achieving the desired levels of plasma density with reasonably good efficiencies. It is important to point out that neither method interferes adversely with the performance of the converter electrodes.

In the theoretical treatments of the transport phenomena in the first generation elementary diode, such as those used in the SIMCON and THRIVE codes, the plasma is divided into three regions: the emitter sheath, main plasma, and collector sheath. In these studies, the sheath regions are usually assumed to be of negligible thickness. The very complex plasma phenomena near the sheath are treated by use of simplified boundary conditions involving random currents and Boltzmann factors. The importance of an additional region between the

emitter sheath and the main plasma region was first pointed out by Hatsopoulos.[1] This relaxation region connects the collisionless emitter sheath, in which the plasma is not in equilibrium, to the collision-dominated main plasma, in which a large degree of the local thermodynamic equilibrium (LTE) has been observed. The understanding of the transport behavior in the relaxation region near the emitter is important because it is the most active region as far as ionization and excitation processes are concerned. The dimension of this non-LTE relaxation region is small, typically less than 0.2mm, and is relatively insensitive to the interelectrode distance. Although this region seems to be insignificantly small in a wide-spaced experimental diode, it occupies most of the interelectrode spacing in a practical narrow gap converter.

This non-LTE region is especially important in the development of second generation converters because of the relatively low emitter temperature. For stainless steel this temperature will be around 1400°K which will lead to a plasma density close to the emitter, considerably smaller than $10^{13}cm^{-3}$. In fact, all thermionic plasmas for the second generation converters, regardless whether they are operated in steady-state or pulsed mode, are expected to be in non-LTE state.

For the first generation converter, the plasma is invariably assumed to be under local thermodynamic equilibrium conditions. This means that the electron density can be determined from the Saha equation, while the excited states are described by the Boltzmann relation and the free electron population is given by the Maxwellian distribution. In other words, by defining three temperatures, the Saha temperature T_s, the Boltzmann temperature T_b, and the Maxwellian temperature T_m, we may write:

$$\frac{N_e^2}{N(1)} = \left(\frac{2\pi\, mkT}{n}\right)^{3/2} e^{-E_i/kT_s} \tag{1}$$

$$\frac{N(P)}{N(q)} = \frac{g_p}{g_q}\, e^{-(E_p-E_q)/kT_b} \tag{2}$$

$$f(E) = \left(\frac{m}{2\ kT}\right)^{3/2} \sqrt{E}\ e^{-E/kT_m} \tag{3}$$

For LTE plasmas $T_s = T_b = T_m$, i.e., one temperature can be used to describe completely the population distributions of all free and bound electrons.

For LTE plasmas, the differential equations governing the transport of particle, momentum, and energy in the interelectrode spacing are given by:

$$\Gamma = -\mu_e \left(N_e E + \frac{kT_e}{e}\frac{dN_e}{dx} + \frac{N_e}{e}(\xi - 3/2)\ k\ \frac{dT_e}{dx}\right) \tag{4}$$

$$Q = \xi kT_e \Gamma - \mu_e \frac{N_e}{e} kT_e(\zeta - \xi^2)\ k\ \frac{dT_e}{dx} \tag{5}$$

$$\frac{dQ}{dx} = -E_i \frac{d\Gamma_i}{dx} - R - \Gamma eE \tag{6}$$

$$\frac{d\Gamma_i}{dx} = SN_e N(1) - \alpha N_e^3 \tag{7}$$

where Γ and Q are the electron particle and energy fluxes, respectively, N_e and N_i are the electron and ion densities, respectively, E is the electric field, μ is the electron mobility, E_i is the cesium ionization energy,

R is the radiative energy loss, S and α are the effective three-body ionization and recombination coefficients, N(1) is the density of ground-state cesium atoms. ζ and ξ are functions of T_e as defined by Nigham.[2] If LTE does not exist, the transitions between two individual energy levels do not balance in detail, so that a microscopic treatment of . quantities such as ion generation S and α recombination are necessary.

However, it is well-known that for electron densities less than $10^{13}cm^{-3}$, or when E/p is large (E: electric field; p: cesium pressure), . significant deviations from the LTE conditions exist. In these cases, it has been shown that the interelectrode cesium plasma can be correctly described by the so-called collisional-radiative (CR) model. For a given neutral density, the parameters typically considered are the electron density and temperature, the electric field sustaining the thermionic discharge, and the populations of the various excited cesium atoms.

Transient studies are usually employed to determine the necessary plasma parameters such as recombination ionization coefficients, the electron temperature and density, and so on. Under transient conditions, departures from LTE are generally larger than those indicated under steady state conditions. Consequently the transient analyses given by the CR model are more sensitive to the proper choices of atomic rate coefficients. Thus, the comparison between the experimental and theoretical results during the afterglow is very powerful in the understanding and critique of the CR model.

Recently, work by Lam[3] shows that there is a basic limitation on the minimum electron density in the interelectrode spacing. This limitation is caused by the formation of a double sheath at the emitter when the emitter temperature is low ($\tilde{-}$1400°K) and the current is modestly high ($J \geq$ lamp/cm^2).

As long as this double sheath exists, the Ohmic resistivity of the plasma is expected to be high and the arc drop will remain at the present 0.4 - 0.5 ev level. The only hope, according to this theory, to significantly reduce the arc drop below the present level for the second generation converter is to increase the ion concentration n_i significantly higher than the Richardson electron concentration n_R.* In fact, Lam's theory indicated that when $n_i/n_R >> 10^2$, the Ohmic resistivity decreases from a relatively constant value of 4 or 5** to a value which is inversely proportional to n_i.

This remarkable theory is seemingly in direct contradiction with previous theories which say that a high electron temperature is undesirable for the thermionic converter because of the high hot electron losses.

It is clear from Lam's theory that in order to produce the high current output (>1 amp/cm^2) needed at relatively low emitter temperatures ($\tilde{-}$ 1400°K), means must be found to heat up the interelectode plasma such that $n_i/n_R \tilde{-} 100$. This means that the degree of ionization would probably be very high. In fact, if one desires to keep the relatively low reservoir temperature (100-150°C), the degree of ionization implied is as high as 30%, in contrast to the 1% value encountered in the first generation plasma. It is thus desirable to study plasma generation and recombination processes at high degrees of ionization and to investigate promising methods of externally generating and sustaining high cesium plasma densities.

---

* $n_R = 2 J_R/< V_e >$ where J_R is the Richardson current and $< V_e >$ is the average thermal velocity of electrons.

** The dimensionless Ohmic resistivity R is defined as the Ohmic plasma voltage drop divided by J/J_E (where J and J_E are the output current and the emitter current, respectively.

II. INVESTIGATION OF THE TRANSIENT CESIUM PLASMA

1. Background

The transient behavior of the recombining plasma has been studied theoretically in the past. It is well-documented that three-body capture

$$Cs^+ + e^- + e^- \rightarrow Cs^* + e^- \text{ (K.E.)}$$

is the initial step of the neutralization process in the plasmas of interest[4,7]; Cs^* represents an excited or ground-state seed atom. This capture step is a radiationless process where the second electron carries away the excess energy as kinetic energy. D'Angelo performed a calculation on a fully ionized gas composed only of protons and electrons[7]. He postulated the aforementioned three-body initial capture step and predicted recombination rates in agreement with several sets of experimental data, but his model has since proven inadequate for dense plasmas ($N_e > 10^{12} cm^{-3}$) because he ignored deexcitation collisions. Bates, et al.[5] and Byron et al.[4,6] have performed more general studies in which they have included this effect.

Once electrons are captured into excited states of the atom, they are not considered to have recombined effectively with the ions since they may have a high probability of being reionized. Byron, et al.[4,6] have shown that the rate-limiting step in the "chain" of three-body-recombination processes is the deexcitation of captured electrons. Their model utilizes the rate-process principle that the slowest step in a rate mechanism is the limiting step. As the system approaches equilibrium, the rate at which electronic levels are crossed in the downward direction toward the ground state determines the net recombination rate. This is true because once the electron has reached the ground state it has a much smaller probability of being reionized than it has in the higher states.

Byron, et al.[6] have shown that there is a minimum in the electronic deexcitation rate at a particular atomic energy level. The location of this level depends strongly on the temperature of the free electron gas.

In their application of the rate-limiting model to potassium ion-electron recombination, it was assumed that the electronic levels above and below a quantum state L^* are continuous bands of energy levels rather than discrete states. The states included in their study or the degeneracies assigned to those states, were not listed. In addition, they approximated the slope of the Gryzinski cross section[8] by a linear function in the electron temperature range, 500°K to 2000°K, over which the calculation was performed.

The model of Bates, et al.[5] has been applied to calculations in pure cesium discharges[9] and in Ar-Cs mixtures[10]. In the work of Norcross and Stone[9] a 26-level cesium model was developed which later was extensively used by researchers in the area of thermionic conversion. We intend to apply their steady state calculations as a reference basis for the transient calculation in the present work.

Up to the present time, relatively very few reliable pulications have reported on the experimental measurements of the transient decay of cesium excited states starting with very high initial degrees of ionization. Most of these studies are concerned primarily with the decay of the electron temperature and density[11,12]. Such data are extremely useful since they lead to quantitative determinations of the recombination coefficients.

Recently, the measurements on the afterglow of neutral helium made by Johnson and Hinnov[13] showed that when the classical cross sections are used, the comparison between the observed excited state population densities and the solution of detailed transition rate equations give a very poor agreement.

In addition, the interpretation of measured recombination rates, in terms of a rate coefficient $\alpha(T_e,N_e)$ that is to be compared with calculated values, is exceedingly sensitive to errors in experimentally determined electron temperatures. In order to get better agreement between CR model calculation and the experimental results, Johnson and Hinnov used semiempirical cross sectional values deduced by comparing observed excited-state population densities with solutions of rate equations with very good results.

From the above reviews it can be concluded that our knowledge about the kinetic process under transient conditioning is still very poor. We hope that this research can lead to a more complete understanding in this field.

2. The Experimental Setup

We used a demountable cesium thermionic diode in a pulsed mode to produce the transient plasma which we investigated by optical diagnostics. The cesium thermionic diode used in the experiments is illustrated schematically in Fig. [1]. Most parts of the diode are made of $1\frac{1}{2}$ inch O.D. Varian high vacuum components with conflat flanges and OFHC copper gaskets. The collector is a 1 inch diameter OFHC copper disc attached to an electrical feedthrough, the emitter is a direct heated swirl filament made of tungsten wire 0.040 inch diameter mounted on a dual current feedthrough. The distance between the electrodes was fixed at 1.7 inches. The discharge region of the diode was made of a pyrex glass cross. Two 2 inch diameter optically flat windows were mounted on a pair of ports of the glass cross to provide optical access to the interelectrode spacing. A 15 liter/sec Varian VacIon pump was employed at the final pumping stage. Both the diode and cesium reservoir were baked at 400°C for more than 24 hours while evacuating until a residual gas pressure of 10^{-8} torr was reached. The bakable valve was then closed. A one gram high purity cesium capsule sealed in a glass

envelope under vacuum was put in the reservoir during assembly. After the bakable valve had been closed the cesium was admitted into the system and the discharge initiated.

Two double walled 2 inch thick asbestos ovens were constructed around the diode and cesium reservoir. Temperature controllers were used to keep the ovens at the desired temperature. Since a constant cesium reservoir temperature is very important in the experiment, a potentiometric recorder was used to monitor its temperature variation. It has been found that the cesium reservoir temperature can be controlled within $\pm$ 3°K during operation. To assure that the reservoir is the coldest spot in the system, the temperature of the converter was kept at least 50°C higher than the temperature of the cesium reservoir.

The pyrex glass discharge tube was the most delicate part of the experimental apparatus. A heating rate slower than 100°C per hour was used to avoid thermal shock to the pyrex glass. The tungsten filament emitter was heated by a D.C. power supply, the temperature of the emitter was controlled manually by adjusting the current through the filament. The electrical circuit for operating the diode in a pulsed mode is shown in Fig. [2]. A Velonex model 340, high power pulse generator was used to energize the discharge. The periodic pulse signal was supplied by a pulse generator and then amplified by the Velonex model 340 providing a negative polarity pulse with positive side grounded internally. The capabilities of the high power pulse generator are pulse voltage from 100 to 1000 volts at 5 amps, pulse width from 100 nano-second to 1 milisecond, and a maximum duty factor of 1%. A 25 ohms non-inductive resistor was put in the circuit which served as the ballast resistor to limit the diode current. The same resistor was also used to measure the current through the diode. The current and voltage of the pulse diode were measured with a Tektronix type 536 oscilloscope.

Since the current measuring resistor was not grounded, a type G plug-in unit (wide band differential preamplifier) was used on the vertical input of the oscilloscope. The I-V characteristic of the diode was taken with two type G plug -in units on both vertical and horizontal input. Figures[3-5]illustrate some of the diode current and voltage recorded. As indicated in those figures, the fast rising voltage causes the cesium vapor break down in a very short period of time. After the ignition of the diode, the impedance of the diode drops to a much lower value than the impedance of the remaining circuit, this phenomenum essentially changes the input to the diode to be a constant current source. The constant diode current during the remainder of the pulse makes the diode voltage decrease as the electron density and the conductance of the diode build up. After the cutoff of the pulse, the cesium ions remain in the interelectrode spacing for some time before they recombine into neutral atoms. The ions neutralize the space charge and are responsible for the positive output voltage after pulse cutoff as shown in Figs. [3-5].

3. Spectroscopic Plasma Diagnostic

a. The spectroscopic apparatus

The arrangement of the optical system is shown in Fig. [4]. The image of the interelectrode spacing was collected by a pair of lenses and was focused on the entrance slit of the spectrometer. The spectrometer used in the experiments was a half meter Jarrell Ash model 82-000 scanning monochromator equipped with an 1180 groove/mm grating. The diffraction grating provides a linear dispersion of 16 Å/mm at the exit slit and the resolution of the spectrometer is determined by the width of the exit slit. Two fixed width exit slits were used in our experiments. During the line shape measurements, a 15 micron slit was used which gives a resolution of 0.24 Å. In all other measurements, a 250 micron slit was

used to cover a wavelength interval of 4 Å, in our case this band width is much larger than the half width of all the lines we are interested in and the line intensity obtained was assumed to be proportional to the total intensity emitted from that line. The monochromator was calibrated by the 5461 Å green line of the mercury lamp, and then checked by other mercury lines including two violet lines at 4047 Å and 4078 Å, two yellow lines at 5770 Å and 5790 Å, and two red lines at 6152 Å and 6234 Å. An EMI 9558QB photomultiplier tube was mounted at the exit slit of the monochromator to measure the intensity of light that came out of the exit slit. The ratio of the number of electrons emitted to the number of incoming photons is a function of wavelength and is referred to as the quantum efficiency $Q(\lambda)$. It is thus necessary to convert the measured intensity (photomultiplier output current) into the true intensity. For a fixed voltage applied to the PM tube, the output current of the PM tube is proportional to the number of electrons emitted from the photocathode, which in turn is related to the true intensity in the following way

$$I_m(\lambda) = N_p Q(\lambda) = \frac{I_T(\lambda)}{hc/\lambda} Q(\lambda) \tag{8}$$

where N_p is the number of photons detected by the photomultiplier, $I_T(\lambda)$ is the true intensity in watt/cm^{3}sec. The measured intensity is then related to the true intensity by

$$I_T(\lambda) = hc \frac{I_m(\lambda)}{Q(\lambda)\lambda} \tag{9}$$

No correction is taken on the line profile, as it involves a region less than 10 Å where the change of $Q(\lambda)$ is too small to be significant.

b. Determination of electron temperature

Assuming the free electrons have a Maxwellian distribution of energy, the electron temperature was determined by measuring the relative continuum intensity from the radiative recombination of free electrons into the 6P state. The 6P state was used, because it gives the strongest continuum radiation in the region of 4000 Å to 5000 Å and this region is relatively free from line radiations.

The radiative recombination mechanism to 6P state can be expressed as

$$Cs^+ + e^- \longrightarrow Cs(6P) + h\nu \qquad (10)$$

where h is the Plank's constant, ν is the frequency of the emitted light and $h\nu$ is the photon energy released as a free electron recombined with a cesium ion and becomes a cesium atom at 6P state. From the conservation of energy we have the relationship

$$h\nu = E_i(6P) + \tfrac{1}{2} m v^2 \qquad (11)$$

where $E_i(6P)$ is the ionization potential of 6P state and $1/2\ mv^2$ is the kinetic energy of the free electron involved. The value of $E_i(6P)$ is about 2.49 ev corresponding to a wavelength of 5080 Å. The intensity of the radiative recombination in the wavelength interval between λ and $d\lambda$ is given by

$$I(\lambda)d\lambda = h\nu N_e N_i v \sigma_{6P}(v) f(v) dv \qquad (12)$$

where N_e is the free electron density, N_i is the ion density, $\sigma_{6P}(v)$ is the velocity-dependent cross section for recombination of the 6P state and f(v) is the electron velocity distribution. The cross section $\sigma_{6P}(v)$ used here was

determined experimentally by Agnew and Summer[17] as

$$\sigma_{GP}(v) = \frac{3.74 \times 10^{-6}}{v^2} \quad cm^2 \tag{13}$$

where v has the unit of cm/sec. Using the relation

$$\lambda = \frac{c}{\nu} \tag{14}$$

where C is the speed of light, after differentiating Eqs. (11) and (13) and substituting into Eq. (12) we can get the intensity of radiative recombination as

$$I(\lambda) = \frac{h^2 \nu^3}{mc} N_e N_i \sigma_{GP}(v) f(v) \tag{15}$$

Assuming f(v) to be Maxwellian

$$f(v) = 4\pi \left(\frac{m}{2\pi kT_e}\right)^{3/2} v^2 \exp\left(\frac{-mv^2}{2kT_e}\right) \tag{16}$$

Combine Eqs. (11, 13, 15, and 16), we find

$$I(\lambda) = 3.74 \times 10^{-6} (hc)^2 \left(\frac{2m}{\pi}\right)^{1/2} N_e N_i (kT_e)^{-3/2} \lambda^{-3} \exp\left(\frac{E_i(GP) - h\nu}{kT_e}\right) \tag{17}$$

or

$$\ln[\lambda^3 I(\lambda)] = \ln C_1 - \tfrac{3}{2} \ln T_e - \frac{hc}{kT_e} \cdot \frac{1}{\lambda} \tag{18}$$

where C_1 is a proportional constant. Since T_e is constant during each measurement, the plot of $\ln[\lambda^3 I(\lambda)]$ versus $1/\lambda$ gives a straight line with a slope equal to $-hc/kT_e$. The electron temperature can thus be calculated by measuring the slope. A typical continuum radiation spectrum of cesium plasma in the region of 4000 to 5000 Å is shown in Fig. [5]. Figure [6] shows the straight line from

which the electron temperature was determined. In actual experimental results, sometimes the light intensity at lower wavelengths is too low to be distinguished from background noise. In such cases, we considered only the region of wavelength above 4500 Å where the light intensity is high compared to the noise.

c. Measurement of electron density

Line profile measurements have been used in determining the electron density of the cesium plasma. There are mainly three kinds of broadening mechanisms which affect the line profile of the bound to bound radiative decay, namely, natural broadening, the Doppler broadening, and the pressure broadening. The natural broadening is due to the uncertainty of the energy of the radiating atoms, which is inversely proportional to the lifetime of the upper level of the transition, and is of the order of 10^{-4}Å in cesium lines. The Doppler broadening is due to the thermal motion of the radiating atom relative to the observer, which is a function of the cesium gas temperature. In a typical cesium thermionic plasma, the gas temperature is low and the Doppler effect usually is responsible for a broadening of about 10^{-2}Å. The pressure broadening results from the interaction of the radiating atom with neighboring atoms. For most thermionic plasmas Stark broadening, which is caused by interaction of the radiating particle with the electric field of charged particles, plays the dominating role. The theory of Stark broadening of spectral lines has been described in a number of papers.[18-22] In general the broadening is treated by perturbation theroy, where the wave functions of the emitting atoms are perturbed by the plasma ion and electron fields. Two different approximations are usually employed in describing the interactions of radiating atoms and charged particles. Electron interactions are treated by the impact approximation while ion interactions are treated by the quasi-static approximation.

These two approximations arise from the difference of the thermal velocities of the ions and electrons. After detailed calculation using the above assumption, the profile of a Stark broadened line can be approximated by a Lorentz distribution

$$I(\omega) = I_{max}\left[\frac{w^2}{(\omega-\omega_o-d)^2+w^2}\right] \tag{19}$$

where $I(\omega)$ is the line intensity at angular frequency ω, I_{max} represents the peak intensity of the line, ω_o is the angular frequency at the maximum intensity for the unperturbed line, d and w are the Stark shift and Stark half width respectively in the unit of angular frequency. The value of d and w are both sensitive functions of the free electron density, and the electron density can be determined by measuring either one of them. The Stark width has been calculated by both Griem[19] and Stone[20], the Stark shift was investigated by Majowski and Donohue.[22] In practice, the Stark width measurement is more frequently used, because it does not need very accurate calibration of the absolute wavelength of the spectrometer. The Stark widths of the cesium fundamental series lines are only slightly temperature dependent (a few percent over temperatures from 2000°K to 5000°K) so the temperature need not be known to determine electron density. In our experiment the electron density was determined by measuring the Stark width of the fundamental series lines and comparing with the calculated values of Stone.

d. Measurement of the relative population of the excited states

The line radiation emitted is a result of the spontaneous decay of the excited state atoms. The mechanism is:

$$Cs(p) \longrightarrow Cs(q) + h\gamma \tag{20}$$

where $p > q$ and $h\nu$ is the energy difference between the states p and q. The number of photons emitted from such a transition within unit time interval and from unit volume is

$$N_p = N(p)\, A(p, q) \tag{21}$$

where

$$A(p,q) = \frac{8\pi^2 e^2 \nu^2}{m_e c^3} f_{qp} \tag{22}$$

is the probability per unit time that an atom emits a photon, and f_{qp} is the absorption oscillator strength for transition from state q to p. If we substitute Eqs. (21 and 22) into Eq. (8), we have

$$I_m(\lambda) = C_2 N(p) \lambda^{-2} Q(\lambda) f_{qp} \tag{23}$$

where C_2 is a proportional constant. Because of the broadening mechanism we have discussed previously, Eq.(23) is true only when the exit slit of the monochromator is wide enough to cover the whole line. In that case the population of the state p can be found as

$$N(p) = \frac{I_m(\lambda)\, \lambda^2}{C_2 Q(\lambda) f_{qp}} \tag{24}$$

Since C_2 is not related to p or q in anyway, the relative population of the excited state can be found by measuring the line radiation originated from that particular state. If the plasma under investigation is in LTE condition, the relative population of the excited states gives the information of electron temperature according to the Boltzmann relation

$$\frac{N(p)}{g_p} = \frac{N(q)}{g_q} \exp\left(\frac{E_q - E_p}{k T_e}\right) \qquad (25)$$

where g_p and g_q are the statistical weight of states p and q respectively, E_p and E_q are the energies of the corresponding states and h is Plank's constant. Table 1 lists all the lines observed in the experiments, where the oscillator strengths used are those given by Agnew and Summer, while the level energies are from Norcross and Stone[9].

Table 1 Observed Cesium Lines

Transition	Wavelength (Å)	Upper Level Energy (ev)	Oscillator Strength
7D - 6P	6973	3.23	0.111
8D - 6P	6213	3.45	0.0439
9D - 6P	5845	3.57	0.0237
10D - 6P	5635	3.65	0.0153
7F - 5D	6870	3.61	0.0409
8F - 5D	6629	3.68	0.0252
9F - 5D	6473	3.72	0.0172
10F - 5D	6366	3.76	0.0123
11F - 5D	6213	3.78	0.0082

4. Experimental Procedure

The cesium diode was operated at constant temperature during each measurement. The region viewed by the monochromator is the middle part of the interelectrode spacing to avoid the background noise from the electrodes. The experimental range for cesium pressure varied from 0.079 to 0.4 torr, while the power pulse width changed from 3 to 10 micro-second. For each operating condition, the line intensity of nD-6P and nF-5D transitions for n from 7 to 10 were recorded as a time function. Free electron density and temperature were measured at various time instances whenever it was possible.

During the line intensity measurements, a 250 micron exit slit was used on the monochromator. Since the wavelength dial of the monochromator is accurate to $\pm$ 2 Å only, the line position had to be located by scanning the monochromator to find the maximum intensity point and fixed at that wavelength. In all experiments, the synchronous signal was set at 500 nano-second before the diode pulse, such that the boxcar integrator was triggered before the radiation signal started. By scanning the boxcar integrator we recorded the time variation of the line radiation for the time interval we are interested in.

Free electron temperature and density were measured using the delay mode of the boxcar integrator. The aperture of the boxcar integrator was set to open at a specified time position which we studied after each trigger pulse while the monochromator was scanned over the wavelength interval of 4000 Å to 5000 Å to record the spectrum of continuum radiation for electron temperature measurements. The same technique was employed to measure the line width of 6629 Å (8F-5D) for electron density determination. A 15 micron exit slit was used on the monochromator during line width measurements. The slit covers a wavelength band of 0.24 Å which is small compared with all the line widths

we have measured, so no correction of the instrument broadening was made. The 6629 Å was chosen for the electron density measurement because it gives both large Stark width and enough intensity to allow for accurate electron density determination.

5. The Experimental Results

The thermionic diode was operated at several conditions to investigate the effects of varying the pulse width at different cesium pressures upon the converter characteristics. The operating conditions are listed in Table 2.

Table 2 Operating Conditions of the Thermionic Diode

Run No.	Pulse Width (microsecond)	Cesium Pressure (torr)	Diode Current (amp)
1	5	0.079	1.4
2	3	0.079	0.12
3	3	0.079	0.40
4	3	0.457	0.48
5	10	0.079	2.0
6	10	0.457	1.2

The line intensity of several diffuse and fundamental series lines had been recorded as a function of time. The electron temperature and electron density at various time instances during the plasma transient were measured whenever the light intensity was high enough. The variation of the excited state populations during the pulsed operation was also estimated.

The line radiation of nD-6P and nF-5D transitions for n = 7, 8, 9 and 10 were recorded during the pulsed operation of the thermionic diode. These lines are emitted from states with energy ranging from 3.23 to 3.76 ev only. The data for higher and lower energy levels are not available at present for the following reasons. The light emitted from the lower energy states either has a very high wavelength which is difficult to be detected by the photomultiplier tube or the transition is resonance radiation when severe trapping makes the data reduction difficult. At the higher energy levels the populations are very low and the light intensities are not strong enough to be detected. Figure [7] illustrates a typical measured intensity of 7D-6P transition where the pulse current was cut off at 3.5 microseconds (the pulse starts at 500 nanosecond after the triggering of the boxcar integrator and has a duration of 3 microseconds). As indicated in the figure, the light intensity increases during the pulse which corresponds to the increasing of population of the upper transition level. After the cutoff of the pulse current, the light intensity continues increasing to a maximum point before it starts to decay. The light intensity increase after cutoff of the pulse was found in all the data we took although the times at which the peak intensity occurred were different in all cases. It is observed that the time needed to reach the maximum decreased as the input pulse power increases, this time also increases

as the cesium pressure increases. Figures [8] and [9] show the position of peak intensity of 7D to 6P transition in the cases of 3 and 10 microsecond pulses respectively. The decay time constants of 7D to 6P transition in Run 1 through Run 4 are almost the same and are found to be about 25 microseconds while the result in Run 5 is 110 microsecond and that in Run 6 is 150 microsecond. Under the same operating conditions, the decay rate in other transitions are usually very close to that in 7D to 6P transition except the 10F-5D and 10D-6P transition in Run 5. Figures [10] and [11] illustrate the time variations of relative population of excited states as deduced from the line radiation measurements. The pulse cutoff time has been used in these figures as the reference time. We have also plotted the relative population versus the bound state energy in Figures [12] and [13] to investigate the distribution of excited state populations during the pulse operation.

Efforts had been made to measure the electron temperature during the pulsed operation of the diode. Unfortunately, the only two cases we have been able to record are those from 10 microsecond pulses. In the case of shorter pulses, the intensity of the continuum radiation spectrum is too low to be detected. It is believed that the electron temperatures in these cases were both very low and changing fast which makes them difficult to measure. Figure [14] shows the electron temperature variation as a function of time as deduced from the experimental data. During the data reduction of the electron temperatures, it is found that after the pulse cutoff, the $\ln[\lambda^3 I(\lambda)]$ vs $1/\lambda$ plots are very close to a straight line at all times while the plot for data obtained inside the pulse appear differently. Figure [15] shows the plot for Run 6 at 7.5 microsecond after the pulse starts. It indicates that the large electric field during the pulse produces a substantial amount of high energy electrons for the excitation of the plasma.

Free electron density had been measured in several cases and the results are shown in Fig. [16]. The measurements show an ionization of about 20% in all cases right after the pulse cutoff. It also shows a relatively slow variation in electron density during the relaxation of the plasma. The very small recombination rate indicated by Fig. [16] is very striking and may prove to be of great practical importance in the thermionic plasma.

6. Theoretical Calculation of the Plasma Relaxation

Up to the present time, the so-called collisional-radiative (CR) model has been used extensively to calculate the distribution of bound states population in a plasma. In this section we will try to formulate the transition processes which represent the mechanisms during the relaxation of a cesium thermionic plasma. The discussion follows closely Bates, Kingston and McWhirter's[5] CR model with the addition of a conservation of particle equation and an energy balance equation. All these equations are solved simultaneously to find the time variation of the plasma parameters.

Under normal plasma conditions for cesium discharges, the mechanisms that are important in determining excited state populations are electron-atom collision processes and radiative decays. Molecular processes are not important because of the low concentration of molecular species. Atom-atom and atom-ion collisions can be neglected since their excitation and ionization rates are much lower than the electron rates. The cesium plasma was assumed to be homogeneous in the region of observation. The free electrons were assumed to be in Maxwellian distribution at all times. The plasma was optically thin for all radiations except for resonance radiations.

Considering an ionized cesium vapor composed of free electrons, singly ionized cesium atoms and neutral atoms in bound states, the rate of change of population

in each state can be expressed as

$$\frac{dN(p)}{dt} = -N(p)N_e K(p,c) - N(p)N_e \sum_{q\neq p} K(p,q)$$

$$-N(p)\sum_{q<p} A(p,q) + N_e \sum_{q\neq p} N(q)K(q,p)$$

$$+\sum_{q>p} A(q,p) + N_e^2\left[N_e K(c,p) + \beta(p)\right] \qquad (26)$$

where N(p) is the density of atoms in level p, Ne is the free electron density, K(p,q) is the collision-induced transition rate from level p to level q, c denotes the electron continuum and K(c,p) is the three-body recombination rate to level p. The spontaneous decay rate from level p to level q is A(p,q) and the radiative recombination rate to level p is β(p). All the transition rates except the spontaneous decay rate are strong functions of free electron temperature T_e.

Similar to the bound state rate equations, the free electron continuity equation can be written as

$$\frac{dN_e}{dt} = N_e \sum_r N(p)K(p,c) - N_e^2\left[N_e K(c,p) + \beta(p)\right] \qquad (27)$$

Assuming that there is no loss of electron energy due to processes other than collision and radiation, the energy balance equation is

$$\frac{dW_e}{dt} = \left(\frac{dW_e}{dt}\right)_{el} + \left(\frac{dW_e}{dt}\right)_{inel} + \left(\frac{dW}{dt}\right)_{rad} \qquad (28)$$

Where W_e is the total electron kinetic energy in a unit volume and can be expressed as:

$$We = Ne \cdot \varepsilon_e = Ne \cdot \tfrac{3}{2} KTe \tag{29}$$

where ε_e is the average energy of an electron. The terms on the right hand side of Eq.(28) represent the electron energy change due to elastic collision, inelastic collision and radiation, respectively. The elastic collision term can be written as

$$\left(\frac{dWe}{dt}\right)_{el} = -2\frac{Me}{Ma}(\varepsilon_e - \varepsilon_a)\nu_{ea} \tag{30}$$

where Me and Ma are mass of electron and cesium atoms, respectively. ε_e and ε_a are the average kinetic energy of each electron and atom as defined in Eq.(4). ν_{ea} is the collision frequency between electron and atom and can be expressed as

$$\nu_{ea} = Ne\,Na\,Vea\,\sigma_{ea} = NeNa\sqrt{\frac{2kTe}{Me}}\,\sigma_{ea} \tag{31}$$

where σ_{ea} is the collision cross section between electron and atom which has an average value of $4 \times 10^{-14} cm^2$. Since the velocity of cesium atoms is much slower than the electron velocity, the relative velocity between electron and atom v_{ea} was replaced by the average electron velocity in Eq.(32). Insert ν_{ea} into Eq.(31), and we find

$$\left(\frac{dWe}{dt}\right)_{el} = 4.24\frac{\sigma_{ea}}{Ma}\sqrt{k^3 Me Te}\,NeNa(Te-Ta) \tag{32}$$

the energy change due to inelastic collision is

$$\left(\frac{dWe}{dt}\right)_{inel.} = \sum_{r}\sum_{q} N_e N(r) K(r,q)\left[E_i(r) - E_i(q)\right]$$

$$-\sum_{p} N_e N(p) K(p,c) E_i(p) + \sum_{p} N_e^3 K(c,p) E_i(p) \qquad (33)$$

where $E_i(p)$ is the ionization potential of level p. The electron energy change due to radiation is

$$\left(\frac{dWe}{dt}\right)_{rad.} = -\sum_{p} N_e^2 \beta(p)\left[E_i(p) + 3/2\, kTe\right]$$

$$-\sum_{p}\sum_{q} N(p) A(p,q)\left[E_i(q) - E_i(p)\right] \qquad (34)$$

differentiate Eq. (29) and we find

$$\frac{dWe}{dt} = 3/2\, k\left[Ne\,\frac{dTe}{dt} + Te\,\frac{dNe}{dt}\right] \qquad (35)$$

substitute Eq. (35) into Eq. (28) and rearrange the terms, we can obtain the temperature rate equation as follows

$$\frac{dTe}{dt} = \frac{2}{3kNe}\left[-3/2\, kTe\left(\frac{dNe}{dt}\right) + \left(\frac{dWe}{dt}\right)_{el}\right.$$

$$\left. + \left(\frac{dWe}{dt}\right)_{inel.} + \left(\frac{dWe}{dt}\right)_{rad.}\right] \qquad (36)$$

Now, the whole system is described by the differential Eqs. (26, 27 and 36). Unfortunately, there are infinite numbers of bound states in the atomic structure and it is not practical to solve the whole set of differential equations. Since the more loosely an electron is bound the greater the relative probability of a collision induced transition versus spontaneous decay, the result is that the high

bound states are in a local thermodynamic equilbrium (LTE) with the electron continuum. Under this assumption the population of the high bound states are given by the Saha equation at the free electron temperature and density, i.e.

$$N_E(P) = g_P\left(\frac{h^2}{2\pi m_e k T_e}\right)^{3/2} N_e^2 \exp\left[\frac{E_i(P)}{kT_e}\right] \qquad (37)$$

where g_p is the degeneracy of level p. It has been found by Norcross and Stone[9] that in a cesium plasma under the condition of Te from 1500°K to 3000°K, Ne from 10^{12} to 10^{15}cm^{-3} and cesium vapor pressure from 10^{-2} to 5 torr, 26 non-equilibrium levels will be sufficient for the calculation of population distribution in the plasma. An additional 27 levels with Saha populations are needed to complete the sums in Eq.(26) giving a total of 53 levels. Higher levels are neglected because of their low population and smaller contribution to the system.

After neglecting the equations describing the high energy levels, we have a set of n+2 simultaneous differential equations to be solved, where n is the number of non-LTE states considered. Each one of the n states is described by a rate equation according to Eq.(26). The other two equations are Eqs.(27 and 36).

A Fortran IV computer program was written to solve the n+2 equations numerically, where n is set to be any number less than or equal to 26. The input data needed for the calculation are cesium reservoir temperature, free electron temperature and density which are measurable quantities in the experiments. To start the calculation we need the distribution of the bound states population as the initial conditions. In the computer program a choice from three kinds of distributions is available, these are (1) LTE, (2) steady state non-LTE and (3) experimental data. The steady state non-LTE condition mentioned above is the

solution of the rate equations when all the derivatives are equal to zero.

With the knowledge of initial conditions all the n+2 equations are integrated simultaneously to find the new distribution of the bound state populations as well as the free electron density and temperature. The numerical method used for the integration was found to be quite critical. As in a typical nonequilibrium problem the differential equations in the present problem can be quite stiff, i.e., they tend to oscillate severely around the equilibrium values when the variables are close to equilibrium. Because of the stiffness of the equations, conventional explicit computation methods such as the Adam-Moulton predictor-corrector formula or the Runge-Kutta method result in extremely long computation time. In this calculation, an implicit integration method is used as recommended by Lomax and Baily[23].

Most of the atomic transition parameters are strong functions of free electron temperature. The calculation of the transition rates involve the integration of the product of transition cross section and the free electron velocity distribution and are very time consuming. Since the numerical method for solving the transient plasma involves the use of several different temperatures during each step of integration, it is not practical to calculate all the parameters each time we change the temperature. In practice, we have calculated each of the transition parameters for several temperatures ranging from 1000°K to 4000°K and then fit these data into a polynomial or an exponential form with the exponent in polynomial form according to the nature of the parameter. The atomic transition rates which appear in the program listing were obtained in this way and were found to have saved a substantial amount of computing time.

7. Discussion

From the results of the experiments it is felt that calculation of the time response of the excited state population densities is not possible at this time. The main reasons are: (1) The initial conditions for the calculation are not available. Because of the short pulse width used in the experiments, the plasma condition at the time of pulse cutoff was far from the steady state non-LTE condition as can be calculated by solving the rate equations.
(2) For a rapid changing plasma as we have observed, the use of detailed balancing technique in finding the atomic parameters is not valid. The difficulties in getting suitable atomic transition parameters is fatal to the theoretical calculation.

Radiation and electron collision are the two major processes which govern the atomic transitions. The rate at which the collisional transition occurs depends strongly upon the amount of energy transferred during the collision. In the atomic structure, the energy of the lower states are relatively widely separated while the higher states are closer to each other, the result is that the collisional transition rates between the higher levels are much higher than those between lower levels. On the other hand, the radiative transition rates are smaller for the hgiher levels because the electrons are more loosely bounded.

It is well known that if the electron collisions dominate the atomic transition processes, the plasma essentially will come to an LTE condition after a time long enough for collisions to take place. In a low density plasma, usually the higher levels are collision-dominated and are in equilibrium with the free electrons while the radiation effect becomes greater at lower levels and the deviation from LTE is significant. It has been shown by Norcross and Stone[9]

that LTE exist in a cesium plasma only if the free electron density is higher than $10^{16} cm^{-3}$. In the same paper, they also found that because of the severe trapping of the resonance radiations, the net transition between the ground state (6S) and the first excited state(6P) is almost purely collisional. In other words, although the lower energy levels deviate from LTE significantly, the relative populations between these two states have a Boltzmann temperature equal to the free electron temperature.

During the pulse operation of a thermionic diode the distribution of the bound state populations are more complicated and we will have to analyze separately the changing of the excited state populations within the pulse and after the cutoff of the pulse.

Almost all the cesium atoms are in their ground states before the pulsing of the diode. Right after the electric field is applied to the electrodes, the free electrons (mainly thermionic electrons) are accelerated by the electric field and gain the energy before all other particles do. The energized electrons then transfer their energy to the neutral atoms through electron-atom inelastic collisions. The rate at which the electrons interact with the neutral atoms determines the population of the excited states during the transfer.

The electron-atom collisional excitation cross section $\sigma(p,q)$ for transition from level p to level q has been investigated by Gryzinski[8]. Since all the excited state populations come from the gound state and the cross section $\sigma(1.q)$ decreases sharply with increasing q, it is obvious that the transition from 6S to 6P is the dominating process which limits the growth of the excited state populations. Assuming a Maxwellian distribution of the free electron velocity, we can obtain the collisional excitation rate coefficient K(1,2) for transition from 6S to 6P as a function of free electron temperature. The

excitation rate coefficient $K(1,2) = \langle\sigma(1,2)v\rangle$ is the average collision frequency of each electron with a ground state cesium atom which induces a 6S and 6P transition. The average time that such a collision occurs to a ground state atom is

$$\tau_{1,2} = \frac{1}{N_e K(1,2)} \tag{38}$$

For a typical steady state cesium themionic plasma with an electron temperature of 2500°K and electron density of $10^{13}cm^{-3}$, the time needed for 6S and 6P states to reach equilibrium with the free electrons is in the order of one milisecond. Since the time necessary to reach the equilibrium is much longer than the pulse width in our experiments, it is clear that the population of the 6P state is always lower than that predicted by Boltzmann distribution at the electron temperature. Figure [17] illustrates the bound state population distribution for different times during the applied power pulse. Curve 1 is the distribution before the pulse is applied. Curve 2 represents the distribution a short time after the pulse started while the population of the 6P state is still far from equilibrium with 6S as discussed above. Once the electrons have been excited to 6P state or higher, they have a much higher collision frequency to be excited to upper states. If the radiative decay rate is negligible compared with the collision transition rate, this means that the absolute value of the slope of the higher energy part of the curve will be smaller than that between 6S and 6P states, but the high radiative rates in the intermediate states keep the population low. Since the radiative rate becomes relatively small at higher levels, the result is that the slope of the population versus energy curve decreases monotonically as the energy increases

until some critical energy where the effect of the radiation is negligible compared with the collisional transition process. Population for levels with energy higher than the critical energy are in collisional equilibrium with the free electrons and the high energy part of the curve shows a constant slope which corresponds to the free electron temperature. In the case of a longer pulse, curve 3 illustrates that more ground state atoms have been excited which in turn give higher excited state and electron populations. The enhancement in electron density produces higher collisional transition rates and makes the critical energy for collision dominated transition move to a lower energy. Curve 4 of Fig. [17] shows the population distribution when the pulse width is so long that a steady state non-LTE condition is achieved. In such a case, both the high energy levels and the population between 6S and 6P states are in equilibrium with the free electron temperature and give the same slope in curve 4, the intermediate states have higher radiative rates and have a slope higher than both sides of the curve.

After the cutoff of the pulse the excited plasma redistributes it population and decays back to the original condition. Since the decay of the plasma is the result of energy loss, it is necessary to analyze this problem from the energy point of view. Although the high energy levels have high collision rates with the free electrons, the effect on electron energy due to these levels are not very important because of their low population and relatively small amount of energy transferred during each collision. So the rate of decay of the electron energy is mainly determined by the low energy states. As we have discussed previously, at the time the pulse is terminated, the free electrons have a temperature higher than the Boltzmann temperature between 6S and 6P states. The high population in the 6S state makes the collision excitation

rate of 6S faster than the de-excitation rate of 6P. A rough estimate shows that for a plasma with ground state population of $10^{15}cm^{-3}$ and free electrons at $10^{14}cm^{-3}$ and 2000°K, the rate of free electron energy loss due to the excitation of 6S to 6P transition is about 0.5 joule/sec., while the total kinetic energy of the free electrons is only 5×10^{-6} joule. In other words, the electron temperature drops very fast initially. The loss of electron energy slows down the excitation rate and makes the de-excitation process more and more important. After the electron energy drops to a point where the excitation rate of 6S and de-excitation rate of 6P becomes comparable the electron energy change due to the inelastic collision becomes relatively small, and the radiative processes which carry the energy out of the plasma dominate the change of electron energy.

As a summary, during the early stage of the relaxation process the electron energy drops drastically but the nature of this drop results in a redistribution of the plasma energy instead of a net loss of plasma energy. It is the radiative processes which result from the decay of the excited state populations that actually drain energy from the plasma.

For the change in high energy level populations, the mechanism is totally different. Figure [18] shows the population distribution for different time instances during the relaxation process. Curve 1 illustrates the populations when the pulse is cut off. Because of the very rapid collisional transitions and long radiative lifetimes, the highest states must be in equilibrium with both the free electron density and temperature, and their populations follows the Saha equation. Immediately after the cutoff of the pulse, the electron temperature decreases rapidly but the electron density does not change very fast. According to the Saha equation, this means that the populations in these states

increase because the lowered electron temperature slows down the collisional ionization rates which in turn causes net recombination to populate the high energy levels. Curve 2 in Fig. [18] shows such an equilibrium between the high energy states at the lower electron temperature. Similarly to the case we have discussed in the excitation of the plasma there exists a critical energy where the rates of collisional transition and radiative transition are comparable. For levels below the critical energy the radiative transition rate is relatively high such that the deviation from Saha equilibrium becomes significant. At later stages of the relaxation process the loss in both electron temperature and density causes an increase in the critical energy and the relatively high radiative transition rates make all the excited states populations drop instead of increasing, which is shown in curve 3 in Fig. [18].

Since there is no energy source for the plasma after the cutoff of the pulse, the behavior of the relaxation process depends solely on the plasma condition at the end of the pulse.

Suppose that we have two plasmas with different degrees of excitation. We thus expect the relaxation of the plasma with a higher degree of excitation to act in the following way:

(1) As we have discussed, the more highly excited plasma should have a smaller difference between the initial free electron temperature and the Boltzmann temperature between the 6S and 6P states. This smaller difference will result in a smaller drop in electron temperature right after the pulse cutoff. Consequently, the expected increase in the excited state populations after cutoff must be smaller.

(2) The higher electron temperature of this plasma during the whole relaxation process keeps the rate of electron recombination lower and should result in a

longer decay time for the plasma with the higher degree of excitation.

The above arguments can interprete some of the observed phenomena such as the longer decay time constant for longer pulse and the fact that the time necessary to reach the peak intensity is longer for those lower current cases, but we are still far from the quantitative understanding of the kinetic process in the transient plasma. Much more data in wider experimental conditions are needed for the quantitative analysis of the relaxation phenomena. It is hoped that this work has provided a good start for future research in this area.

III. VIBRATIONALLY EXCITED MOLECULAR NITROGEN AS AN IONIZATION SOURCE IN THE THERMIONIC PLASMA

1. Background

In laser work the vibrational levels of molecular species often serve as storage tanks of energy obtained from electrical discharges. Nitrogen is particularly useful in this respect because its excited vibrational energy levels are exceptionally long lived due to the fact that the nitrogen molecule possesses no electric dipole moment. Once the molecular vibrational levels are excited they cannot decay to the found state ($v=0$) levels through electric dipole radiation[24]. Deactivation can proceed only by collisions with other molecules or atoms or with the walls of the confining vessel. The wall deactivation coefficient of nitrogen is small[25] (about 1×10^{-3} for stainless steel, the same order or less for most other common surfaces) so most of the deactivation proceeds by collisions with neutral cesium atoms which often result in cesium ionization (see Fig. [1]).[26]

In this work we report experimental observations on the direct ionization of Cs atoms by vibrationally excited N_2. It has been known for some time that molecular nitrogen in the presence of alkali atoms (Na, K, Cs) will quench

resonance radiation under a variety of laboratory experimental conditions.[27,28] The reverse process, i.e., the excitation of alkali atoms by vibrationally excited N_2 has also been reported.[29,30] These reactions are important in the understanding of certain types of aurora in which strong alkali metal radiation is observed. In recent years, interest in the transfer of vibrational energy from N_2 to excite other atomic or molecular gases has been expanded because of the rapid development of high power lasers. For such lasers the vibrationally excited N_2 is produced either by a discharge or by the rapid gas dynamic expansion technique.

The present study has been carried out to investigate the possibility of using N_2 as a gas additive for the development of thermionic topping generators. In such generators, it is desirable to produce an enhanced Cs ionization in the interelectrode spacing. In the following section the experimental procedure used in the present study will first be described. This will be followed by a discussion on these experimental observations.

2. Experimental Measurements

The plasma under investigation is produced in a thermionic discharge tube which is completely demountable, constructed with 1.5" I.D. high vacuum components. The emitter is made of a swirling tungsten filament made of 0.040" wire and the collector is a 1" diameter stainless steel disk. The interelectrode spacing is set at 0.5". The system is outgassed at 350°C for 24 hours until the gas pressure of 10^{-7} torr is reached. High-grade nitrogen (impurity levels less than 0.5 parts per million) is introduced into the system through the stainless steel transfer line. Cesium vapor is then introduced into the system by connecting the cesium reservoir. The test section during the experiment is maintained at a temperature about 50°C higher than the reservoir temperature. The emitter is

heated to a temperature of 1180°K for all runs and it is determined by pyrametric measurement through an optically flat window.

The I-V characteristics with the cesium pressure fixed at 0.1 torr and the nitrogen pressure varying from 0 to 1 torr basically correspond to cesium thermionic discharges in which the nitrogen acts as an energy absorber which quenches the cesium radiation produced by the discharge.

As the nitrogen pressure continues to increase a new phenomenon is observed as indicated in Fig. [19]. Here, the discharge produced at high ignition voltages (>30 volt for our experiments) is similar to a pure nitrogen discharge. This is verified by spectroscopic measurements (Fig. [20]) which show predominantly the first and second positive bands of N_2. The intensity of the nitrogen radiation decreases monotomically from point 1 and approaches zero near point 3. However, the intensity of the cesium radiation first decreases as the applied voltage decreases; but from point 2 to point 3, cesium radiation increases, reaching a maximum at point 3 before plunging down to zero. Cesium radiation is also observed but at much lower intensity. After the ignition further increase in voltage does not lead to any noticeable increase in current. However, if one steadily reduces the voltage, a significant increase in current appears. This is demonstrated in Fig. [21] in which we see that when the voltage is reduced manually in steps, step-increases in current occur. The step-increase is very small initially; but increases drastically as the voltage is further reduced, reaching a maximum and then dropping sharply to zero. All step-increases in current take place after a delay of about a couple of seconds wherever the voltage is reduced. It appears for all cases that a minimum voltage is required to maintain the nitrogen discharge. Below this voltage, the current drops to zero and the discharge is extinguished.

The ignition voltages are directly proportional to the nitrogen pressure and are relatively independent of the cesium pressure because of the large values of the pressure ratio used in our experiments ($P_{N_2}/P_{Cs} \geq 40$). At high Cs pressure the increase in current is so pronounced that plasma oscillations occur.

3. Discussion of Results

The portion of the curves where the current shows a delayed increase after decreasing the voltage, is to the best of our knowledge, the first experimental observation of the ionization of cesium atoms by the vibrationally excited N_2 in an N_2-Cs discharge which can be described in the following reaction

$$N_2^* + Cs \rightarrow N_2 + Cs^+ + e + \Delta E \tag{39}$$

To answer the question as to the nature of the vibrationally excited states N_2^* in reaction (39), we propose that the vibrationally excited ground states N_2^* ($X\text{-}\Sigma g^+$) are responsible for the ionization of cesium by either a one-step process

$$N_2^* \ (\nu \geq 15) + Cs(6S) \rightarrow N_2(\nu = 0) + Cs^+ + e + \Delta E \tag{40}$$

or a two-step process

$$Cs(6S) + e \rightarrow Cs(6P) + e + \Delta E$$

$$N_2^*(\nu \geq 10) + Cs(6P) \rightarrow N_2(\nu = 0) + Cs^+ + e \tag{41}$$

Figure [22] shows the relative energy diagrams for N_2 and Cs. As was pointed out by Haug et al.[28], neither reaction (40) or (41) requires perfect energy matching between the vibrational transitions in N_2 and the ionization energies (E_{6S}-$F_{continuum}$= 3.89v, E_{6P}-$E_{continuum}$= 2.45v). The excess energy appears as the kinetic energy of the product ion or electron ΔE.

The generation of $N_2^*(X^1\Sigma g^+)$ with $\nu > 10$ can come from the decay of high electronically excited states[31]

$$N + N + M \rightarrow N_2^*(C^3\Pi u) \text{ or } N_2^*(B^3\Pi g)$$

$$N_2^*(C^3\Pi u) \xrightarrow[\text{2nd positive}]{10^{-7}S} N_2^*(B^3\Pi g) \xrightarrow[\text{1st positive}]{10^{-8}S} N_2^*(A^3\epsilon_u^+) \xrightarrow{1\,S} N_2^*(X^1\Sigma g^+) \qquad (42)$$

The first and second positive bands are observed (Fig. [20]), thus reaction (42) definitely contributes to the generation of the vibrationally excited $X^1\Sigma g^+$ in our experiment. Judging from the fact that the first and second positive bands disappear completely just before the current drops sharply to zero (Fig. [21]), the contribution from reactions (42) must play a dominating role in the production of the vibrationally excited $N_2^*(X^1\Sigma g^+)$. The contribution of direct electron excitation of $N_2^*(X^1\Sigma g^+)$ depends on the electron temperature. The cross section for such excitations has a sharp peak when the electron energy is around 2.1 ev[32]. Our average electron temperature is expected to be much less than 2.1ev. Thus, the contribution from direct electron impact production of vibrationally excited $N_2(X^1\Sigma g^+)$ is believed to be less important than reaction (42).

The deactivation rate of the vibrationally excited states $N_2^*(X^1\Sigma g^+)$ is governed by collisions with cesium atoms and the walls of the test section. Since the surface deactivation rate of $N_2^*(X^1\Sigma g^+)$ is very small[33], most of the

vibrationally excited states are used either to excite or to ionize Cs atoms. When the deactivation rate is larger than the rate of generation, reaction (39) reverses its direction and the current plunges rapidly to zero.

To assess the effect of lowering the applied voltage on the rate of generation of the vibrationally excited state, it is important to point out that the distribution if highly non-Boltzmann.[34]

The population distribution is a very sensitive function of gas kinetic temperature. A very small reduction in the kinetic temperature T can lead to drastic increases in the vibrational population in this region. Since the oven temperature is maintained at a temperature 50°C higher than the reservoir temperature, the kinetic temperature of N_2 must be larger than the oven temperature due to the collisions with hot electrons. As the voltage is reduced, T must be decreased accordingly which causes the observed increase in current. The observed delayed time (~ 2 sec) can be attributed to the time necessary for the vibration population distribution to relax from one temperature to another.

IV. PLASMA SUSTENANCE BY THE RESONANT APPLICATION OF MICROWAVE POWER.

1. Background

It has been known for some time in fusion plasma research that significant plasma densities can be achieved by the application of microwave power. Such plasma generation methods are quite attractive because they do not require the insertion of extraneous electrical leads as is required in the triode configuration of the thermionic converter. Moreover it allows for continuous power producing operation by the steady application of microwave power for plasma sustenance, in contrast to the pulsed modes of converter operation which can provide power output only during the off cycle of the applied ion generating pulse. Moreover employment of microwave energy for plasma support offers the possibility of utilizing resonant configurations with well established plasma conditions.[35] It is believed that such resonant application of microwave power to plasma support will prove an energetically inexpensive means of plasma sustenance.

Tonks[36,37,38] and others in 1931 noticed that when an electric field was applied perpendicular to the axis of a cyclindrical plasma, resonances occurred. Later Dattner[47] experimentally determined that these resonances were dipolar and they are due to oscillations of charge.

There are three kinds of RF discharge in a plasma depending on the background pressure and driving frequency.[39,40,41] These RF discharges are multipacting plasma, resonantly sustained plasma or a diffusion controlled plasma. At pressure of approximately 0.1 torr, when collisions are dominant in the plasma, we have a diffusion controlled discharge. At a lower pressure of about 10^{-3} torr, the RF plasma has the characteristic of a plasmoid which is characterized by sharp luminous boundaries and the fact that it can be maintained by a relatively low power driving source, and is called a

resonantly sustained discharge. For very low pressure, approximately 10^{-5} torr, the plasma is a multipacting discharge.[42-50]

Taillet[51] observed that in resonantly sustained plasma, the electric field in the plasma is much larger than the field in the absence of the plasma. The response of an ionized gas to very high frequency electric waves has been the subject of many investigations. Oscillations in the neighborhood of 10^9 hertz was originally found by Penning and was further investigated by Tonks and Langmuir using the low pressure mercury arc. They found that the observed high frequency oscillations corresponded to the plasma electron oscillations as shown by the following equation.

$$f_p = (N_{res}\, e^2/\pi m_e)^{1/2} = 8980 N_{res}^{1/2} \qquad (43)$$

where f_p is the oscillation frequency, m_e is the electron mass, n_p is the plasma density.

An important property of plasma oscillation is that its half period represents a response time in which the plasma reacts to an externally applied electric field. Thus if a field of frequency f_m is applied to a plasma where the plasma electron oscillation frequency f_p is larger than f_m, electrons will move so as to oppose the applied field by setting up a field between them and the stationary ions. The shielding movement tends to reduce the net field in the interior of the plasma to zero. However, if $f_m > f_p$, the electrons cannot respond rapidly enough to cancel the externally applied field, and consequently the field penetrates the plasma. Thus for $f_p/f_m < 1$, the field penetrates the plasma, i.e. the plasma is transparent, whereas for $f_p/f_m > 1$, the electron motion shields the interior and the plasma is opaque to the externally applied fields. At $f_p = f_m$, a critical relation holds

between the applied microwave field and the plasma resulting in absorption of most of the applied microwave power. The state which corresponds to a plasma density of N_{res} (cut-off or critical density) is dynamically unstable and the plasma cannot be resonantly sustained at this value at a steady state.

With enough incident microwave power and appropriate tuning of the cavity, the critical density of the plasma can be increased by about a factor of ten.[48,49,57] The reason for being able to sustain the plasma above the critical density can be explained by Fig. [23] in which we plot power in relative units versus the plasma density. A family of curves is presented corresponding to different values of incident power. Also shown in Fig. [23] is a power loss line which represents the power lost in the plasma due to inelastic ionization, excitation,and diffusion losses to the walls. For an incident power of P_2, there are two points where the power absorbed by the plasma is equal to the power lost by the plasma. In resonantly sustained plasma, the power absorbed is indeed equal to the power loss in the plasma. Thus with steady operation of incident power P_2, there are two equilibrium states A and B as shown in Fig.[23]. State B is in a stable equilibrium while state A is an unstable equilibrium because at point B, any reduction in the plasma density has the tendency to increase the power absorbed by the plasma, which in turn causes an increase in ionization, hence increases the plasma density. On the other hand an increase in plasma density at point B has the tendency to reduce the power absorbed by the plasma, which in turn causes a reduction in the plasma density. Hence state B is in stable equilibrium.

For the same reason, point A is unstable because an increase of plasma density will increase the absorbed power, which will eventually bring the plasma to point B. But a decrease of the plasma density at point A will

extinguish the plasma. So point A is unstable. The resonantly sustained plasma density must be above N_{res} where the plasma begins to be opaque to the applied field. That is why it is sometimes difficult to resonantly sustain a dense plasma.

The interaction of microwave power with plasmas is a complex phenomenon which strongly depends on the geometry of the apparatus and the frequency and power of the applied microwave field.[52-59]

2. Experimental Setup

a. The Microwave Cavity

A reentrant type cavity is used as the resonant microwave cavity because of its easily accessible size in our frequency range, its tuning capability and the adjustability of the strength of the electric field in the gap inside the cavity. The reentrant cavity is composed of an inner and an outer conductor. A sliding short is installed between the conductors to adjust the length of the cavity. A hole of 1-7/8" in diameter is made on one of the end walls of the cavity so that the glass tube housing the converter can be inserted inside the inner hollow conductor tube. The location of the interelectrode space is the same as the gap between the inner conductor and the end plate as shown in Fig. [24].

By moving in and out the inner conductor, the gap distance can be adjusted contributing to better tuning. The inside diameter of the outer conductor and the outside diameter of the inner conductor are 3" and 1-7/8" respectively. The characteristic impedance of the cavity is determined by Z_o, where

$$Z_o = 138\sqrt{\mu_r/\varepsilon_r}\,\log b/a \qquad (44)$$

and μ_r is the relative permeability and ϵ_r is the relative dielectric constant. In this case, both μ_r and ϵ_r are both equal to 1, while 2a and 2b are the O.D. of the inner conductor and the I.D. of the outer conductor which are equal to 1-7/8" and 3" respectively. By Eq. [42] the characteristic impedance of this cavity Z_o is found to be 30 Ω. The approximate cutoff wavelength for the first higher order mode wave, besides the principal TEM mode wave, which can exist in the cavity is given by

$$\lambda c = \pi(a+b) = 19.5 \text{ cm.} \tag{45}$$

So if the applied frequency is below the cutoff frequency, only the principal TEM waves will exist inside the cavity. For TEM waves,

$$E_z = H_z = 0 \tag{46}$$

and for the wave propagation in the +Z direction

$$E_x/H_y = -E_y/H_x = Z_o \tag{47}$$

whereas for propagation in the -Z direction

$$E_x/H_y = -E_y/H_x = -Z_o \tag{48}$$

At low frequencies, the resonant circuit is represented by an inductor and a capacitor combination either in series or in parallel. Resonance occurs when there are equal average amounts of electric and magnetic fields around the inductor and the electric field between the capacitor plates. At microwave frequencies, the LC circuit is replaced by a closed conducting enclosure or cavity. The electric and magnetic energy are stored in the field within the cavity at an infinite number of discrete frequencies, the

resonant frequencies. There are equal average amounts of electric and magnetic energy stored in the cavity volume. Thus, in calculating the resonant frequency of the cavity, the combined capacitive susceptance due to the proximity of the metallic wall and that due to energy storage in the inner and outer conductors, and also the gap capacitance should be taken into account. On the other hand, the susceptance must be equal in magnitude to the short circuited inductive susceptance offered by the transmission line to the cavity.

The combined capacitance of the cavity, C, is the sum of the gap capacitance, C_o, and the equivalent capacitance of the cavity, C_1. The equivalent capacitance of the gap is obtained by

$$C_o = \varepsilon_o \pi (a^2 - a'^2)/d + \varepsilon_o \pi a'^2 \gamma/d, \quad (a' = a - 1/2'') \tag{49}$$

where γ is a capacitance reduction factor for the open hole on the end plate as compared to the geometry without the hole. The equivalent capacitance of the cavity is given by

$$C_1 = 4 \varepsilon_o a \ln \frac{2.718\sqrt{(b-a)^2 + h^2}}{2d} \tag{50}$$

So the total combined capacitance is

$$C = \varepsilon_o \pi (a^2 - a'^2(1-\gamma))/d + 4\varepsilon_o a \ln \frac{2.718\sqrt{(b-a)^2 + h^2}}{2d} \tag{51}$$

The inductance of the cavity is given by L, where

$$L = \frac{\mu_o h}{2\pi} \ln b/a \tag{52}$$

As a result, the resonant frequency can be computed by equating the total reactance of the cavity to zero and the resonant frequency is

$$f_{res} = \frac{1}{2\pi\sqrt{LC}} \tag{53}$$

At each fixed gap distance, the resonant frequencies of the cavity in the range of 1-2 GHz can be measured experimentally by adjusting the cavity length. We have also investigated the resonant frequencies of the cavity with different gap distances, starting from 0.05" to 0.45" at intervals of 0.05". The measurements agree very well with the theoretical predictions of equations 49, 50 and 51.

b. The Vacuum System

The demountable cesium thermionic diode and the vacuum components used in this experiment are shown in Fig. [24]. The cesium thermionic diode is composed of one inch diameter stainless steel disc, the collector, separated by one inch from a swirl tungsten emitter inside a pyrex glass tube housing. The glass tube is connected to a cesium reservoir. The glass tube is connected to a bakable valve through a tee. The bakable valve connects to the pumping system which consists of a mechanical pump, a diffusion pump, an ion pump, and a pressure gauge. The system is pumped down to a pressure of 10 microns by the mechanical pump, then down to a pressure of 10^{-4} torr by the diffusion pump. An ion pump is used for the final stage of pumping. Both the diode and the cesium reservoir are baked at 250°C and the tungsten filament is outgassed for more than 24 hours while pumping until a residual gas pressure of the order of 10^{-8} torr is reached. Then the bakable valve is closed and the cesium reservoir connected. The microwave cavity and the diode are heated in an oven which is made of two double walled two inche thick asbestos insulating blocks. The cesium reservoir is also

heated in an oven located just below the oven of the converter diode. Temperature controllers are used to keep the ovens at the desired temperature. Chromel-Alumel thermocouples are placed at various positions for temperature measurements.

c. The Microwave Setup

A sketch of the microwave system is shown in Figs. [25] and [26]. The microwave signal is generated by a 1 - 2 GHz sweep oscillator. This oscillator produces a quite stable frequency signal easily adjustable in the sweep range at a power of about 20 mw. This microwave signal is amplified by a travelling wave tube amplifier (TWT). The amplified output power ranges from 0 - 20 Watts.

A circulator is installed between the TWT and the rest of the system to protect the TWT's output helix from damage by the reflected microwave power. The third port of the circulator is connected to a matched load which can absorb up to 150 W of reflected power.

A pair of directional couplers are used to measure the incident and reflected power. The reflected signal power level is measured by a power meter and is displayed on an oscilloscope. It serves to indicate the resonance condition. A section of coaxial slotted line is used to measure the input impedance of the cavity. A reference plane is established on the slotted line for a short circuit load. The phase of the cavity impedance is measured by the difference of the null and the reference plane in the SWR pattern which also serves as an indication for a resonant condition of the plasma - cavity system.

After going through the tuner, which adjusts the matching between the microwave source and the cavity, the signal is sent into the cavity through a 0.141" O.D. semi-rigid high temperature (250°C) low attenuation coaxial cable to excite the magnetic field inside the cavity. A loop configuration excites the magnetic field at the TEM wave. Furthermore, the loop is placed in a location where the concentration of magnetic field lines threading the loop is highest, which is near the shorting plate since the magnetic fields are directly proportional to rf current in the walls and the strongest current lines in a transmission line is at the short.

d. The Electrical Circuit

The electrical circuit configurations used to discharge the plasma are shown in Fig. [26]. Both D.C. and rectified A.C. signals are used to ignite or discharge the cesium plasma. A variable non-inductive resistor is connected in series with the power supply as a ballast resistor to limit the diode current.

D.C. power supply of 0-60 V and 0-15 amp. is used to discharge the plasma so that its I-V characteristics can be plotted on a X-Y recorder. Besides using D.C., a 220 V A.C. power supply is stepped down to 120 V A.C. through an isolation transformer to discharge the plasma. With A.C. discharge, the I-V characteristics can be displayed on an oscilloscope. In the A.C. discharge circuit, a rectifying diode is used in series with the A.C. power supply so that most of the negative voltage cycle is rectified.

3. The Experimental Results

The performance of a thermionic converter or diode can be improved substantially by lowering the plasma arc drop. The quality of the performance of a converter diode can be deduced from its I-V characteristic curve. The

transition point (the "knee") of an I-V characteristic curve of a thermionic diode is also the point of maximum performance of the diode at a certain emitter temperature. The arc drop voltage of the diode measured at the transition is the potential drop across the interelectrode space required to produce just enough ions to balance the plasma losses. In order to maintain the plasma density level, the electron temperature of the plasma must be sufficiently high to produce ions as rapidly as they are lost by the diffusion to the electrodes and by volume recombination. So the reduction of the arc drop voltage of the diode when the plasma is sustained by microwave power can be measured by the shift of the output voltage at the transition point when we compare the I-V curves with or without applied microwave power.

The experiments were carried out under the following conditions:

The cesium reservoir temperature ranges from 150°C to 200°C which corresponds to a relatively low cesium pressure from 0.01 to 0.1 torr.

The emitter temperature is about —1300°K, which implies an emitter current density of the order of or less than 1 amp/cm^2. The microwave signal at the output of the TWT amplifier ranges in power between o and 20 watts at a rather low microwave frequency region, i.e., 1-2 GHz.

It is immediately evident that the thermionic diode is not operated at the optimum performance region or in the positive power quadrant.

We measured the I-V characteristics on the oscilloscope or the X-Y recorder D.C. and A.C. discharges of the cesium plasma in the converter diode. Emitter temperature at T_E=1025°K and T_R=423°K, the D.C.power supply ignites the cesium plasma at 3.6 V as shown in Fig. [27]. In the same

figure, with additional microwave heating, the plasma can be ignited at 1.8 V. At the same time, the diode voltage at the transition point is decreased by 1 V. At the same cesium pressure and T_E at 1150°K, the I-V curve with and without microwave is shown in Fig. [28]. Three typical I-V characteristic curves measured with and without applied microwave power are shown in figures [29], [30] and [31].

It is found that with microwave heating, the I-V curve of the diode shifts from the negative power quadrant into positive power quadrant. The ignition voltage of the plasma and the arc drop are shown in Table 1 with T_R at 473°K and T_E from 935°K to 1300°K.

An interesting method of evaluating the performance of the thermionic converter is provided by Lam who summarizes the plasma arc drop in terms of a single parameter. This parameter is the normalized plasma resistance R which, according to Lam's theory, has a minimum value of 4 or 5 as long as there exists an emitter motive peak.[3]

The converter arc drop is related to the normalized plasma resistance R by the equation

$$\dot{\gamma} = \frac{1}{1 + \exp \frac{\dot{\gamma} R - V_d}{\tau}} \qquad (54)$$

If the emitter motive peak is suppressed, $J_E = J_R$. Without external heating, R cannot be determined experimentally because of the simultaneous changing of J_E and τ below the transition point of the I-V curve, where the emitter motive exists. This can be explained by Fig. [32] which shows the potential diagram between the electrodes at four points on the I-V curve. At point 1, the plasma is unignited and the current density is very low. At point 2, the plasma is in negative resistance region

where the plasma is not completely ignited and the emitter motive peak still exists. At either point 1 or 2, the emitter net current density J_E cannot be determined because J_E is a function of τ and $\Delta\hat{X}$ which are both varying during the transition from point 1 to point 3. It is only when point 3 is reached which is the transition point or the "knee" of the I-V curve, that the plasma is completely ignited and the emitter motive peak disappears, and $J_E = J_R$ becomes a constant. At point 4 the plasma is in a saturation region. In Fig. [35] shows that the I-V curve and the potential diagrams of the converter diode with microwave heating. The "knee" of the I-V curve disappears and the plasma is sustained at high current density when both A.C. and microwave power are applied while at low current density the plasma is sustained only by microwave power. Because of the disappearance of the emitter motive peak, there is no sudden jump of diode current and $J_R = J_E$ is constant can be assumed. As a result, Eq. (59) can be used to relate $j = (J/J_R)$ and V_d at a certain value of R and τ. The normalized I-V characteristics of the diode with external heating are plotted as j versus V_d. The best fit of these experimental I-V curves with respect to the parameters R and τ into the curves provided by Lam's theory can provide us with the best values of Rand τ. A family of Lam's plot at $\tau = 5$ and a family of I-V curves with different microwave input power are shown in Fig. [34] and Fig. [35] respectively. The normalized plasma resistance, R, and normalized electron temperature, τ, are tabulated in Table 3 with different emitter temperatures and at $T_R = 473$ K. It is shown that at $T_E = 935^{\circ}$K and n_R/n_p=0.45, R is equal to 10 and the best value of τ is also 10. As the ratio of n_R/n_p increases to 13.4 at T_E=1055°K, R increases to 25 and τ decreases to 5 which is almost constant until

$T_R = 473^{\circ}K$

T_E(°K)	R	$N_{res}{}_{10}{}^{10}$	$n_R{}_{10}{}^{10}$	n_R/N_{res}	τ
935	10	2.7	1.22	0.45	10
965	10	2.7	6.30	2.33	8
995	15	2.7	18.00	6.67	7
1025	20	2.7	32.40	12.00	5
1055	25	2.7	36.20	13.40	5
1085	25	2.7	33.90	12.56	5
1115	25	2.7	31.70	11.74	5
1180	25	2.7	26.3	9.7	5
1210	30	2.7	20.29	7.51	5
1240	30	2.7	19.49	7.22	4
1270	50	2.7	19.20	7.15	3
1300	50	2.7	19.00	7.04	3

TABLE 3

PLASMA PARAMETERS

T_E=1180°K. From T_E=1210°K to 1300°K, R is greater than 30 and τ is less than 4 even though the ratio n_r/n_p decreases. The table shows that as τ decreases, the plasma resistance increases, which is an indication that in order to reduce plasma resistance or arc drop, higher electron temperature is required.

Finally, an extended plot of the I-V characteristics of the diode with and without microwave heating is shown in Fig. [33] at T_E=935° K to demonstrate the improved performance of the diode with external microwave heating.

4. Discussion

It is believed that microwave power shows great promise as a source of energy to sustain the cesium plasma in a thermionic converter. At the lower operating temperature of 1400°K the emitter in the advanced converter can no longer supply sufficient ionization levels. An external source of ion generation is needed which does not interfere with the emitter and collector electrodes. Externally supplied microwave power may prove to be the best agent to perform the task. It is attractive in many ways. There is considerable flexibility in that we may adjust both the power and the frequency of the applied microwave power to achieve the desired plasma condition. In supplying microwave energy we do not interfere with the interelectrode spacing by the insertion of extraneous electrodes. We may operate in the continuous mode in contrast to pulsed systems which would not be available for power generation during the pulse on condition. Furthermore the geometrical dimension of the emitter collector distance envisioned is the correct order of magnitude to allow support of the plasma by microwave fields in a resonant mode. The energy expenditure of microwave power at a resonant plasma system

is expected to be smaller in comparison to alternative energy sources. We hope to proceed to an accurate analysis of the microwave power consumption needed to support a required level of plasma density in the near future. The technology of microwave power generation and transmission is well advanced with many off-the-shelf items available to utilize in our systems.

We have seen in our analysis of the experimental data a trend that tends to support Lam's theoretical treatment clearly. More work is needed in this area to provide a comprehensive understanding of the plasma in the thermionic converter. The simplicity of a microwave supported plasma in an optimum diode could allow for easily interpreted data from which conclusions could be drawn about the proper plasma density level for highest overall efficiency. We thus believe that microwave power sustenance of a thermionic plasma in a resonant configuration is indeed a very attractive choice.

REFERENCES

1. G. N. Hatsopoulos, Proc. Thermionic Specialist Conf., San Diego, pp. 1, (1965).

2. W. L. Nighan, J. Appl. Phys., 39, 223, (1968).

3. H. S. Lam, U. S. Energy Research and Development Administration Report COO-2533-3, (1976).

4. S. Byron, P. I. Bortz and G. Russell, Proc. of Fourth Symposium on Engr. Aspect of Magnetohydrodynamics, Univ. Calif., April 10-11, 1963.

5. D. R. Bates, A. E. Kingston and R. W. P. McWhirter, Proc. Roy. Soc. (London), Ser. A, 267, 297 (1962).

6. S. Byron, R. Stabler and P. Bortz, Phys. Rev, Letters, 8, 376 (1962).

7. N. D'Angelo, Phys. Rev., 121, 505 (1961).

8. M. Gryzinski, Phys. Rev., 115, 374 (1959).

9. D. W. Norcross and P. M. Stone, J. Quant. Spect. Rad. Transfer, 8, 665 (1968).

10. J. V. Dugan, NASA Report No. TDE-2004 (1964).

11. B. Sayer, J. C. Jeannet, J. Lozingot and J. Berlande, Phys. Rev., A8, 3012 (1973).

12. M. Alesdovskii, Soviet Physics JETP, 17, 570 (1963).

13. L. C. Johnson and E. Hinnov, Phys. Rev., 187, 143 (1969).

14. J. B. Taylor and I. Lanmuir, Phys. Rev. 51, 753 (1937).

15. H. Shelton, R. F. Wuerker and J. M. Sellen, ARS Meeting, San Diego, 1959, Paper No. 882-59.

16. L. L. Marino, A. C. H. Smith and E. Caplinger, Phys. Rev., 128,2243 (1962).

17. L. Agnew and C. Summer, Proc. of VII International Conference on Phenomena in Ionized Gases, Belgrade, Vol. II, pp. 574, 1965.

18. H. Griem, M. Baranger, A. C. Kolb and G. Oertel, Phys. Rev., 125, 177 (1962).

19. H. Griem, Phys. Rev., 128, 515 (1962).

20. P. Stone and L. Agnew, Phys. Rev., 127, 1157 (1962).

REFERENCES (Cont.)

21. M. Baranger, Phys. Rev., 112, 855 (1958).

22. R. Donohue and R. Majkowski, J. Appl. Phys., 33, 3 (1962).

23. H. Lomax and H. E. Bailey, NASA Technical Note, TN D-4109 (1967).

24. W. L. Nigham, Appl. Phys. Lett., Vol 20, No. 2, 96 (1972).

25. G. Black, H. Wise, S. Schechter and R. L. Sharpless, J. Chem. Phys., Vol. 60, No. 9, 3526 (1974).

26. C. N. Manikopoulos, Tao Chang, D. T. Shaw, Proceedings of Thermionic Power Generation Conference, Eindhoven, The Netherlands, 1975.

27. A. C. Mitchell and N. W. Zemansky, "Resonance Radiation and Excited Atoms" (Cambridge Univ. Press, London, 1961) p. 189.

28. D. R. Jenkins, Proc. Roy. Soc. (London) A, 303, 453 (1968).

29. R. Haug, G. Rappenecker and C. Schmidt, Chem. Phys., 5, 255 (1974).

30. H. F. Krause, J. Frick and W. L. Fite, Chem. Phys., 56, 4563 (1972).

31. C. M. Sadowski, H. I. Shiff and G. K. Chow, J. Photochem, 1, 23 (1972).

32. G. J. Schulz, Phys. Rev., 125, 229 (1962).

33. G. Black. H. Wise, S. Schechter and R. Sharpless, Chem. Phys., 60, 3626 (1974).

34. G. E. Caledonia and R. E. Center, Chem. Phys., 55, 552 (1971).

35. R. M. Fredericks, I. A. Asmussen, Jr., J. Appl. Phys., 42, No. 9, 3647 (1971).

36. L. Tonks, Phys. Rev., Vol. 37, pp. 1458-1483; June, 1931.

37. E.Z. Stowell, Phys. Rev., Vol. 37, pp. 1452-1457; June, 1931.

38. L. Tonks, Phys. Rev., Vol. 38, pp. 1219-1223; Sept., 1931.

39. C.C. Wang, J. Appl. Phys., Vol. 16, pp. 351-366; June, 1945.

40. D. J. Rose and S. C. Browns, J. Appl. Phys., Vol. 23, pp. 1028-1034; Sept., 1952.

41. K. Fujisawa, IRE Transactions on Microwave Theory and Techniques, pp. 344-358; Oct. 1958.

REFERENCES (Cont.)

42. A. Dattner, Phys. Rev. Letters, Vol. 10, pp. 205-209; March, 1963.

43. J. V. Parker, J. C. Nickel and R. W. Gould, Phys. of Fluids, Vol. 7, pp. 1489-1500; Sept.,1964.

44. R. L. Ramey and T. S. Lewis, J. Appl. Phys., Vol. 39, pp. 1747-1751; Feb., 1969.

45. P. Leprince, Phys. Letters, Vol. 26A, pp. 431-432, March, 1968.

46. A. W. Vlachos and C. S. Hsuan, J. App. Phys., Vol. 39, pp. 5009-5016; Oct.,1968.

47. R. B. Hall, J. App. Phys., vol. 40, pp. 30-36; Jan.,1969.

48. A. M. Messiaen and P. E. Vandenples, App. Phys. Letters, Vol. 15, pp. 30-33; July, 1969.

49. S. L. Halverson and A. J. Hatch, Appl. Phys. Letters, Vol. 14, pp. 79-81; Jan.,1969.

50. G. Kent and R. Heintz, J. App. Phys., Vol. 39, pp. 1741-1746; Feb.,1968.

51. J. Taillet, Am. J. of Phys., Vol. 37, pp. 423-441; April, 1969.

52. A.M. Messiaen and P. E. Vandenplas, Phys. of Fluids, Vol. 12, pp. 2406-2417; Nov.,1969.

53. G. Lisitano, M. Fontanesi and E. Sindoni, App. Phys. Letters, Vol. 16, pp. 122-124; Feb.,1970.

54. B. Agdur and B. Enander, J. App. Phys., Vol. 33, pp. 575-581, Feb.,1962.

55. G. Kent and D. Sinnott, J. App. Phys., Vol. 42, pp. 2847-2851; June 1971.

56. W. P. Allis, S. C. Browns and E. Everhard, Phys. Rev., Vol. 84, pp. 519-522; Nov.,1951.

57. R. Fredericks and J. Asmussen, IEEE Proceedings Letters, pp.315-317; Feb.,1971.

58. E. River and M. V. Lapisardi, IEEE Transactions on Microwave Theory and Techniques, Vol. 19, pp. 309-314; March,1971.

59. D. T. Shaw, C. H. Lee and C. N. Manikopoulos, 11th IECEC, pp. 1625-1627, 1976.

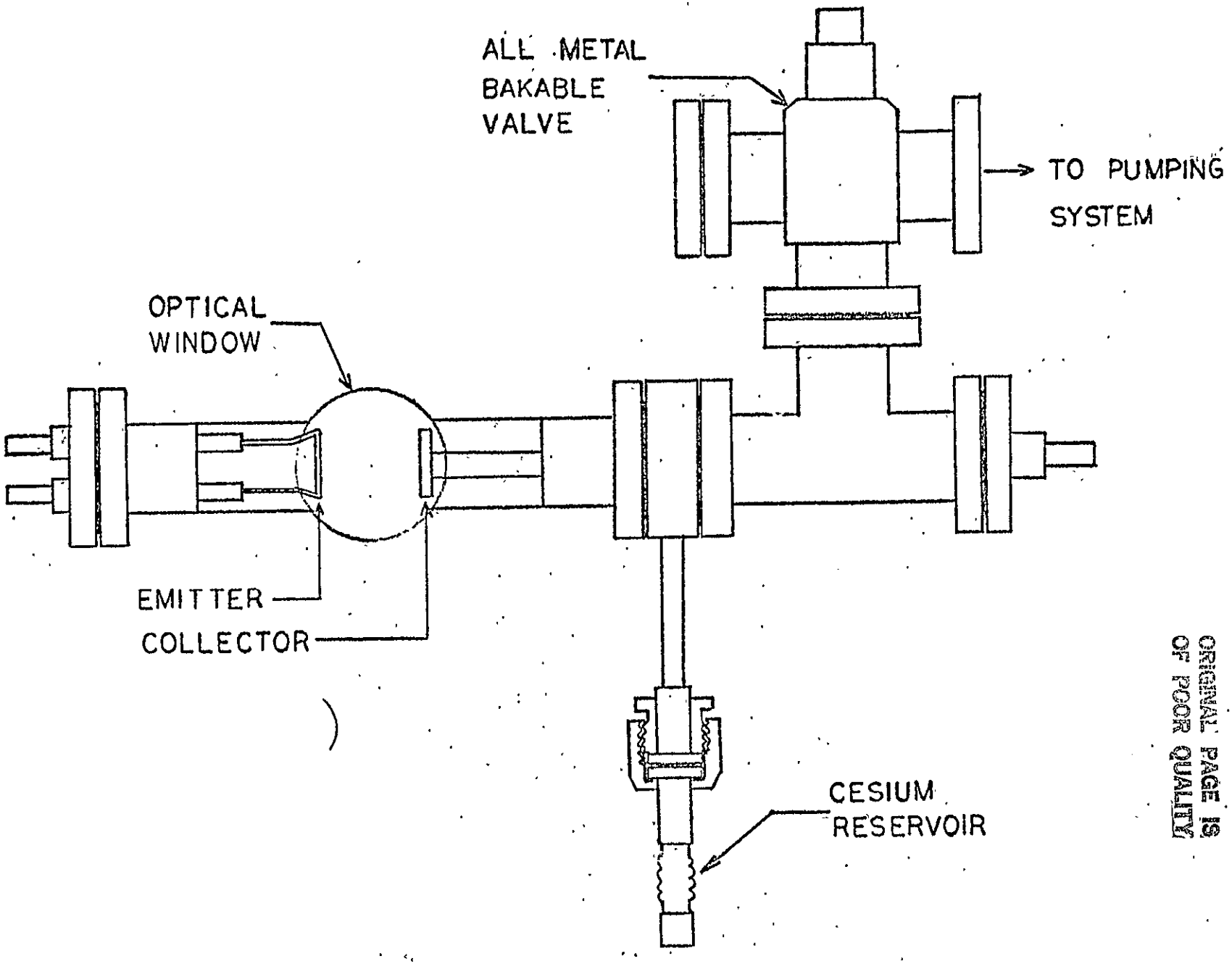

Fig. 1 Schematic Drawing of the Thermionic Diode

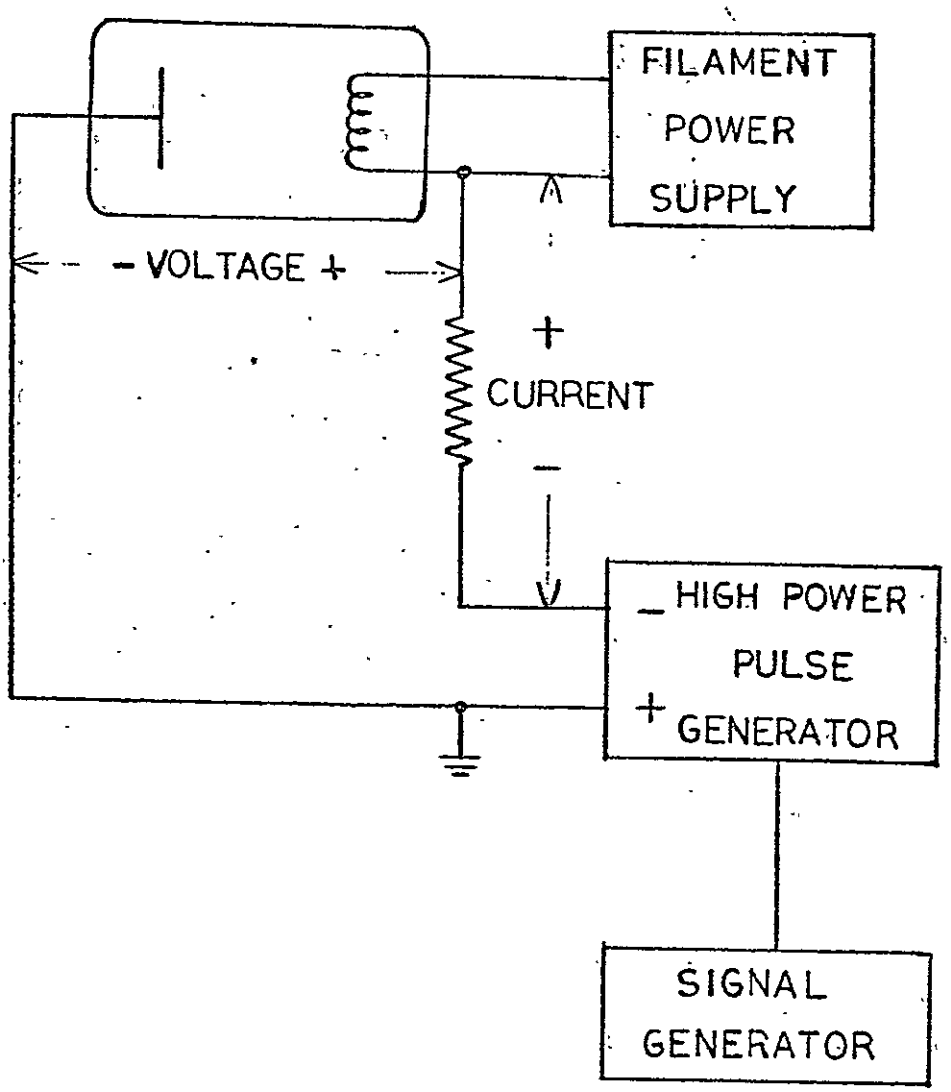

Fig. 2 Electrical Circuit for Pulsing the Diode

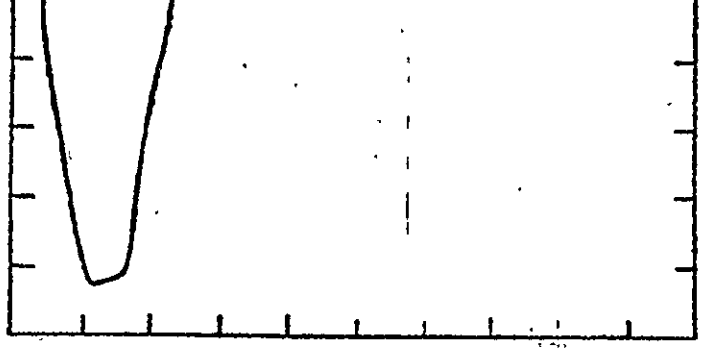

Vertical Scale : 10 v/div.

Horizontal Scale : 2 μs/div.

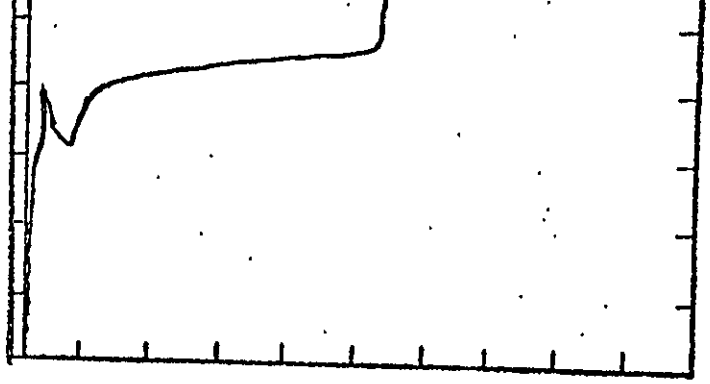

Vertical Scale : 20 v/div.

Horizontal Scale : 2 μs/div.

(b)

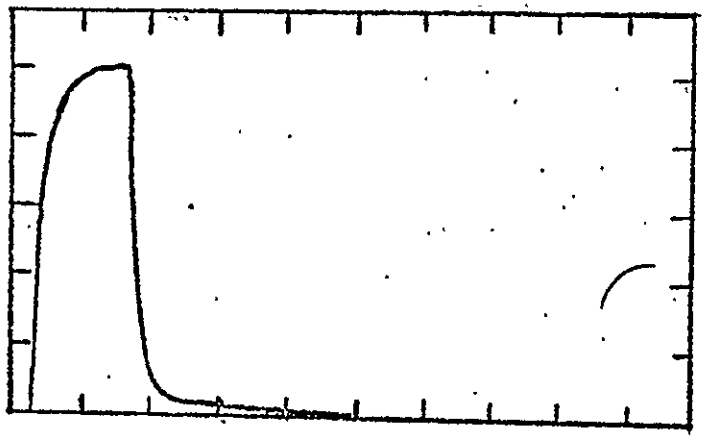

Vertical Scale : 80 ma/div.

Horizontal Scale : 2 μs/div.

Diode Characteristic for a 3 μs pulse:

(a) Converter Diode Voltage vs Time

(b) Converter Diode Current vs Time

(b)

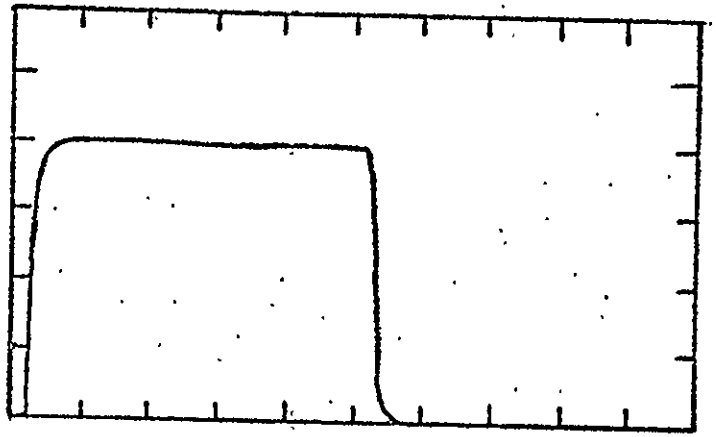

Vertical Scale : 0.4 a/div.

Horizontal Scale : 2 μs/div.

Diode Characteristic for a 10 μs pulse

(a) Converter Diode Voltage vs Time

(b) Converter Diode Current vs Time

Fig. 3.

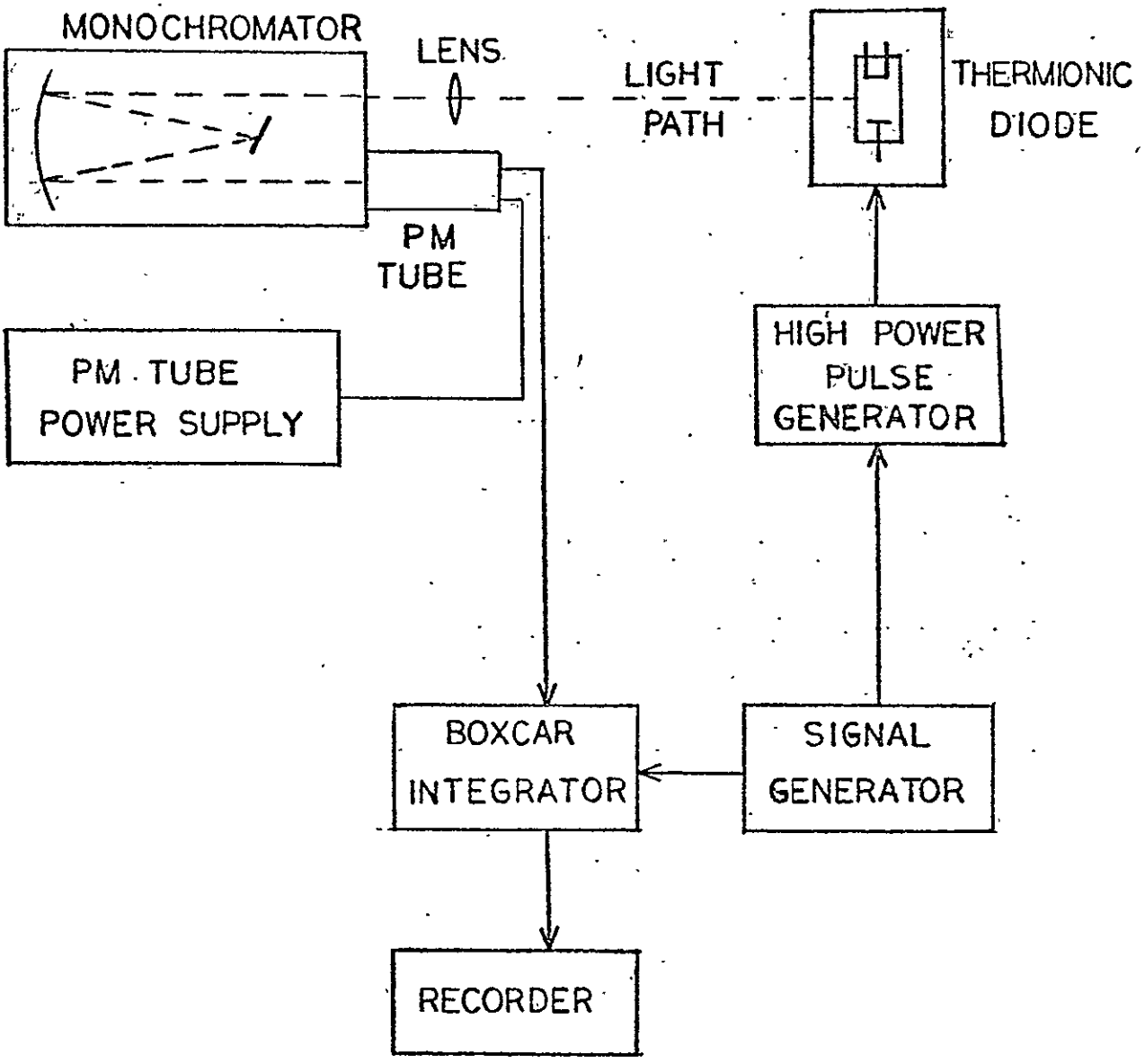

Fig. 4 Schematic Drawing of the Spectroscopic Apparatus

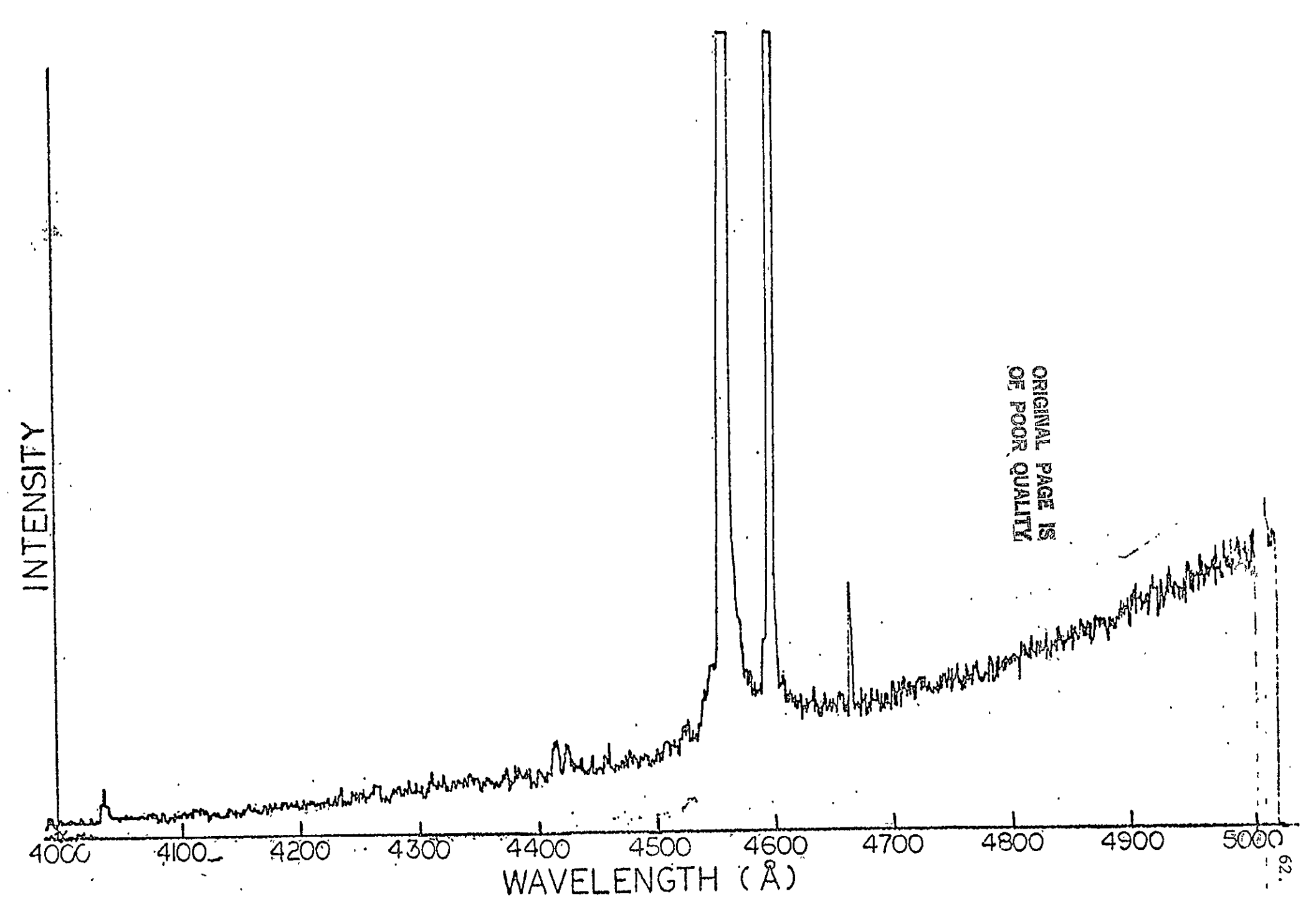

Fig. 5 Typical Experimental Data of the Continuum Spectrum

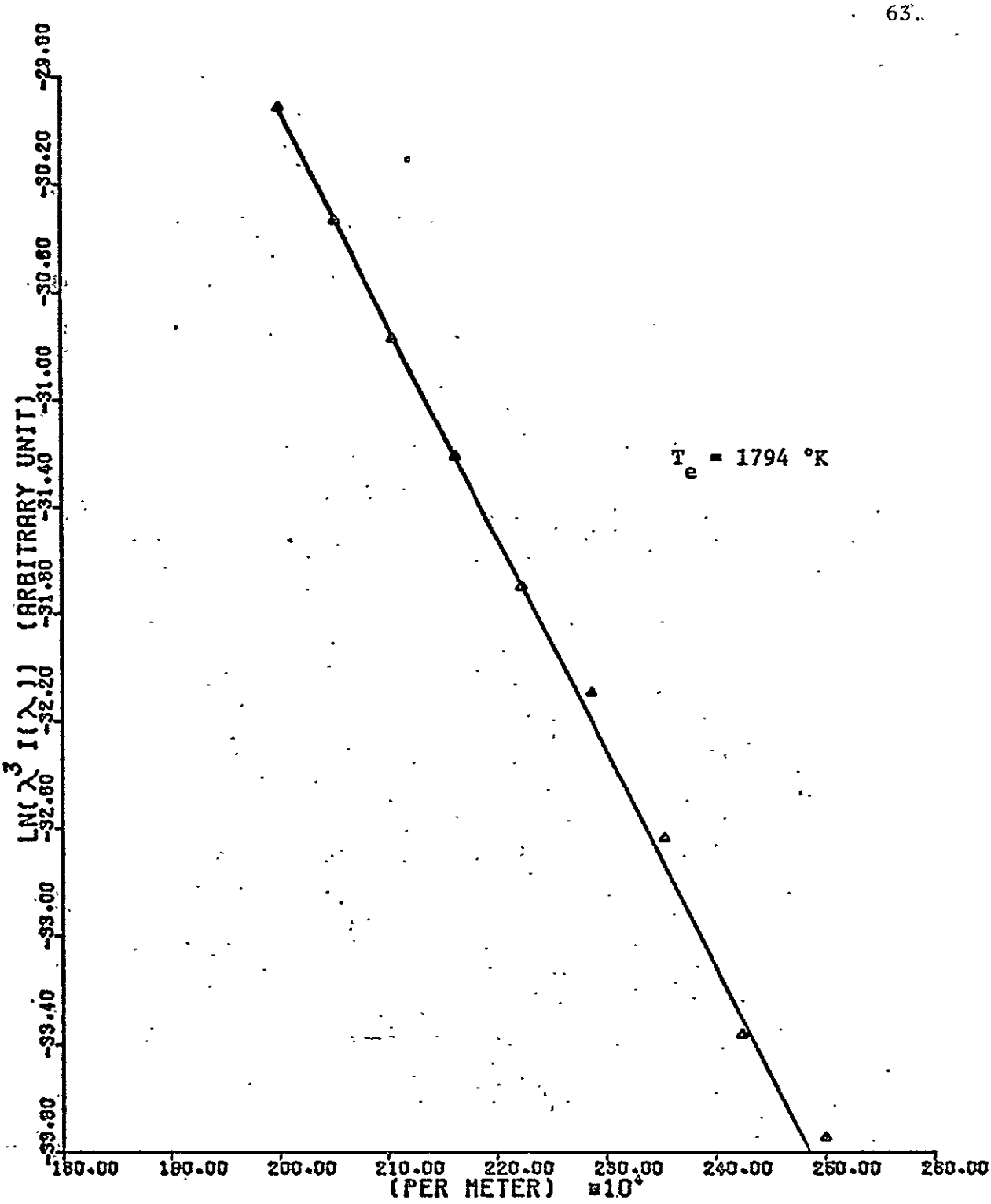

Fig. 6 Data Reduction of Fig. 5 for the Determination of Free Electron Temperature

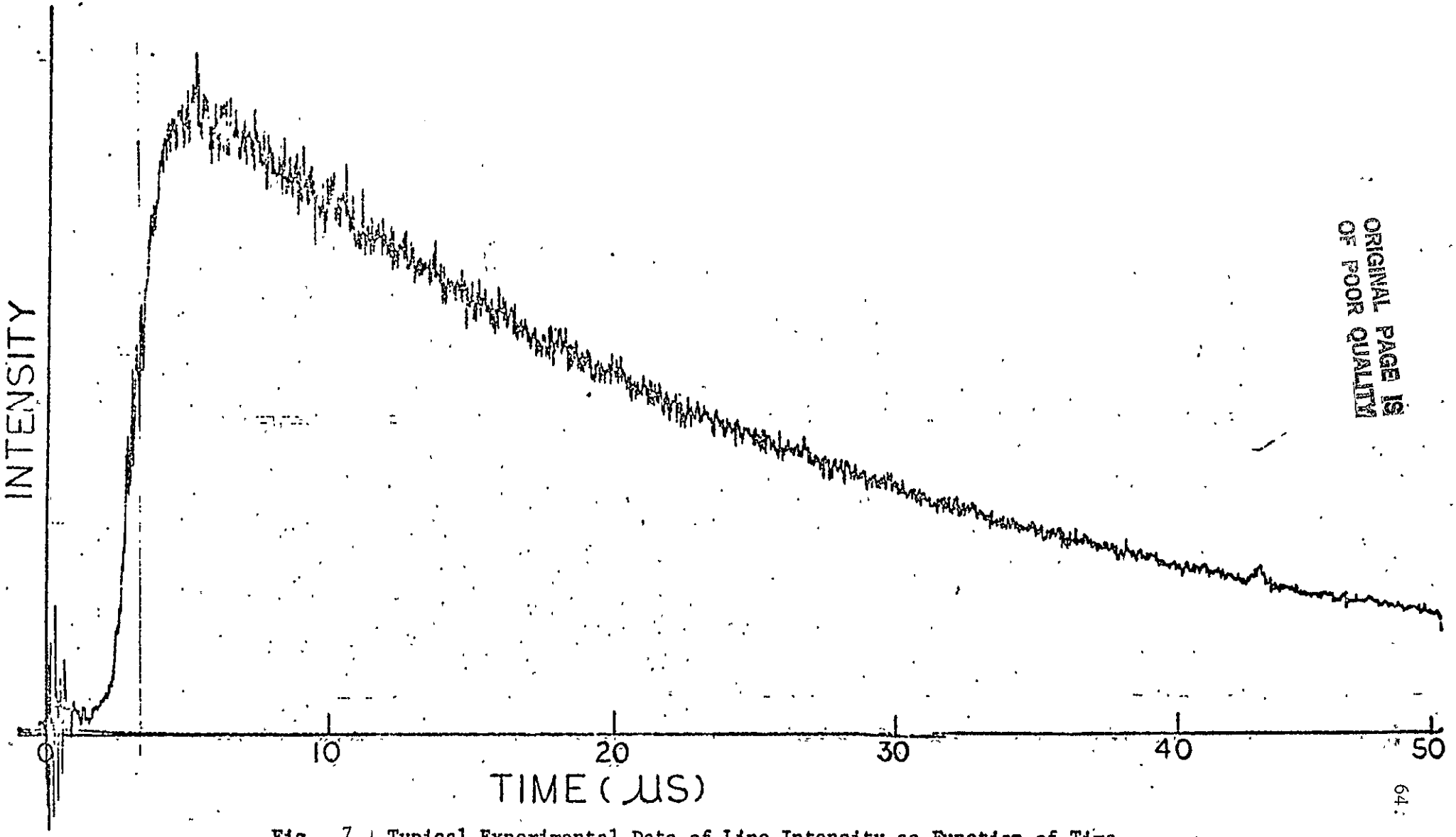

Fig. 7 Typical Experimental Data of Line Intensity as Function of Time

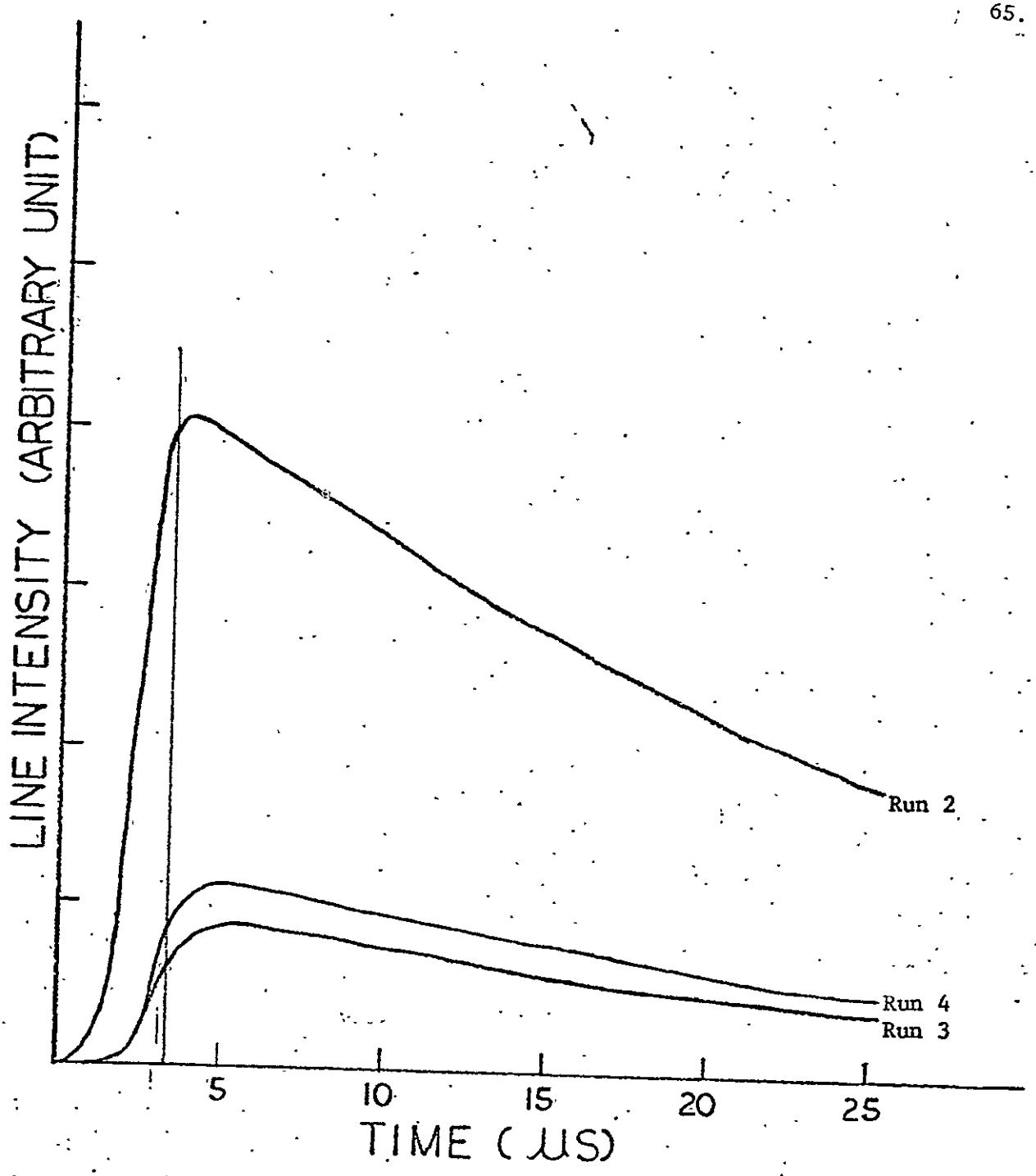

Fig. 8 Variation of the 7D - 6P Line Radiation for Plasmas Excited by 3 μs pulse.

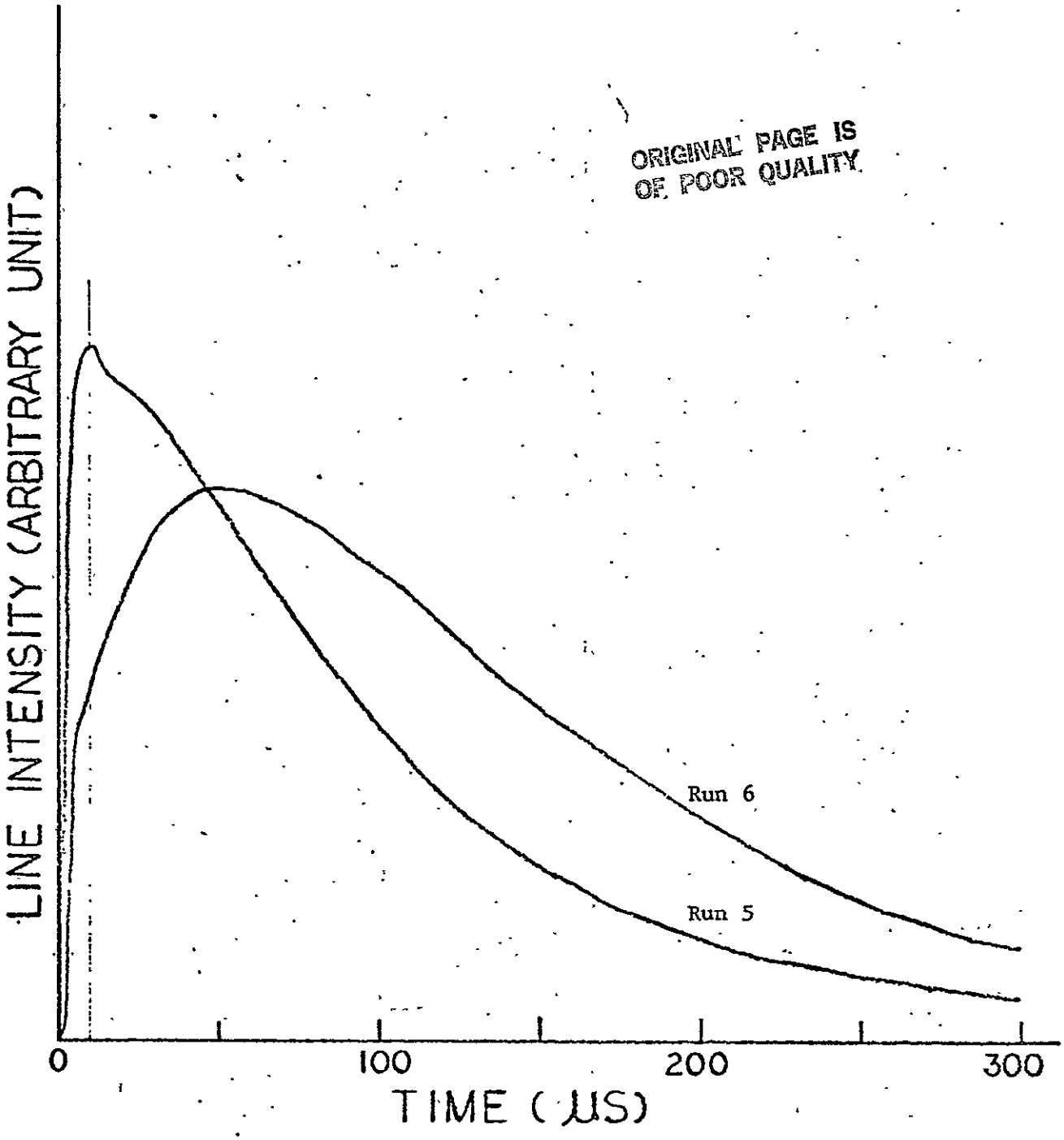

Fig. 9 Variation of the 7D - 6P Line Radiation for Plasmas Excited by 10 μs pulse

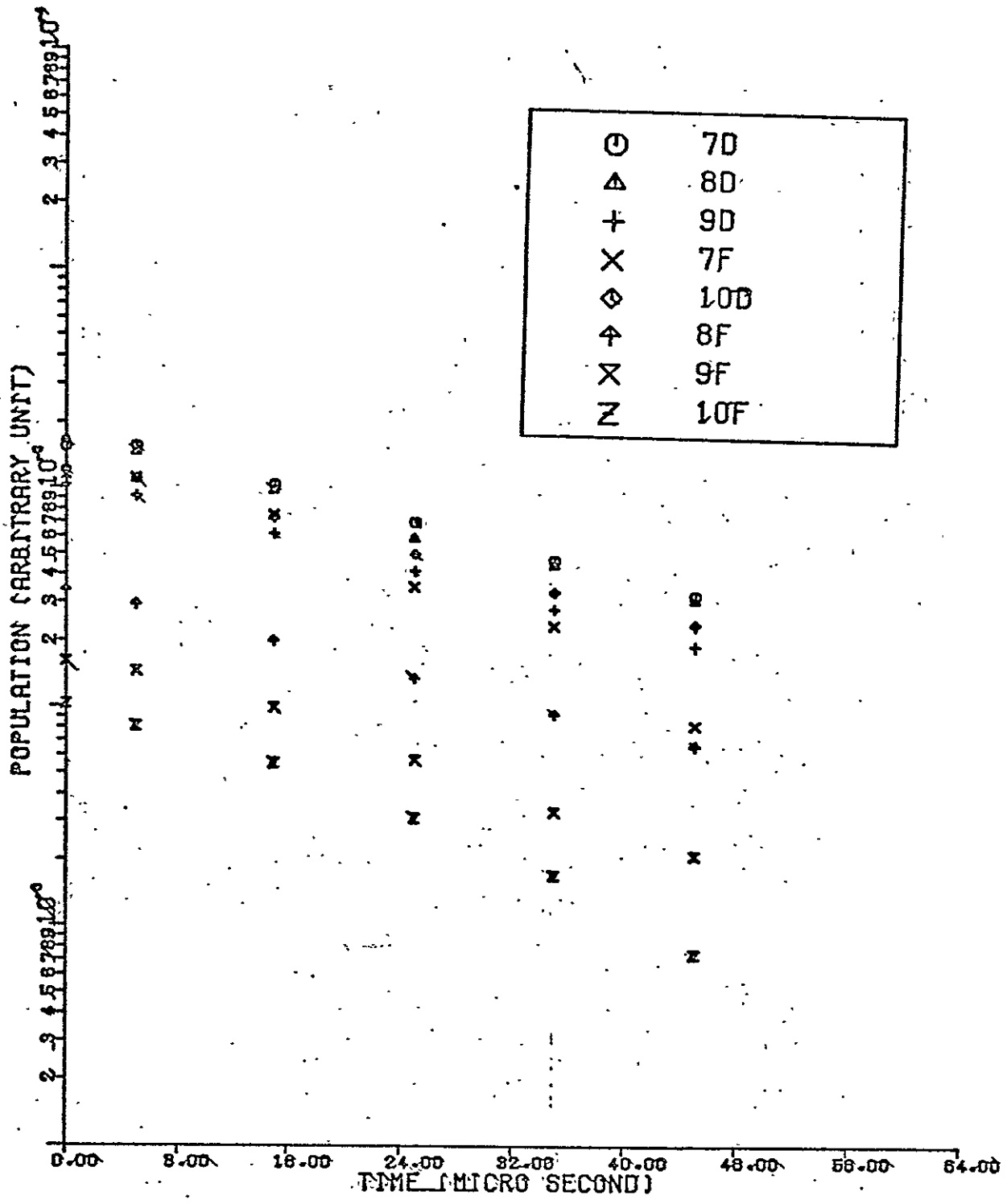

Fig. 10 Variation of the Excited State Populations During the Decay of Plasma in Run 1

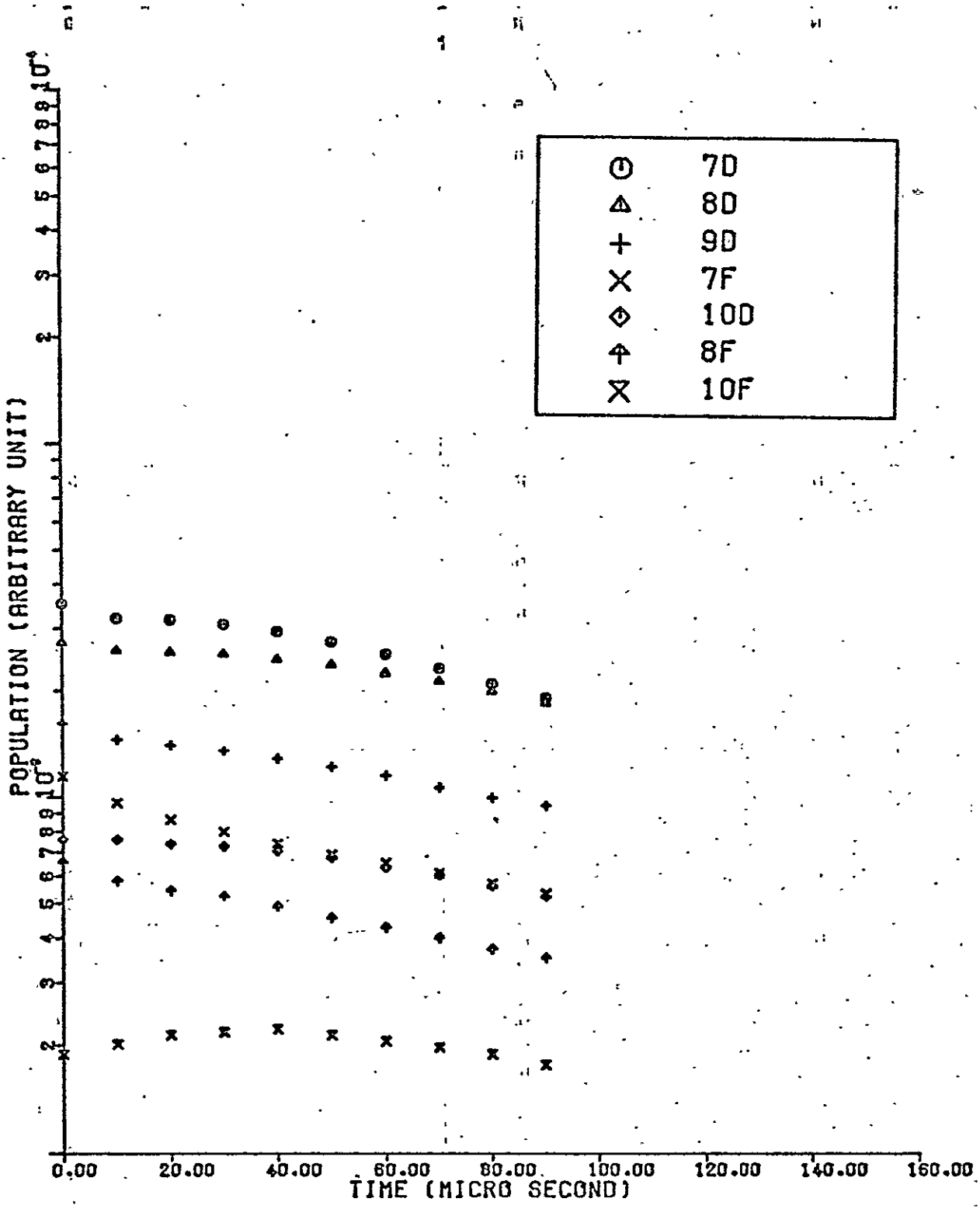

Fig. 11 Variation of the Excited States Population During the Decay of Plasma in Run 5

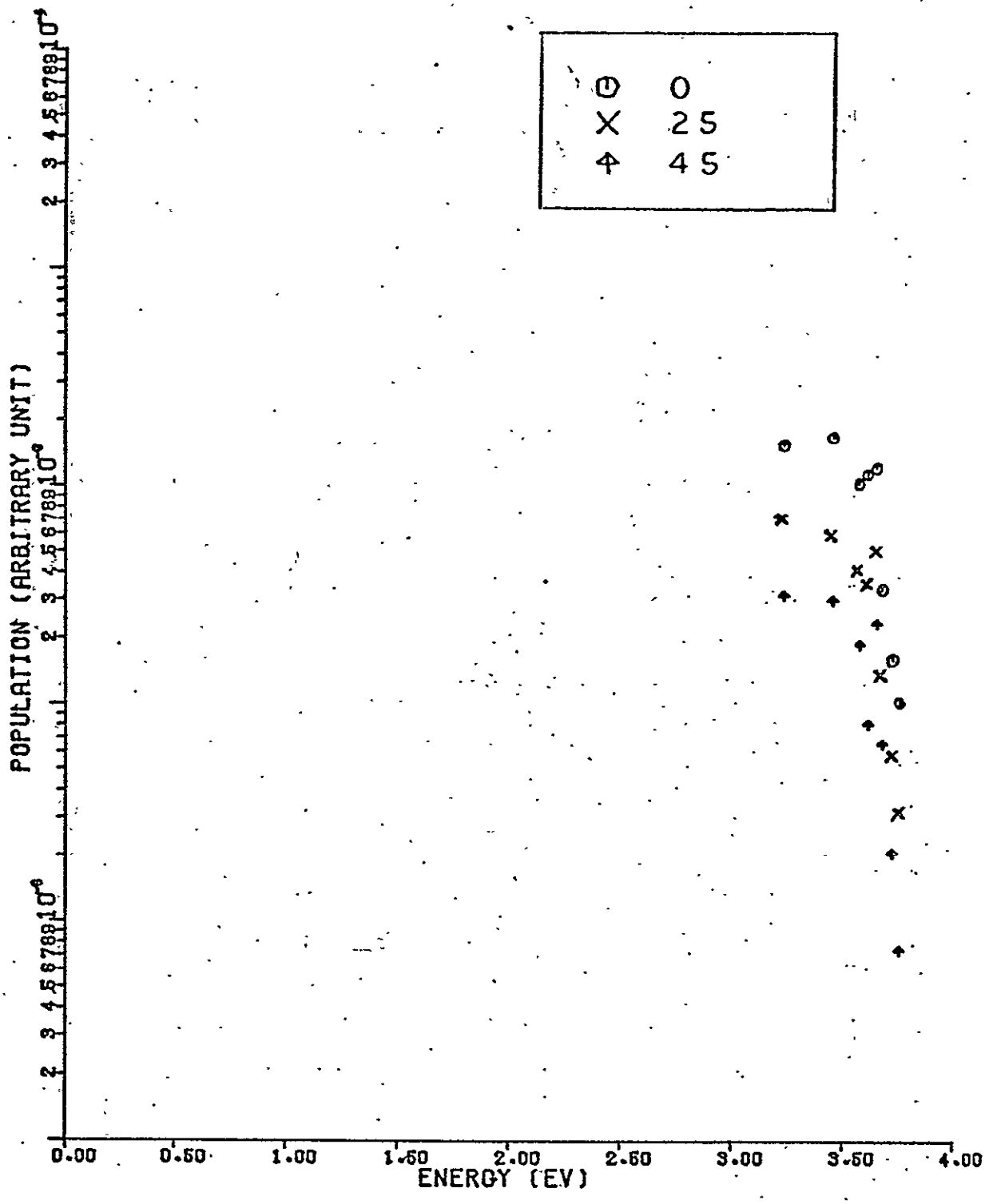

Fig. 12 Distribution of Excited States Population for Several Time Instances in Run 1

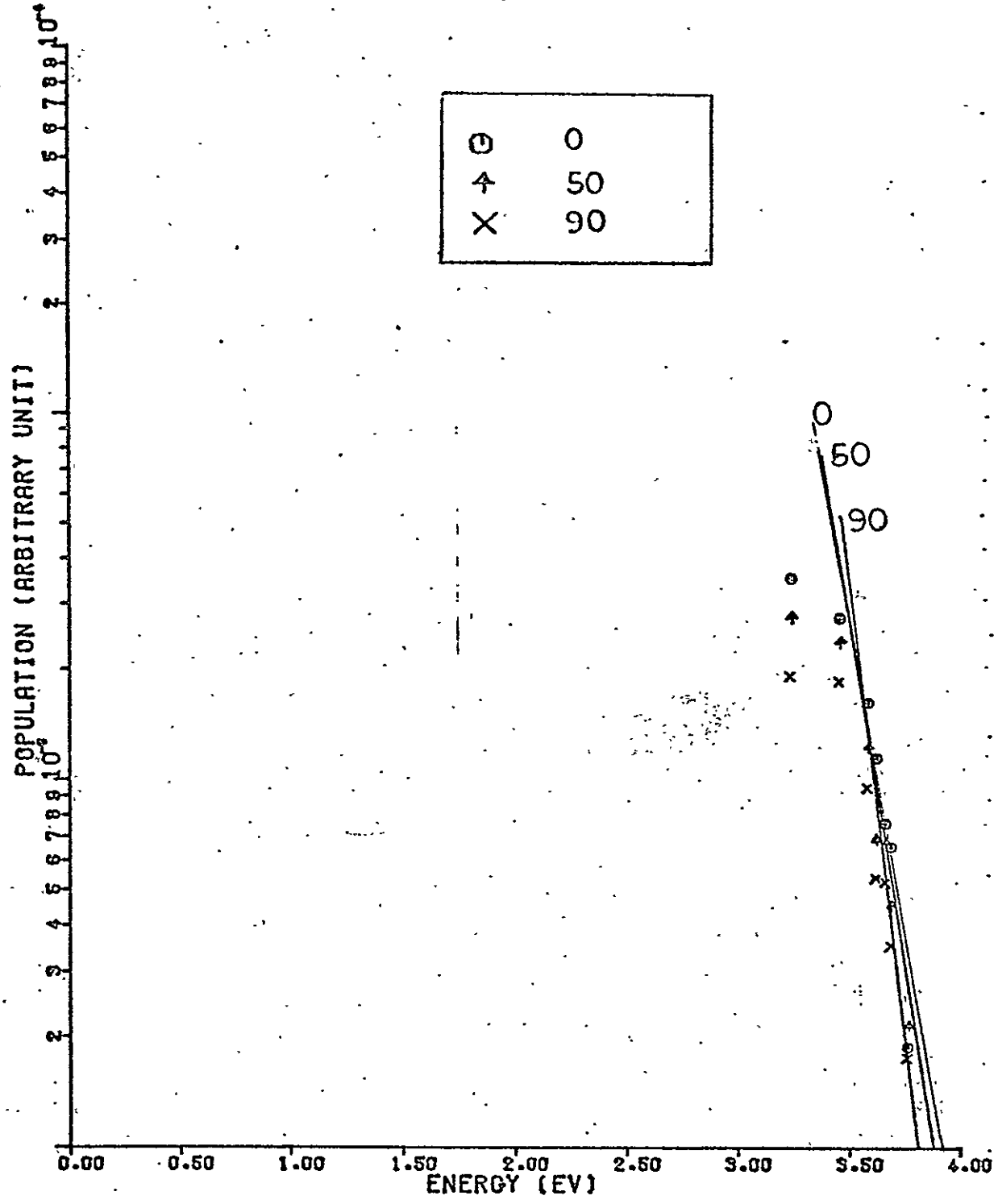

Fig. 13 Distribution of Excited States Population for Several Time Instances in Run 5

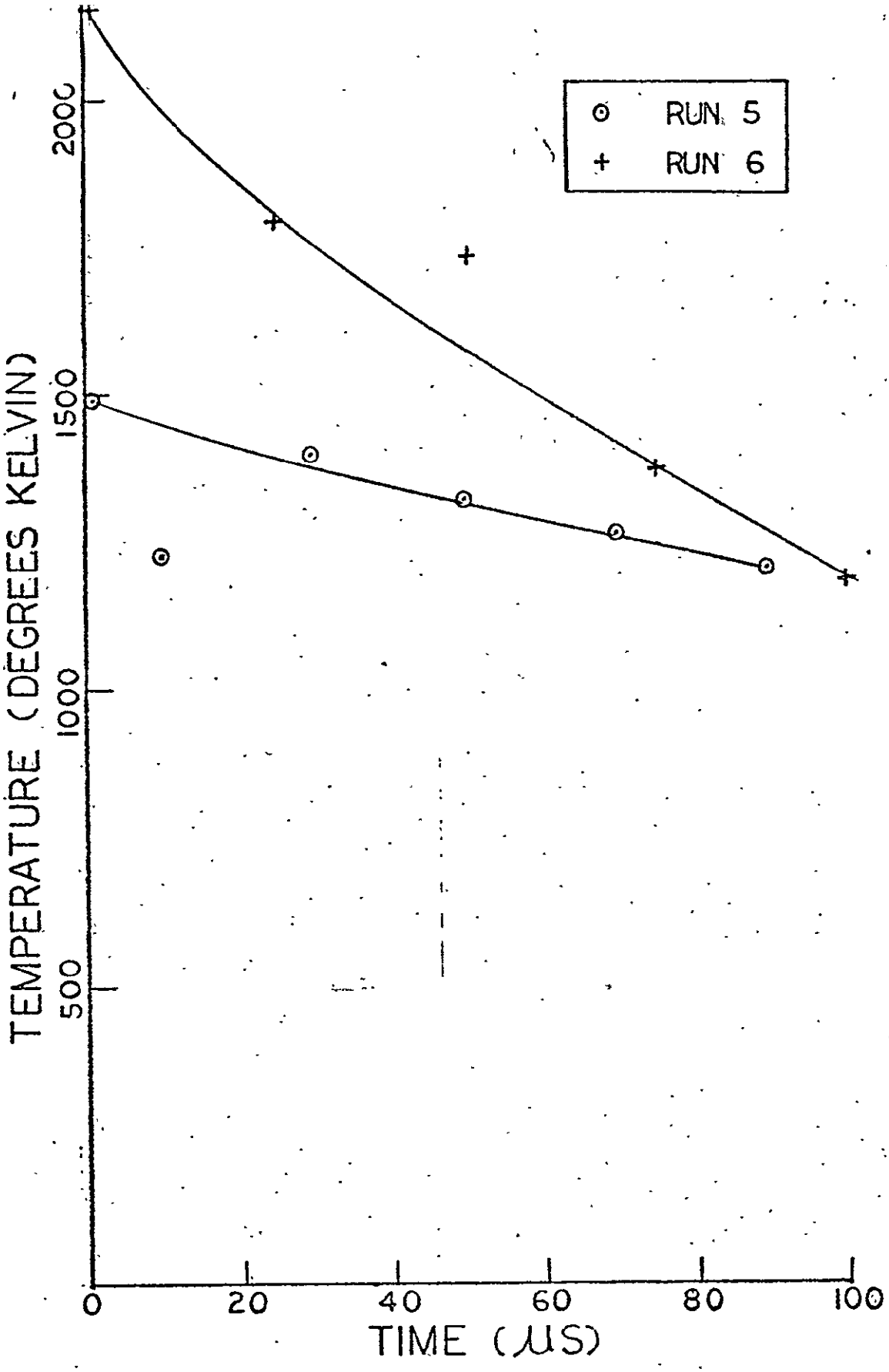

Fig. 14 Variation of Free Electron Maxwellian Temperatures

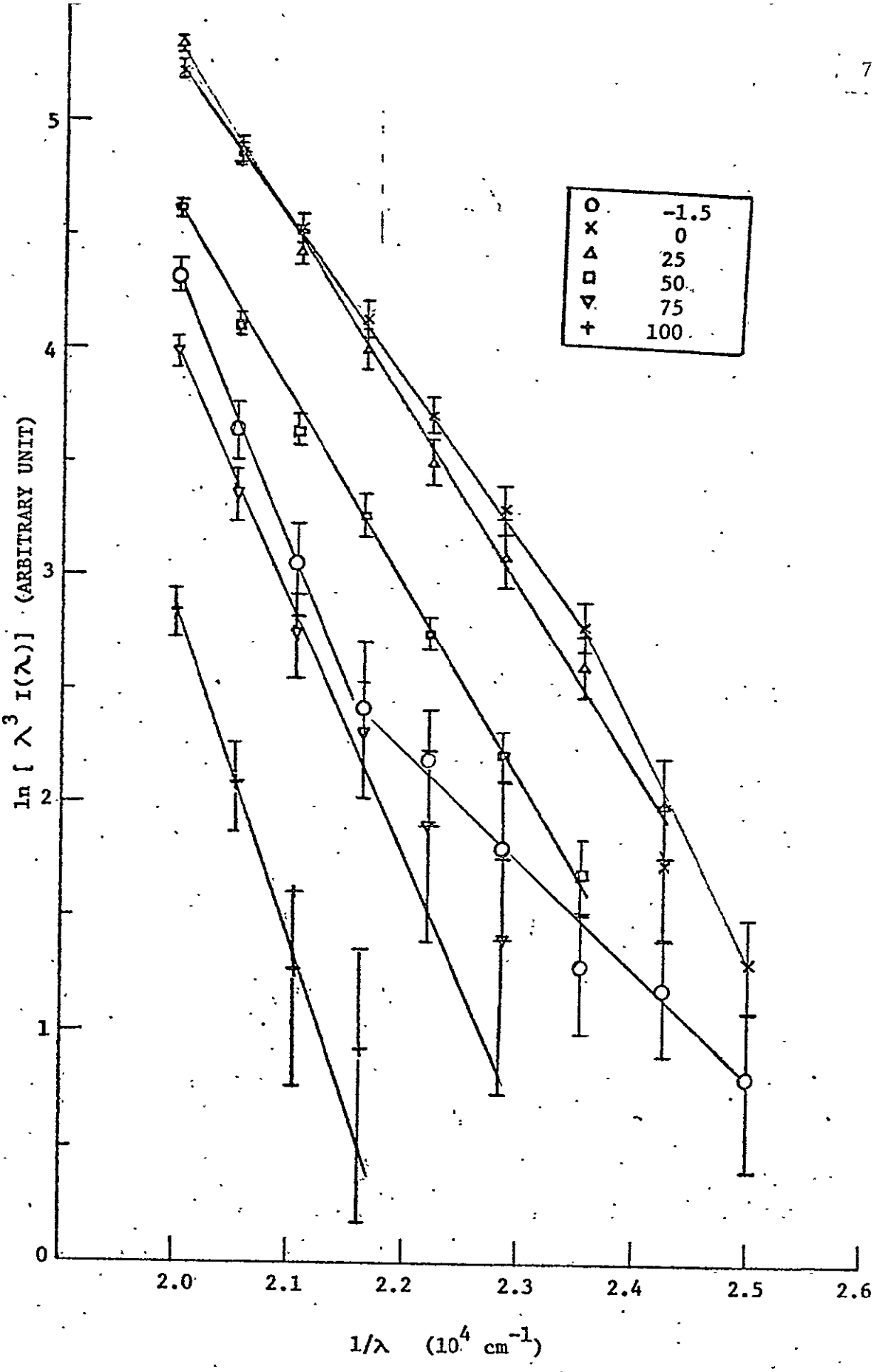

Fig. 15 Data Reduction of Free Electron Temperature for Run 6

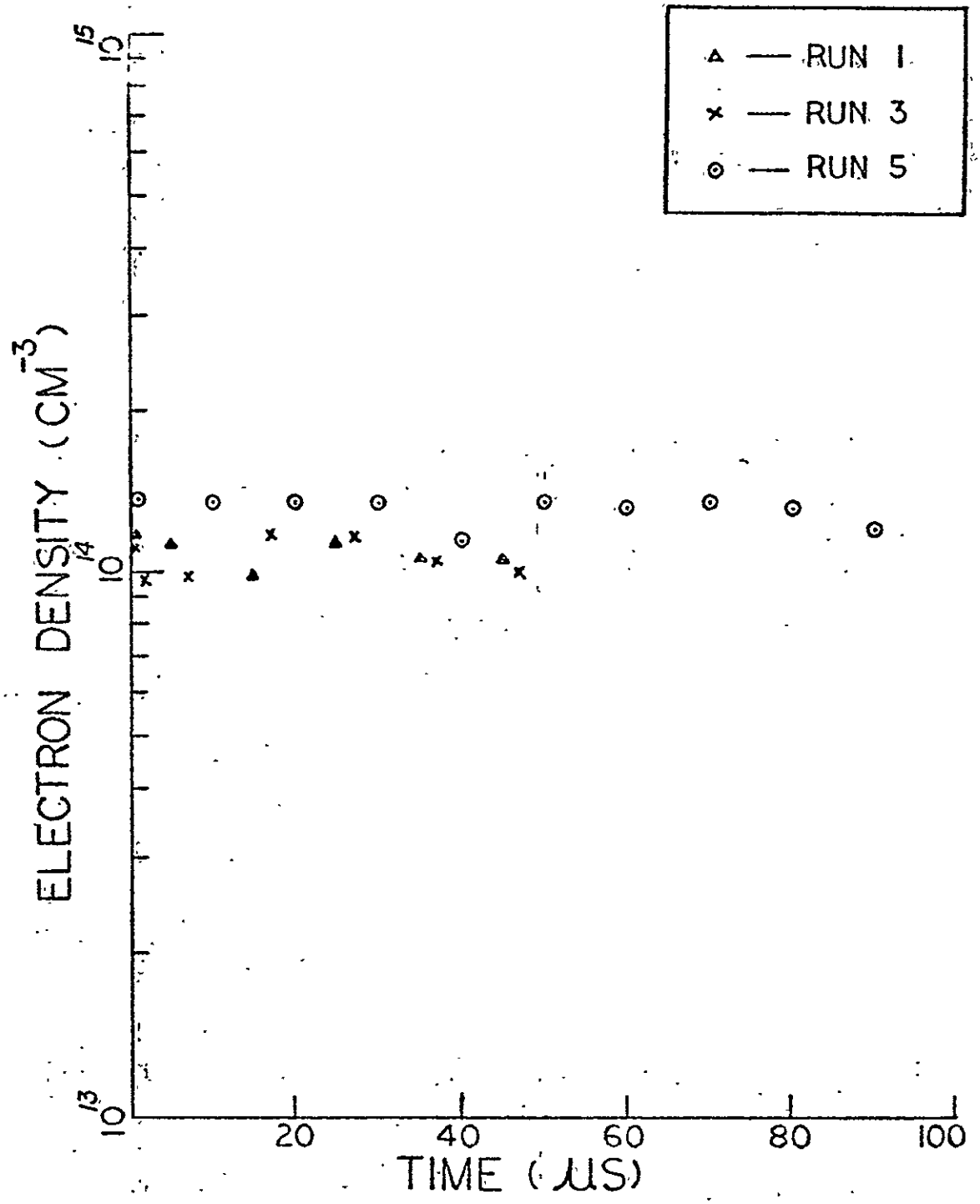

Fig. 16 Variation of the Free Electron Density During the Decay of the Plasma

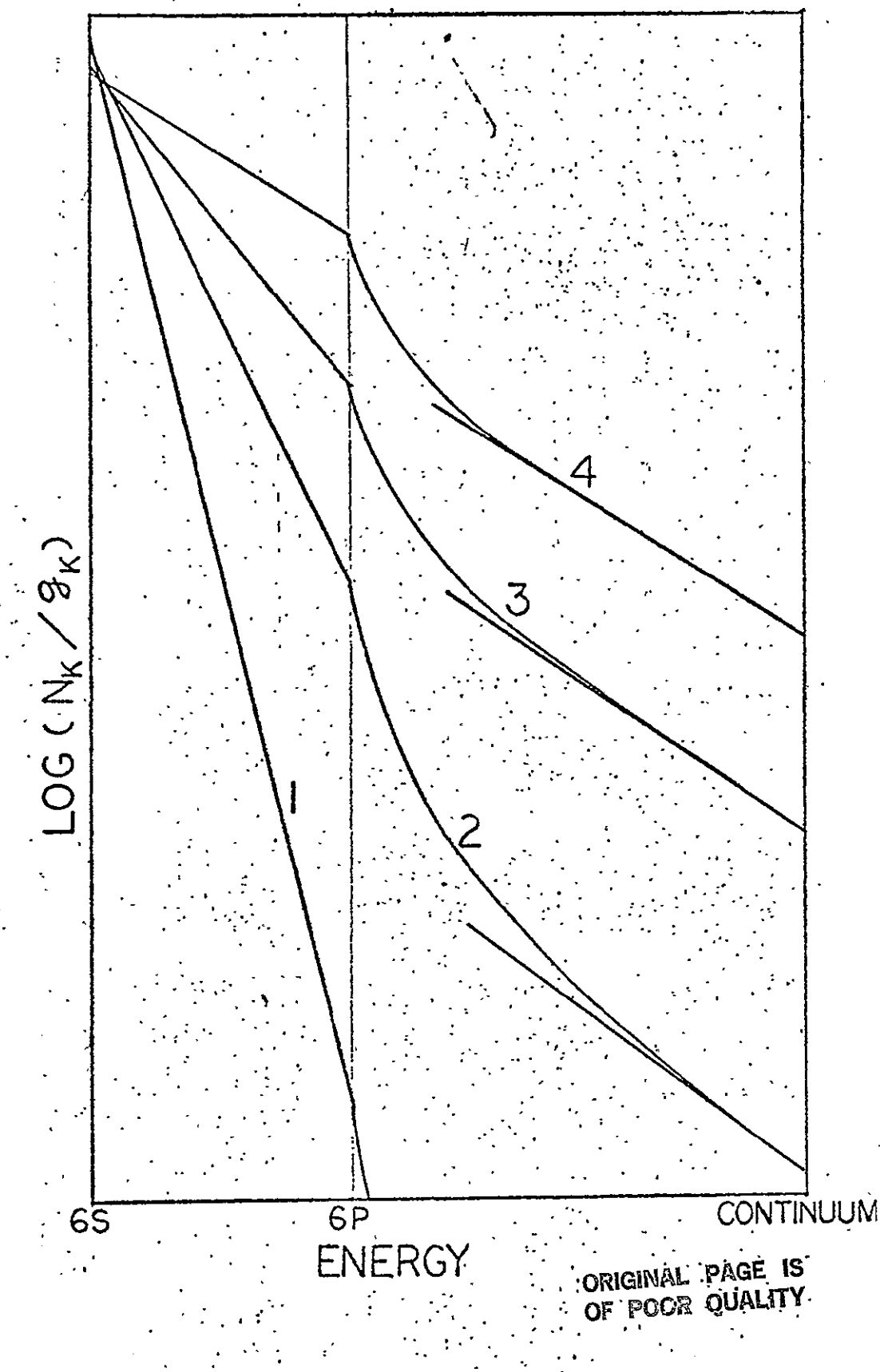

Fig. 17 Excitation of a Cesium Plasma

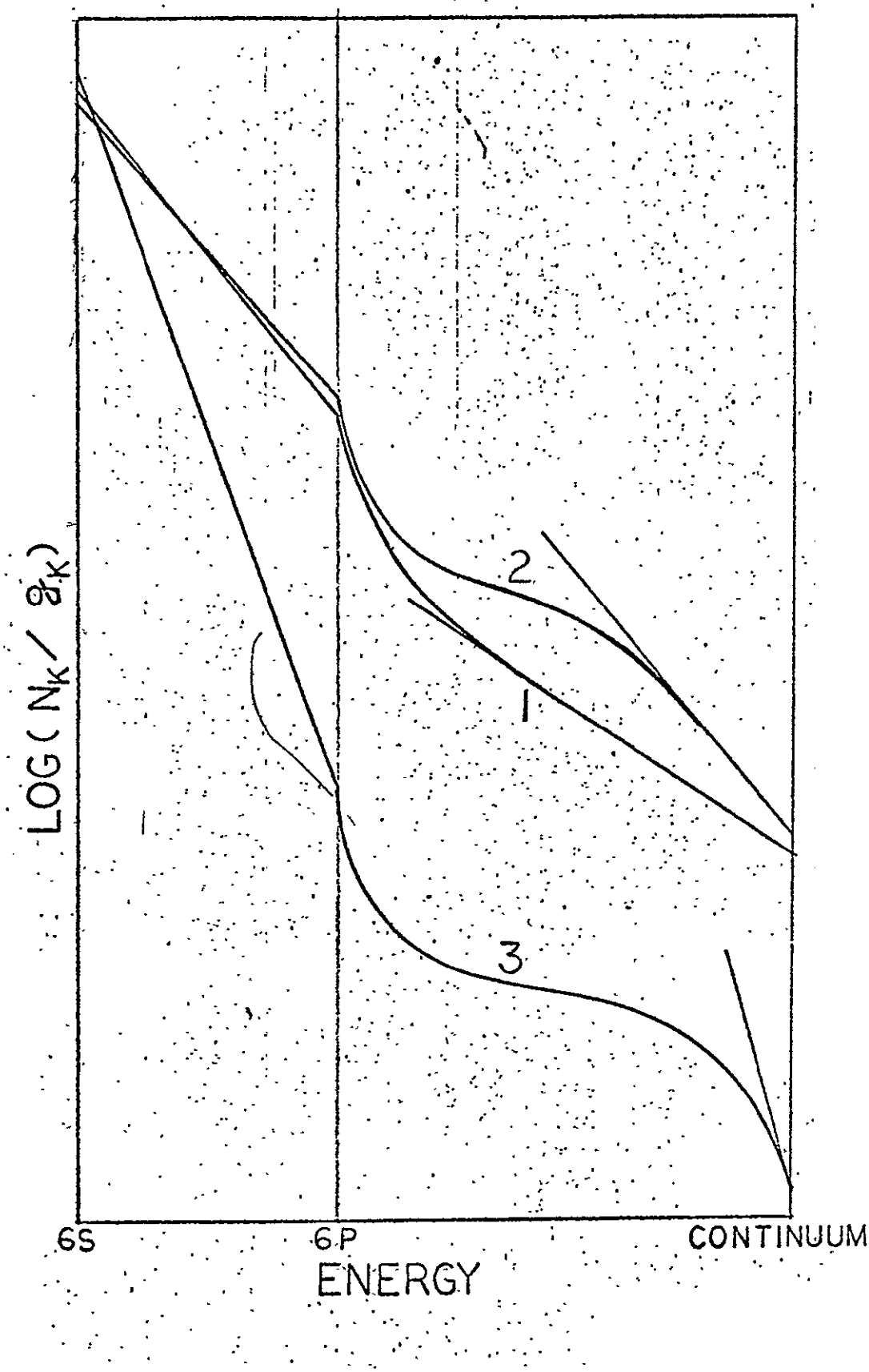

Fig. 18 Decay of a Cesium Plasma

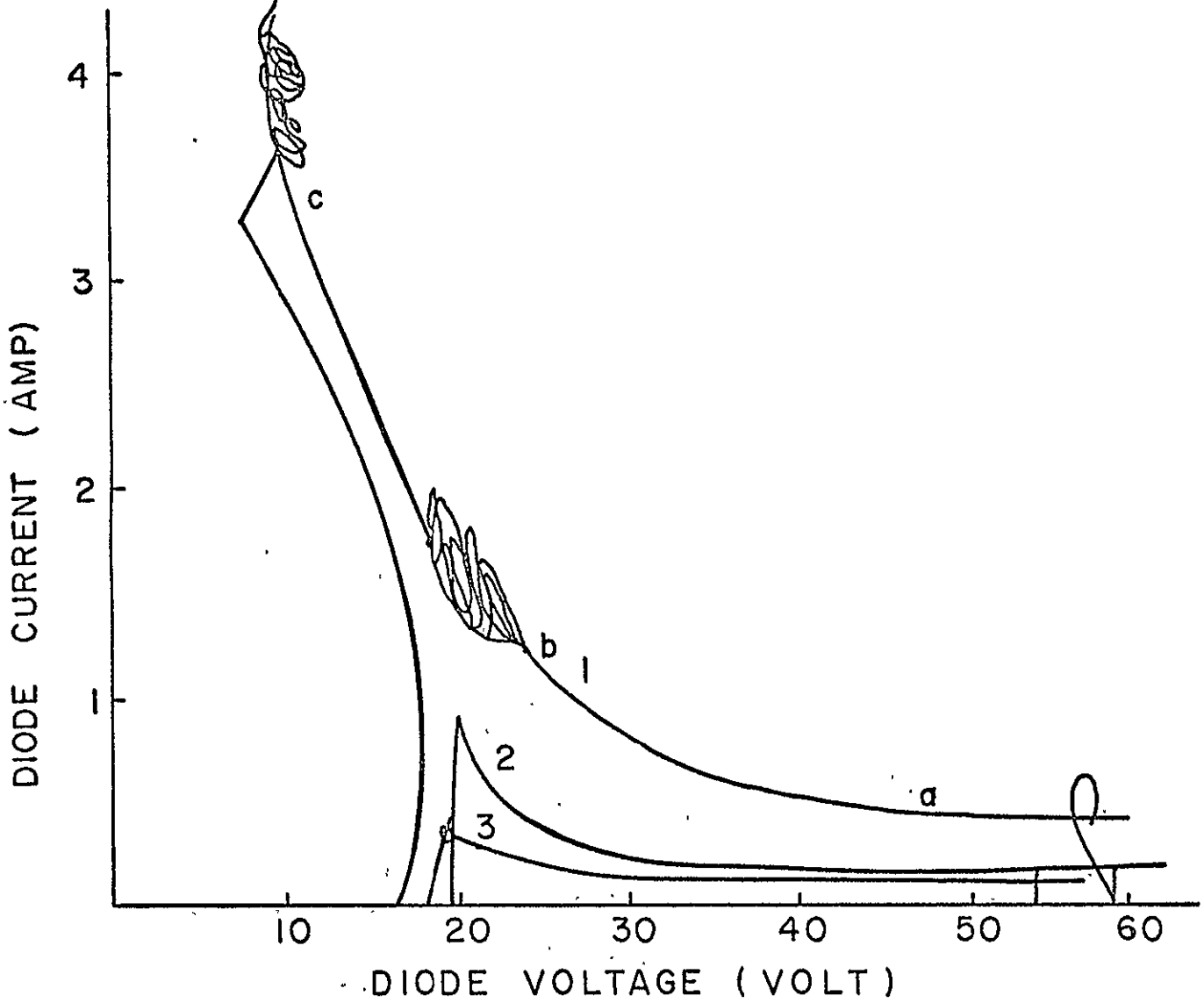

Fig.19 I-V characterisitcs of N_2-Cs thermionic discharge

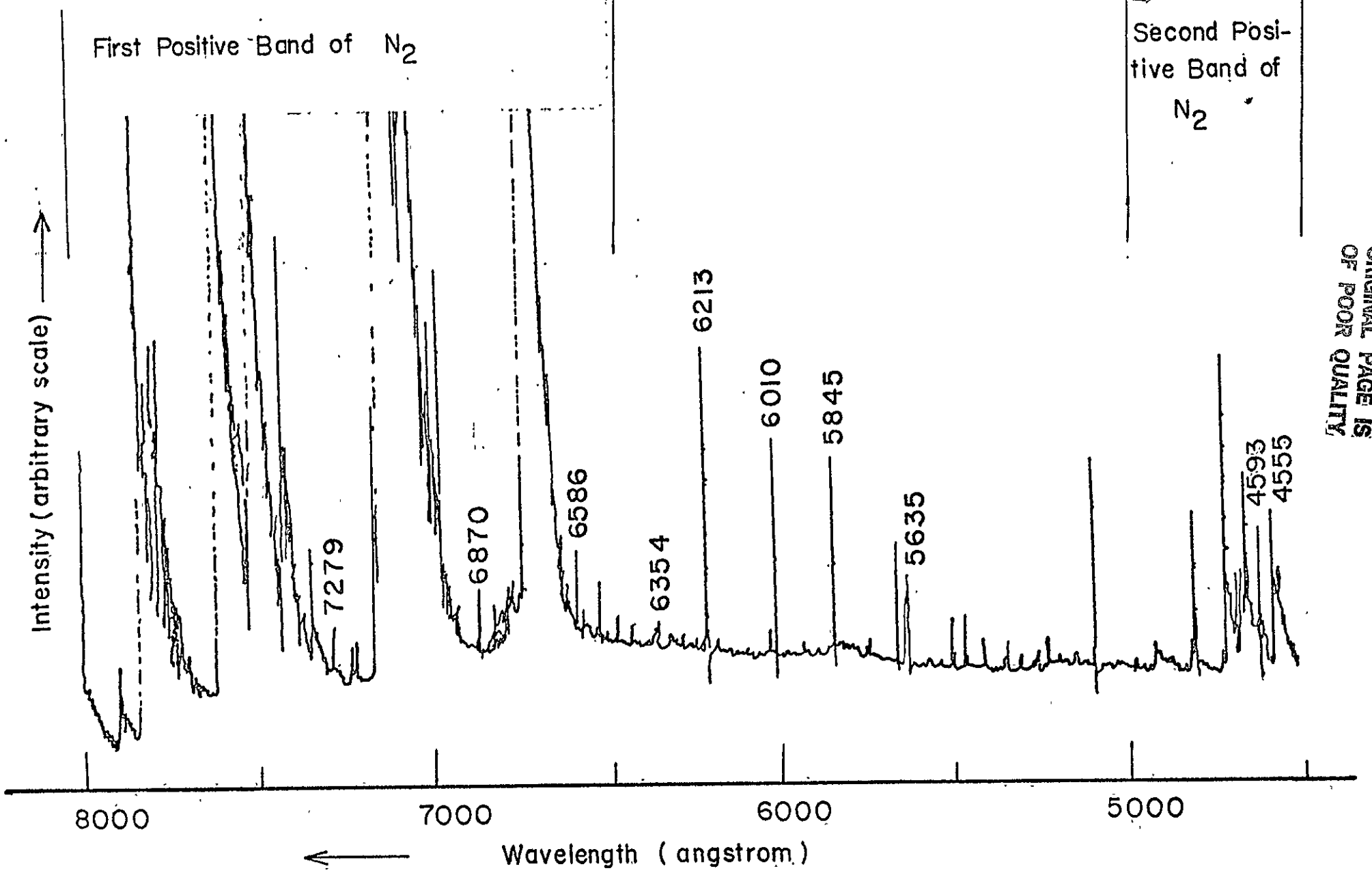

Fig. 20 Spectroscopic lines-radiation measurements.

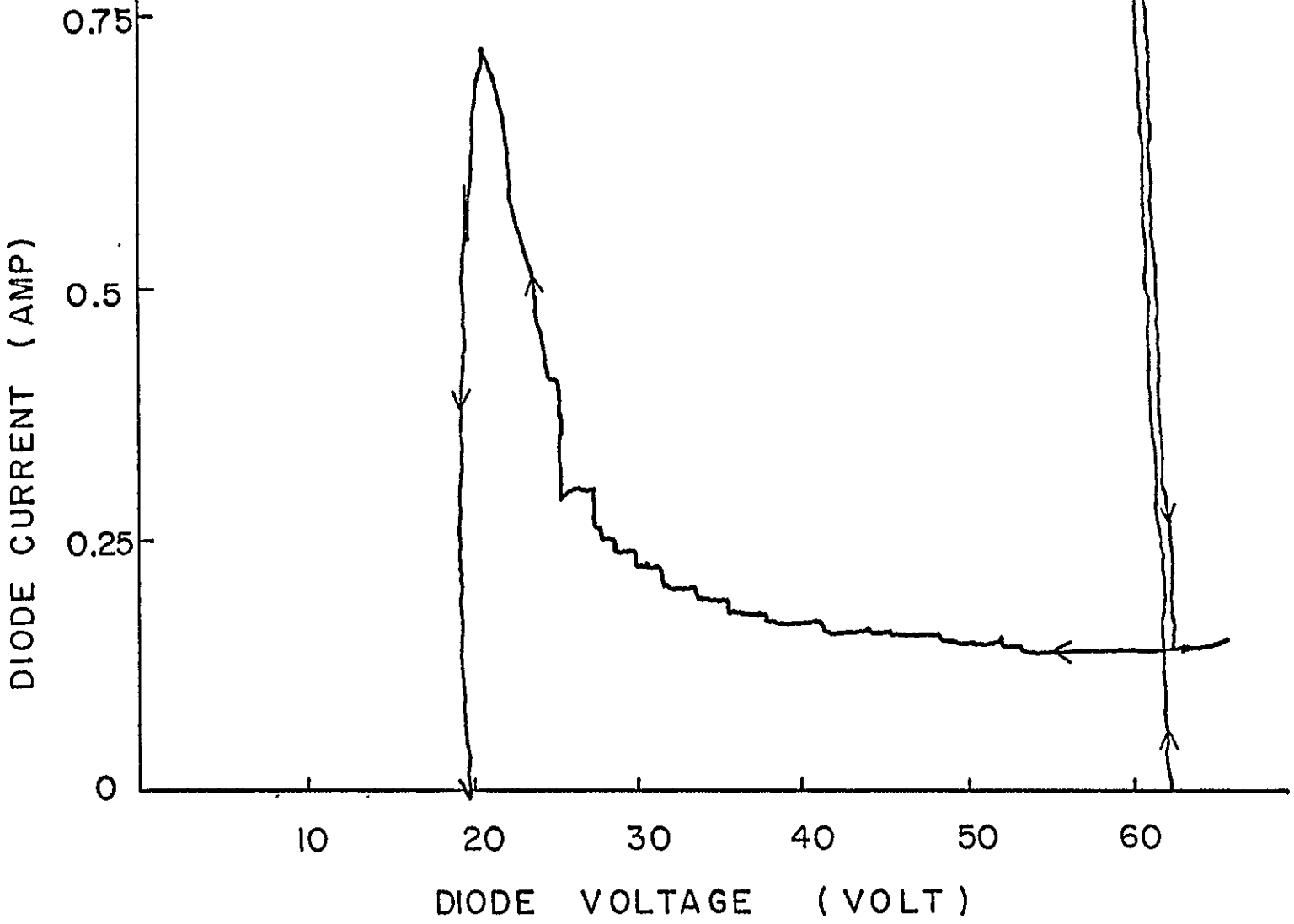

Fig. 21 I-V characteristics showing step-size increases in current.

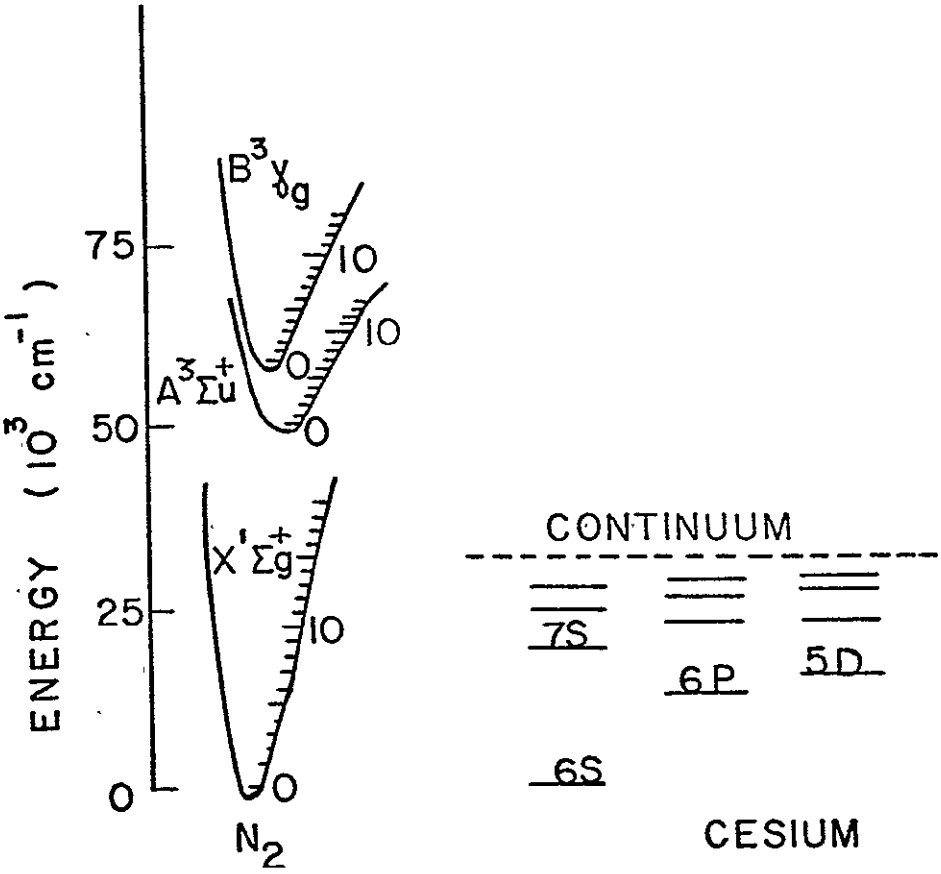

Fig. 22 Energy levels of N_2 and Cesium.

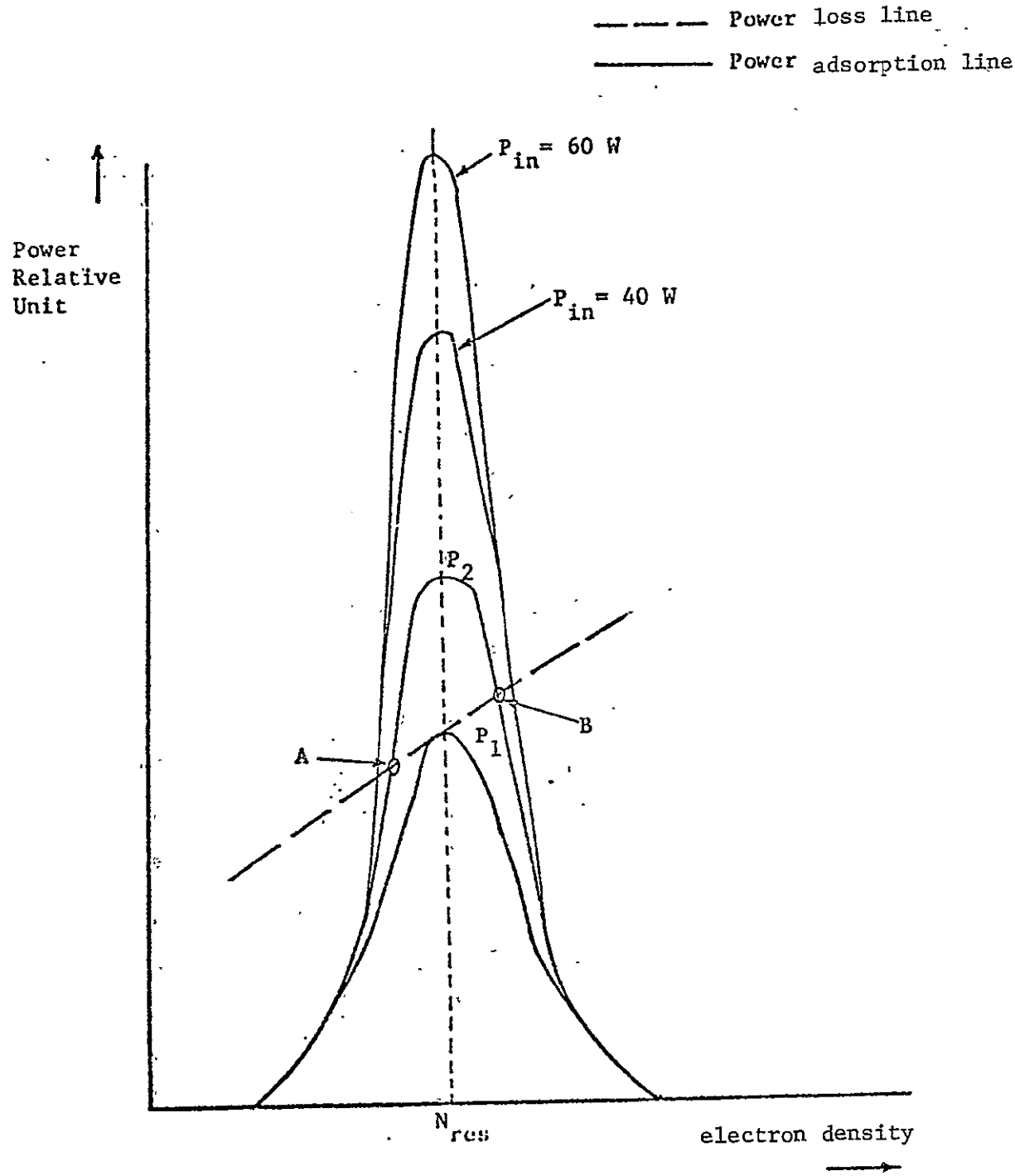

FIG. 23 POWER ABSORBED AND LOST VS PLASMA DENSITY

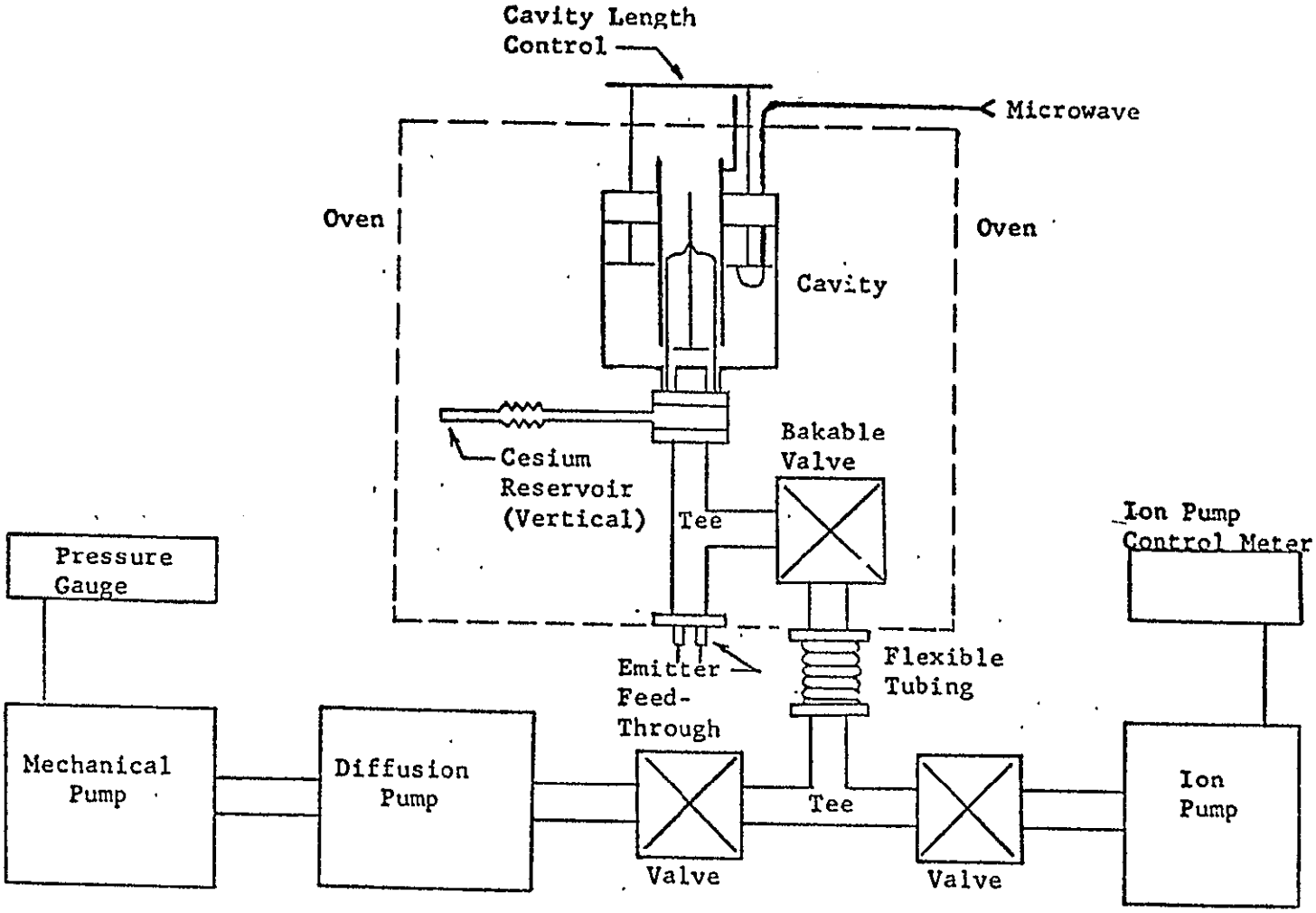

FIG. 24 VACUUM SYSTEM SET UP

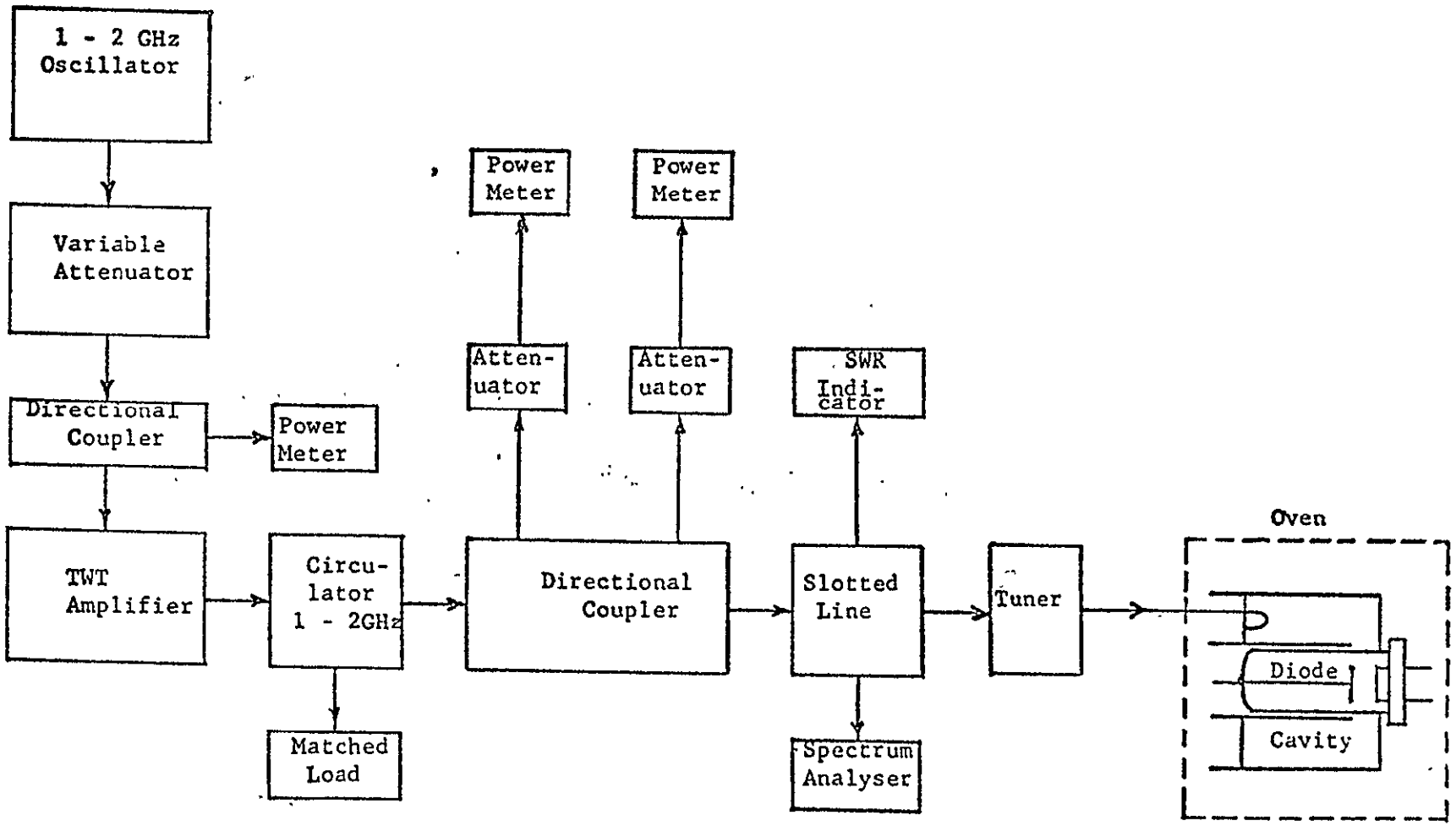

FIG. 25 MICROWAVE SYSTEM SET UP

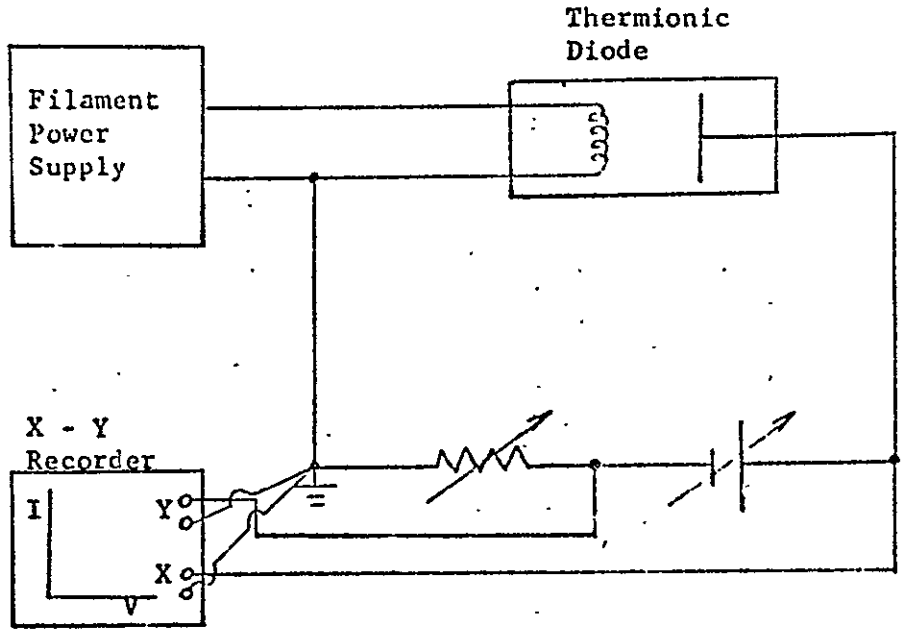

a.) DC Discharge

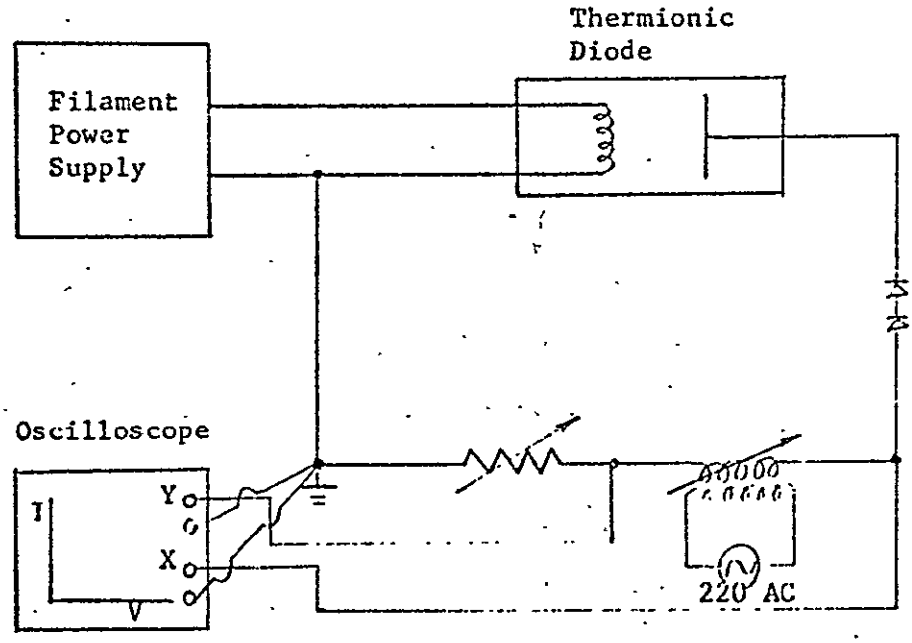

b.) AC Discharge

FIG.26 THERMIONIC DIODE ELECTRICAL CIRCUIT SET UP

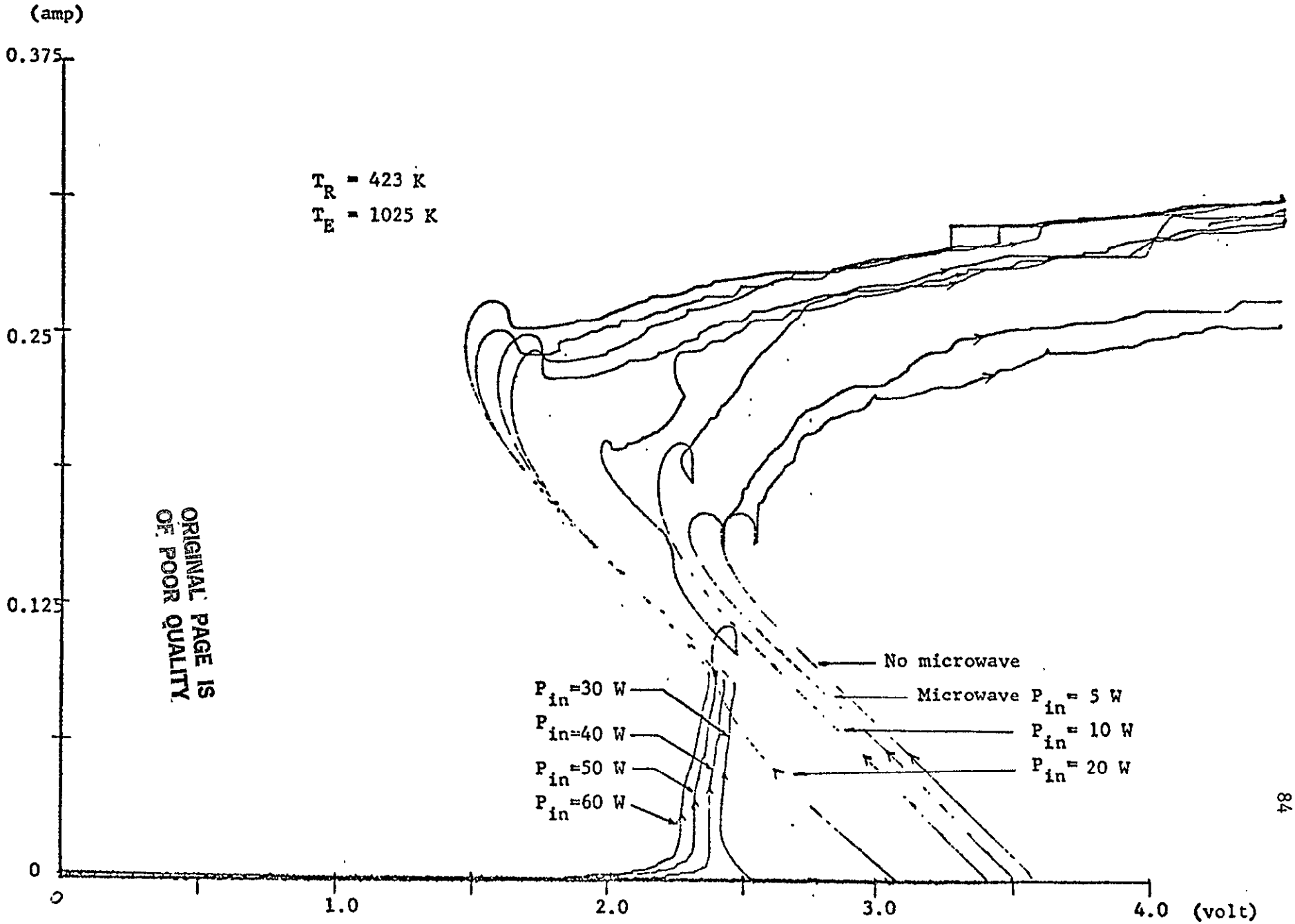

FIG. 27 I - V CHARACTERISTIC AT T_R=423 K AND T_E=1025 K

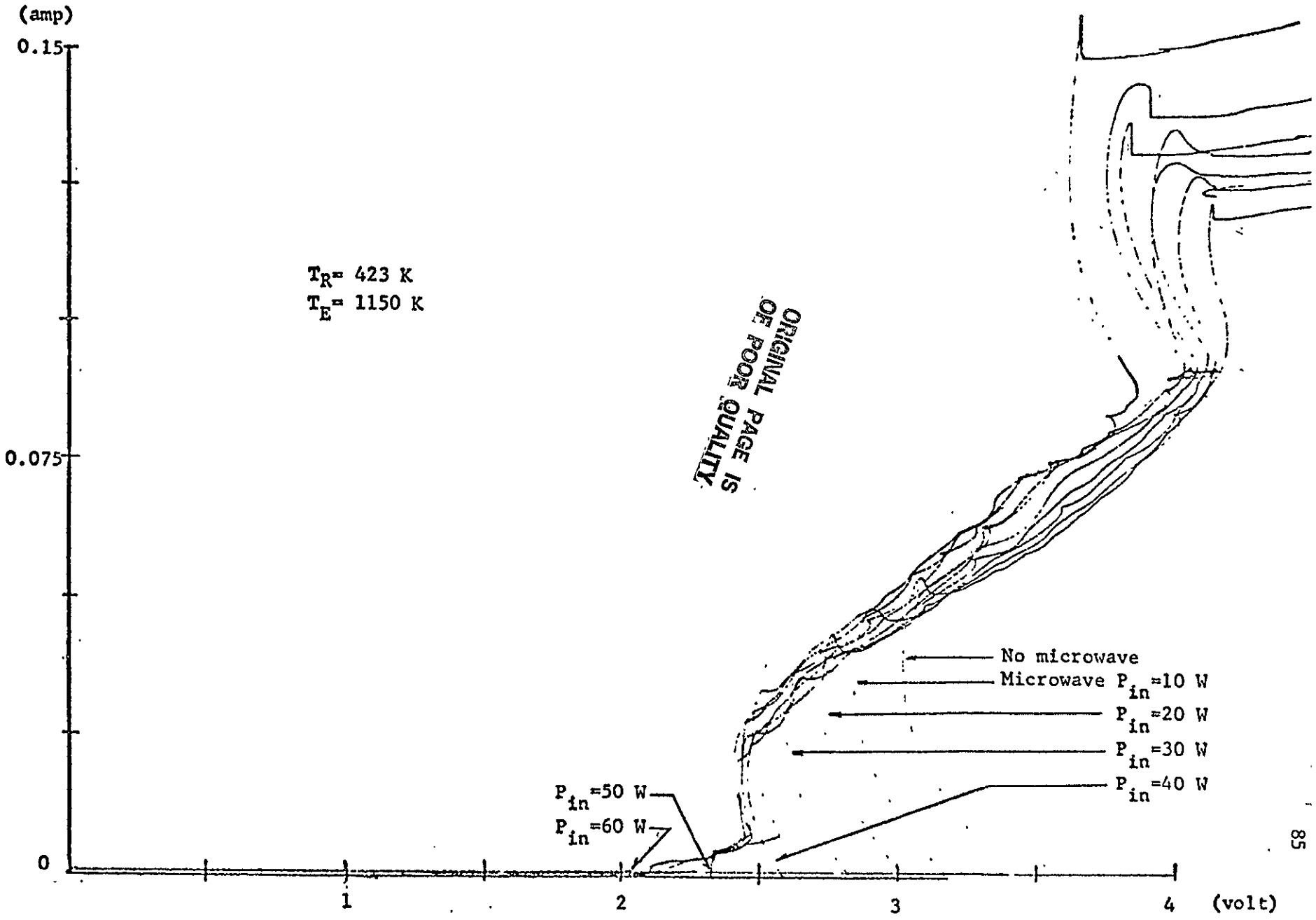

FIG. 28 I - V CHARACTERISTIC AT T_R=423 K AND T_E=1150 K

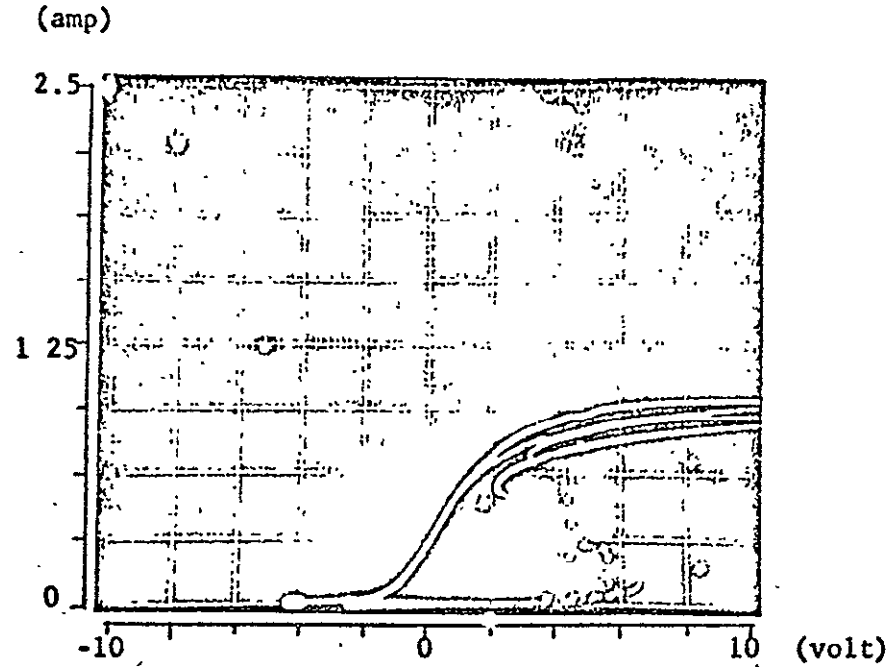

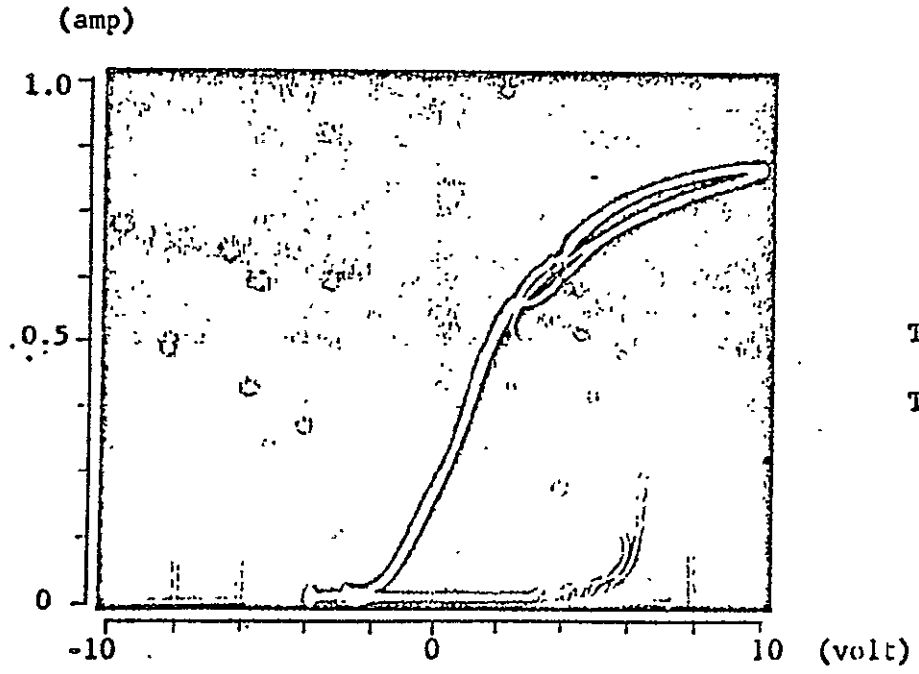

FIG. 29 I - V CHARACTERISTIC AT T_E=1115 K AND T_E=1180 K

(BOTH PICTURES ARE SHOWN WITH AND WITHOUT MICROWAVE)

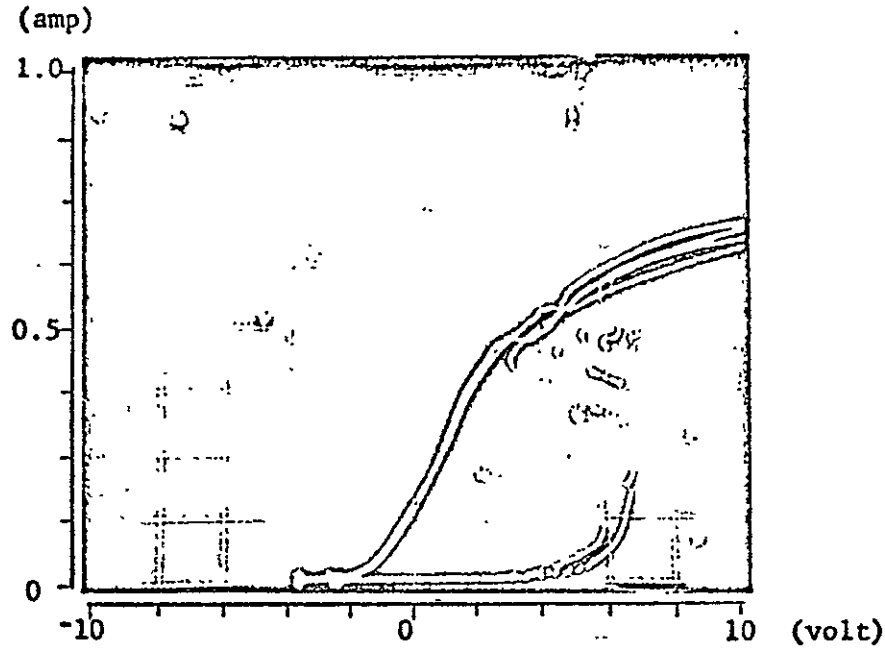

T_E = 1210 K

T_{CS} = 473 K

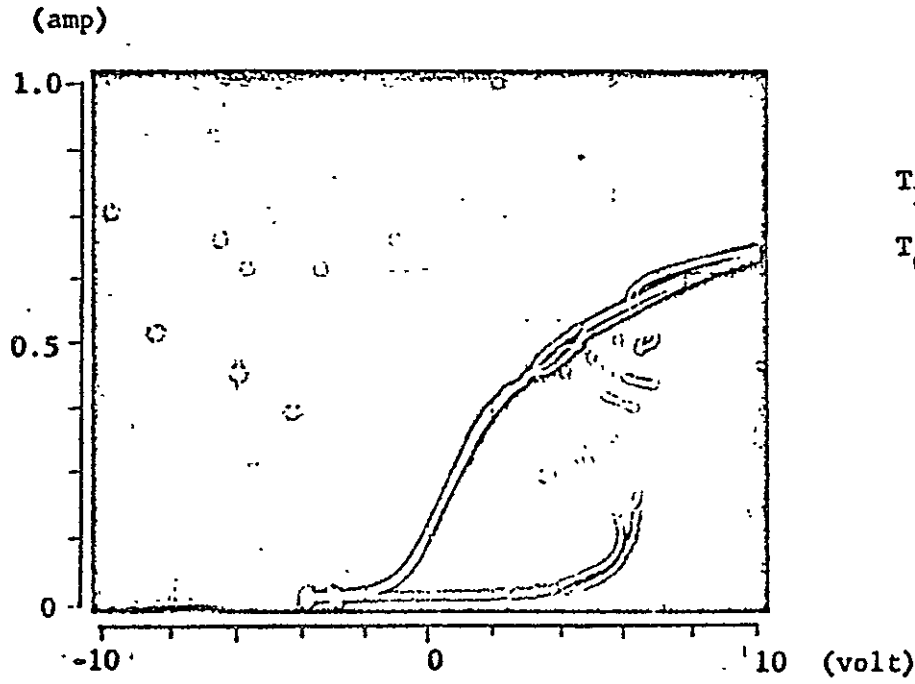

T_E = 1240 K

T_{CS} = 473 K

FIG. 30 I - V CHARACTERIESTIC AT T_E=1210 K AND T_E=1240 K

(BOTH PICTURES ARE SHOWN WITH AND WITHOUT MICROWAVE)

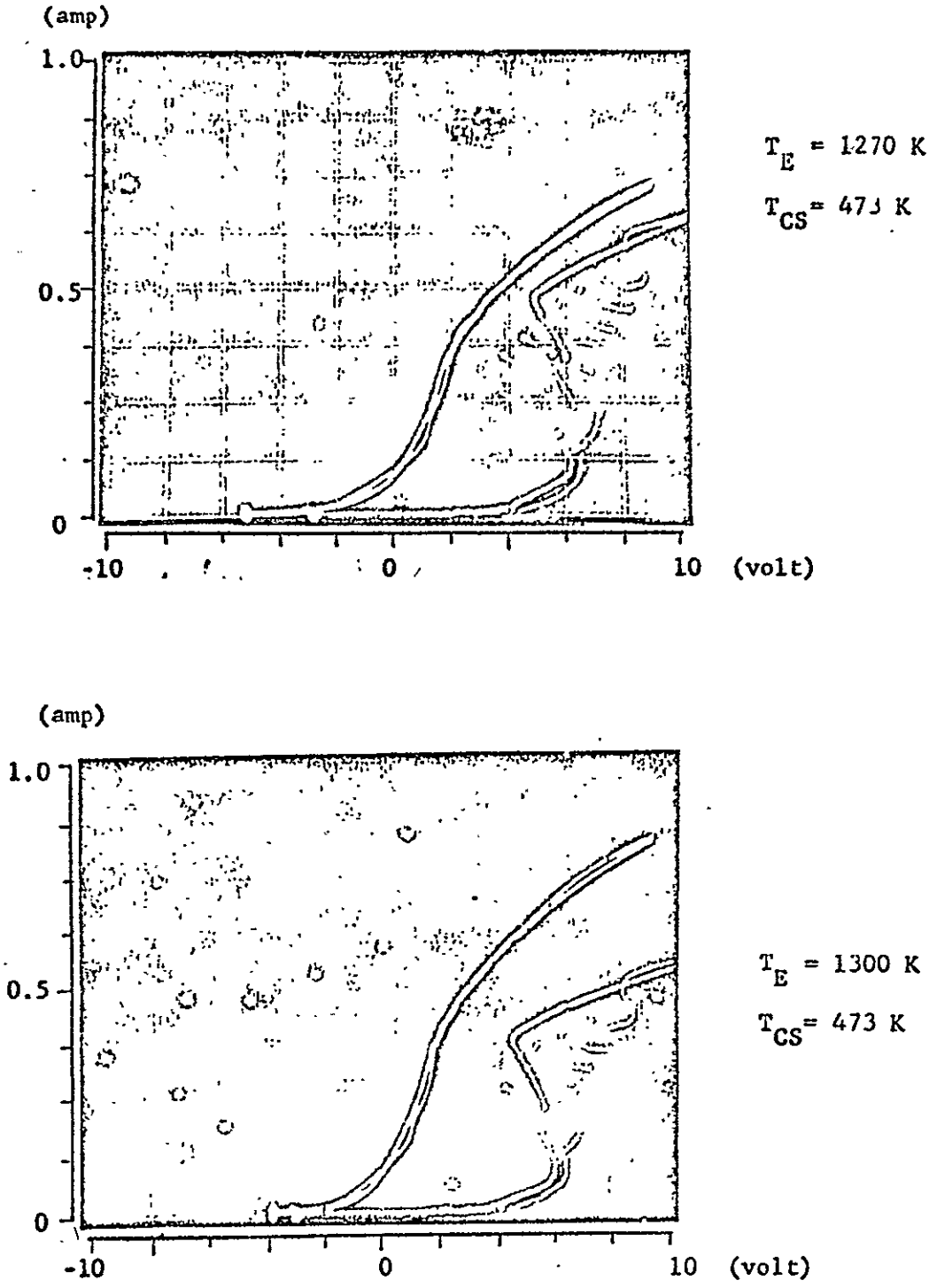

FIG. 31 I - V CHARACTERISTIC AT T_E=1270 K AND T_E=1300 K

(BOTH PICTURES ARE SHOWN WITH AND WITHOUT MICROWAVE)

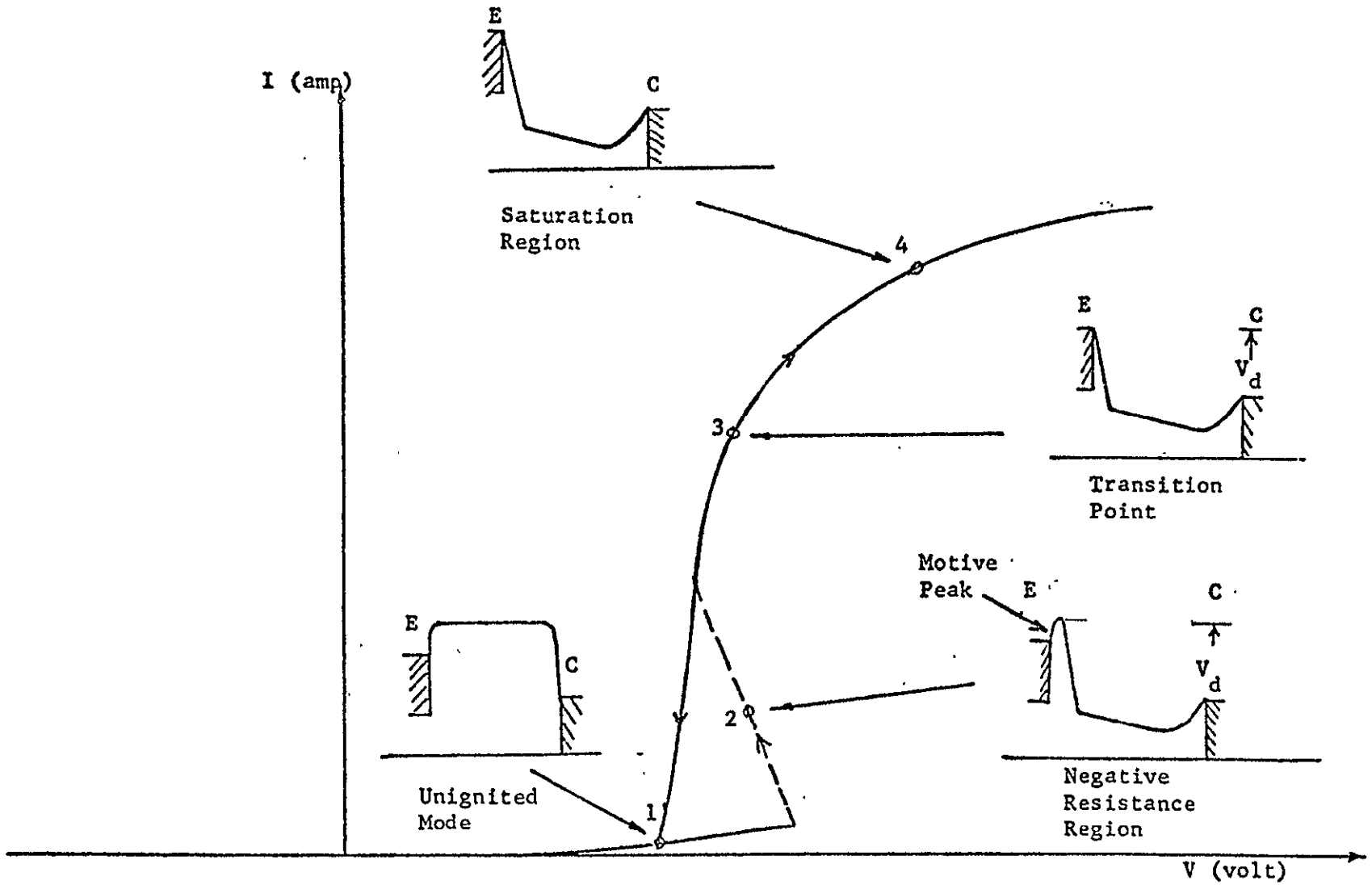

FIG. 32 TYPICAL I - V CHARACTERISTIC CURVE OF CESIUM THERMIONIC DIODE IN NEGATIVE POWER QUADRANT AND THE POTENTIAL DISTRBUTION DIAGRAMS

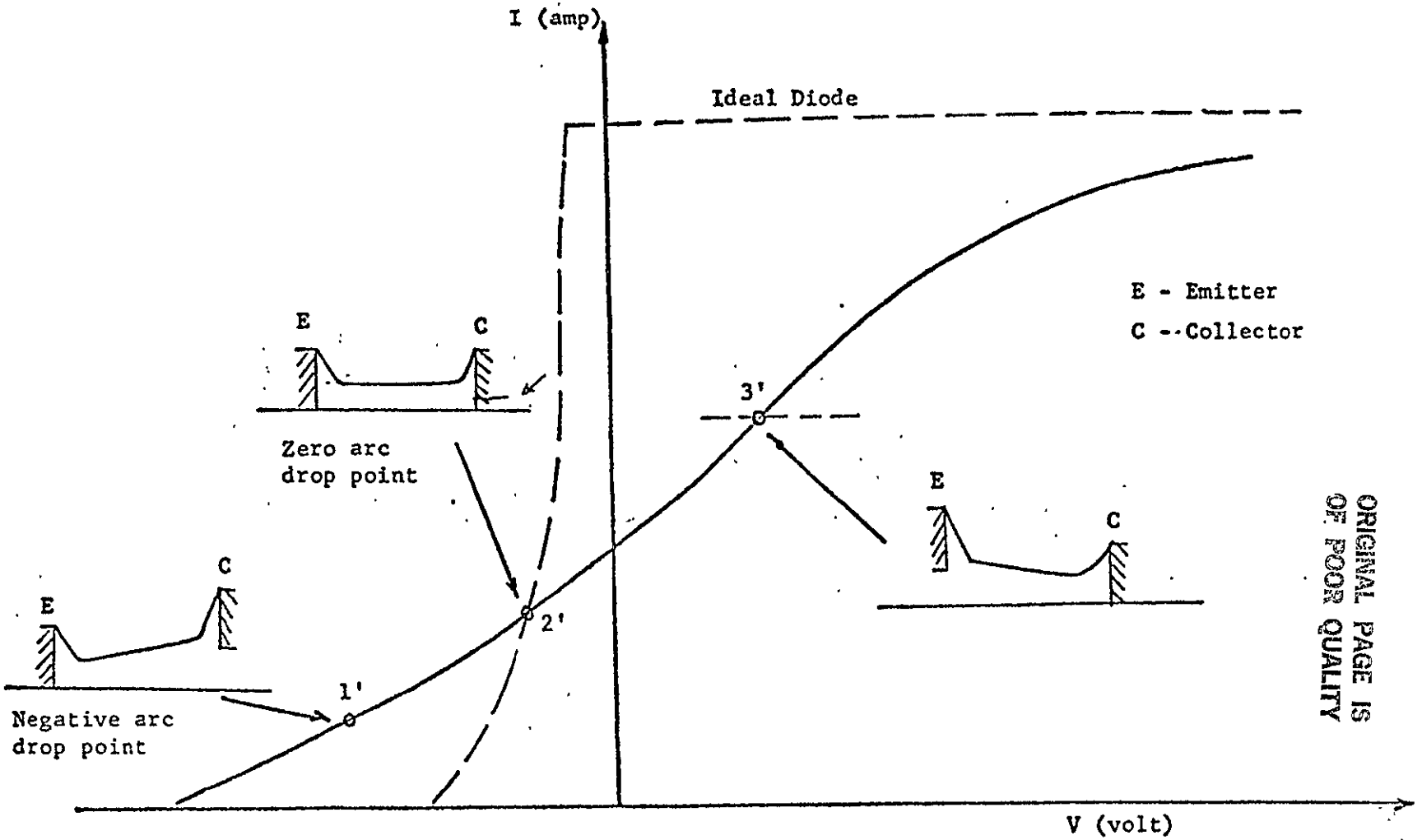

FIG. 33 TYPICAL I - V CHARACTERISTIC CURVE OF MICROWAVE CAVITY THERMIONIC DIODE AND POTENTIAL DISTRIBUTION DIAGRAMS.

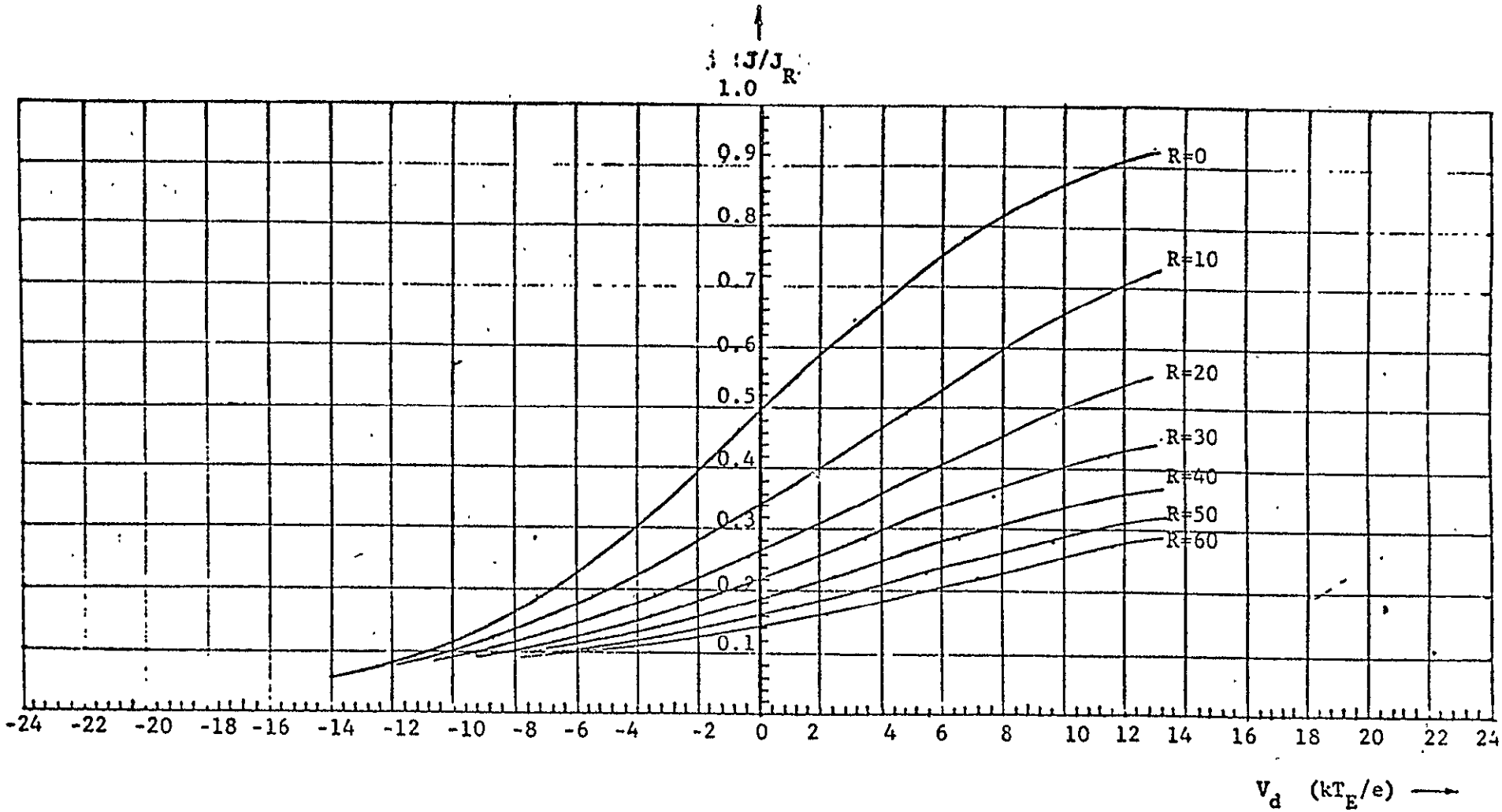

FIG. 34 NORMALIZED I - V CHARACTERISTIC EXTERNALLY HEATED CASE USING LAM'S THEORY AT $\tau = 5$

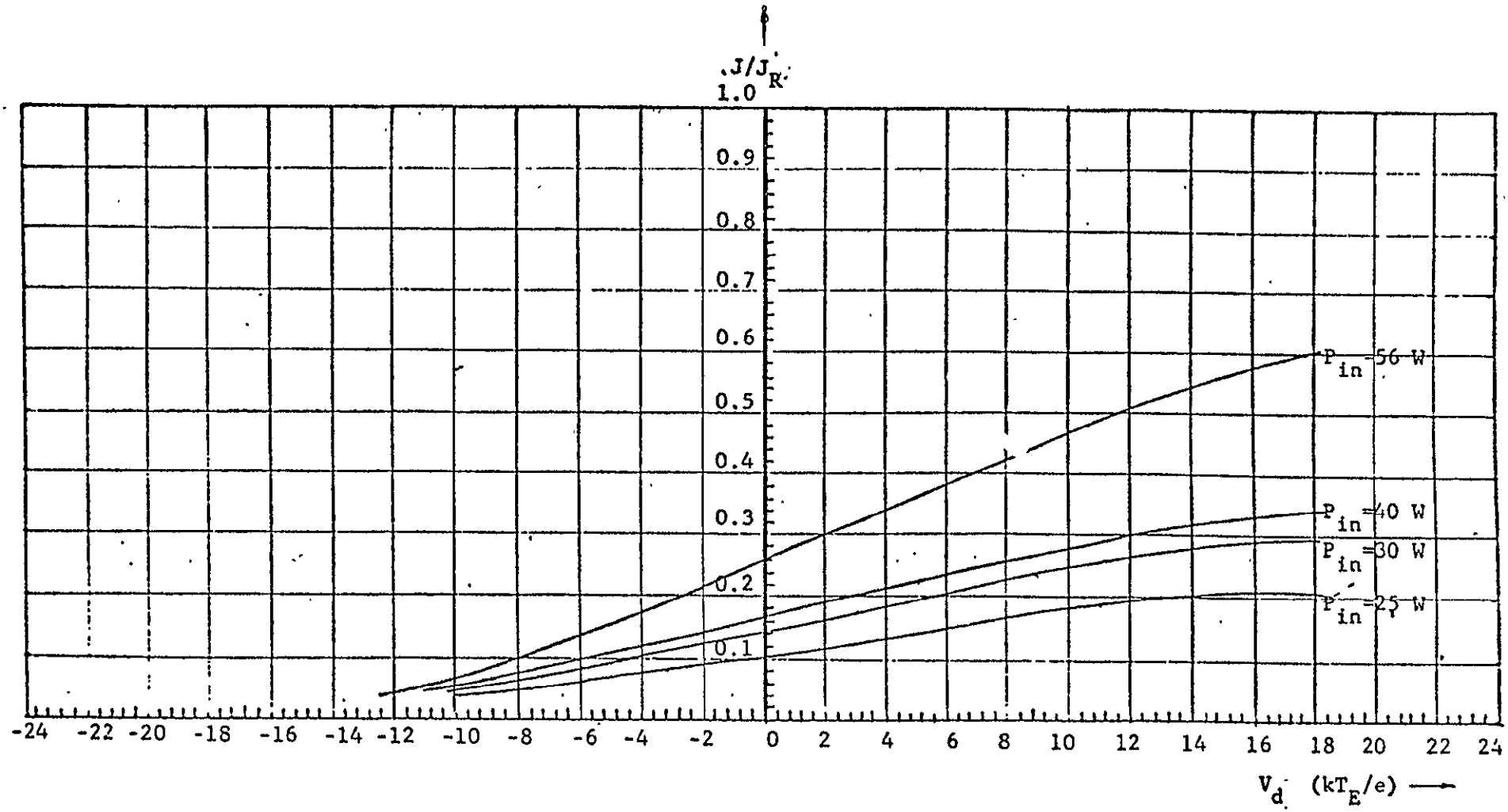

FIG. 35 NORMALIZED I - V CHARACTERISTIC WITH DIFFERENT INCIDENT RF POWER LEVELS

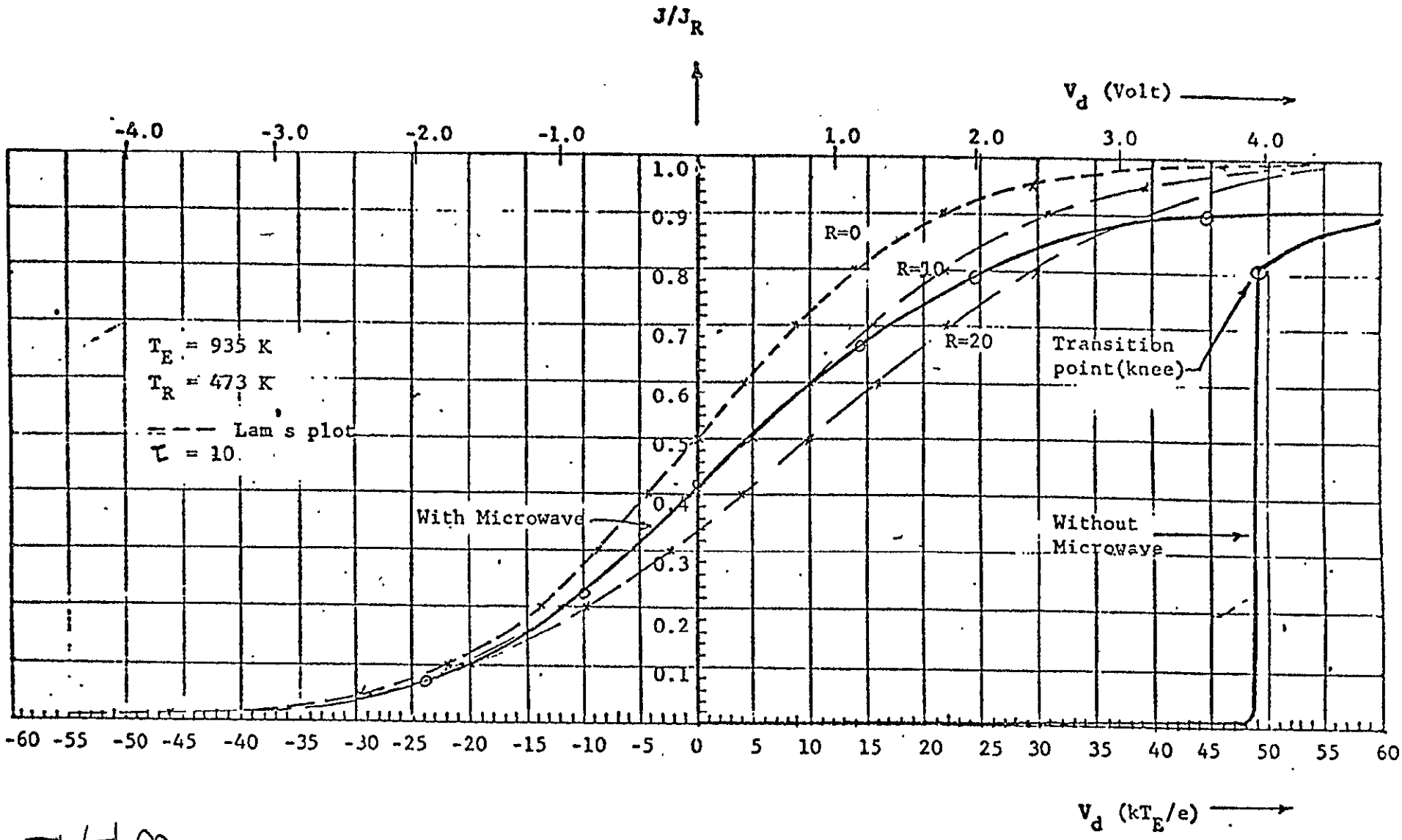

FIG. 36 I - V CHARACTERISTIC WITH AND WITHOUT MICROWAVE